# Boron and Oxygen Isotope Systematics of Two Hydrothermal Systems in Modern Back-Arc and Arc Crust (PACManus and Brothers Volcano, W-Pacific)

*Manuscript in preparation for a special issue in Economic Geology*

***Lucy E.M. Schlicht[1*], Olivier Rouxel[2], Jeremy Deans[3], Stephen Fox[4], Yaron Katzir[4], Kouki Kitajima[5], Simone A. Kasemann[1], Anette Meixner[1], Wolfgang Bach[1]***

## *Affiliations*

*[1]Faculty of Geosciences and MARUM-Center for Marine Environmental Sciences, University of Bremen, Leobener Str. 8, 28359 Bremen, Germany*

*[2]IFREMER, Unité de Géosciences Marines, Plouzané, France*

*[3]School of Biological, Environmental, and Earth Sciences, the University of Southern Mississippi, Walker Science Building, 117601-266-5381, USA*

*[4]Department of Earth and Environmental Sciences, Marcus Family Campus, Ben Gurion University of the Negev, Be´er Sheva 84105, Israel*

*[5]Department of Geoscience, University of Wisconsin, Madison WI 53706, USA*

---

**corresponding author, email address: lucy.schlicht@uni-bremen.de*

## Abstract

A better characterization of subsurface processes in hydrothermal systems is key to a deeper understanding of fluid-rock interaction and ore forming mechanisms. Vent systems in oceanic crust close to subduction zones, like at Brothers volcano and in the Eastern Manus Basin, are

known to be especially ore rich. We measured B concentrations and isotope ratios of unaltered and altered lava that were recovered from drilling sites at Brothers volcano and Snowcap (Eastern Manus Basin) to test their sensitivity for changing alteration conditions with depth. In addition, for Brothers volcano, quartz-water oxygen isotope thermometry was used to constrain variations in alteration temperature with depth. All altered rocks are depleted in B compared to unaltered rocks and point to interaction with a high-temperature (> 150 °C) hydrothermal fluid. The $\delta^{11}B$ values of altered rocks are variable, from slightly lower to significantly higher than those of unaltered rocks. For Brothers volcano, at the Upper Cone we suggest a gradual evolution from a fluid- to a more rock-dominated system with increasing depth. In contrast, the downhole variations of $\delta^{11}B$ at Snowcap as well as $\delta^{11}B$ and $\delta^{18}O$ variations at the NW Caldera (Site U1530) of Brothers volcano are suggested to indicate changes in w/r-ratios, and in the latter case also temperature, with depth due to permeability contrasts between different lithology and alteration type boundaries. Furthermore, $\delta^{11}B$ values from the NW Caldera (Site U1527) might point to a structural impact on the fluid pathway. These differences in the subseafloor fluid flow regime that range from more pervasive and fluid-controlled towards stronger controlled by lithological and structural features have significant influence on alteration conditions and may also impact metal precipitation within the seafloor.

## Introduction

Water-rock (w/r) interactions in seafloor hydrothermal systems cause intense exchange of mass and heat between oceanic crust and seawater and can form seafloor massive sulfide deposits of economically important base and noble metals. Hydrothermal activity in back-arc and arc settings is of particular interest because of the commonly observed formation of high-grade and Au-rich ore bodies (e.g., Yang and Scott, 1996) and the similarity to porphyry-type and epithermal ore deposits on land (e.g., Whitney, 1975; Audétat, 2019). The formation of

high-grade ore deposits requires a large source of metals from which metals are leached and an ore trap in which the mobilized metals are concentrated efficiently. This mobilization and precipitation of metals in hydrothermal systems strongly depends on the fluid flow regime that is influenced by the presence of faults and fractures as well as by interbedding of more and less permeable strata that can act as barriers for uprising metal-rich fluids (e.g., Zierenberg et al., 1998). Isotopic tracers are useful recorders of temperature of water-rock interactions and the intensity of fluid flow in different domains of the basement (e.g., Kesler, 2005).

Boron is a highly fluid-mobile element and can also show a moderately volatile character, depending on the salinity of solutions (Foustoukos and Seyfried, 2007). In unaltered volcanic rocks B is hosted in clinopyroxene and to a minor extent in plagioclase (Raffone et al., 2008), and also is abundant in the glassy matrix or rather in volcanic glasses (e.g., Marschall et al., 2017). The B concentrations of unaltered whole rocks from back-arc and arc crust are usually elevated (up to 37 µg/g B) compared to MOR (mid-ocean ridge) basalts (< 1 µg/g B) due to addition of B derived from the dehydration of subducted altered oceanic crust and sediments (e.g, Hoog and Savov, 2018). In volcanic rocks that were affected by seafloor hydrothermal alteration, clay minerals like smectites, illite and also chlorite are the major B hosting mineral phases and dominate the B concentration of the altered whole rocks. At low alteration temperatures (< 150 °C) B concentrations of altered whole rocks > 100 µg/g commonly occur due to uptake of B by secondary minerals (mainly clay minerals), while high temperature (> 150 °C) altered volcanic rocks usually show B concentrations lower than the unaltered rock due to leaching (e.g., Thompson and Melson, 1970; Spivack and Edmond, 1987; Smith et al., 1995; James et al., 2003; Yamaoka et al., 2015a).

Boron has two stable isotopes, $^{10}B$ and $^{11}B$, whose ratio (expressed as $\delta^{11}B$) in different reservoirs in back-arc and arc hydrothermal environments strongly deviate. While seawater

71 shows high isotopic values ($\delta^{11}B \approx +40$ ‰), unaltered oceanic crust in back-arc and arc
72 settings shows highly variable but generally lower isotopic values than seawater ($\delta^{11}B \approx -9$ to
73 +16 ‰; Hoog and Savov, 2018; Marschall, 2018 and references therein). The $\delta^{11}B$ values of
74 unaltered volcanic rocks in supra-subduction zones are commonly higher than the MOR
75 basalt average ( $-7.1 \pm 0.9$ ‰; Marschall et al., 2017) due to release of B from the subducting
76 slab. Because of the variable isotope ratios of sources, B concentrations and isotope ratios are
77 potentially useful tracers for hydrothermal w/r interaction processes.

78 This study reports B concentrations and isotope ratios of unaltered rocks from the seafloor
79 and of variably altered rocks from subseafloor sections of active seafloor hydrothermal
80 systems in two supra-subduction zone locations in the Western Pacific. One location is
81 situated in the Manus back-arc basin of Papua New Guinea (Ocean Drilling Program (ODP)
82 Leg 193) and the other location is Brothers volcano in the Southern Kermadec arc, New
83 Zealand (International Ocean Discovery Program (IODP) Expedition 376 "Brothers Arc
84 Flux"). Both cruises were executed aboard the *D/V JOIDES Resolution*. At Brothers volcano,
85 we also measured O isotope ratios of hydrothermal quartz crystals to constrain the
86 temperature range of precipitating fluids and measured Sr isotope ratios for one unaltered rock
87 and several altered rock samples. At both locations, previous work on the composition of
88 discharging fluids (Reeves et al., 2011; de Ronde et al., 2011) and secondary mineralogy (de
89 Ronde et al., 2005; Seewald et al., 2019) indicate reactions between basement rocks and
90 seawater-derived fluids, as well as influx of magmatic vapor rich in $H_2O$ and $SO_2$ into the
91 hydrothermal systems. Our goal was to obtain a deeper understanding of B isotopic
92 fractionation and the overall variations in B isotopic composition in seafloor hydrothermal
93 systems and to investigate what downhole variations in $\delta^{11}B$ values in combination with $\delta^{18}O$
94 based temperature estimates can tell us about changes in the fluid flow regime in the sub-
95 seafloor that is an important controlling factor of ore mineral precipitation in hydrothermal
96 systems.

# Geological Setting

*Snowcap, Manus Basin*

The Manus back-arc basin opened along the Manus spreading center and is delimited to the north by the now inactive Manus trench and to the south by the actively subducting New Britain trench (Martinez and Taylor, 1996). ODP Leg 193 drilled several holes in the Pual Ridge, a neovolcanic zone and part of the Southeast Ridges (SER) between the Djaul and Weitin Transforms in the eastern Manus Basin (Fig. 1). Pual Ridge hosts several hydrothermal vent areas, including Snowcap, which is part of the large PACManus hydrothermal area (Binns and Scott, 1993). Snowcap (ODP Leg 193, Site 1188) is in a water depth of 1640 mbsl (meters below sea-level) and features mainly diffusive, low-temperature fluid discharge (6 °C) through a dome-shaped area, interpreted as volcanic dome or cryptodome (Thal et al., 2014). A small cluster of chimneys in the northwestern section of Snowcap dome about 60 m WNW of ODP Site 1188 vents hydrothermal fluids with temperatures between 150 and 180°C (Reeves et al., 2011). Beneath the seafloor, Snowcap consists of dacitic lava flows (Paulick et al., 2004; Thal et al., 2014) that range from unaltered to extensively altered. The discharging fluids at Site 1188 are at 6 °C, and a maximum temperature of 313 °C was measured at 360 mbsf (meters below sea-floor) within borehole 1188F eight days after drilling, which indicates a steep geothermal gradient (Shipboard Scientific Party, 2002). Fluid inclusions in anhydrite indicate high temperatures at depth (270–385°C) but both low and high temperatures in the shallower section, suggesting variable mixing with entrained seawater (Vanko et al., 2004). The presence of abundant native sulfur (Thal et al., 2014) is interpreted as relict of prior venting of acid-sulfate fluids involved in advanced argillic alteration.

120 *Brothers Volcano, Kermadec Arc*

121 Brothers volcano is located in the southern part of the Kermadec arc and represents an active,
122 submarine caldera volcano of 3 to 3.5 km in diameter, approximately 2200 mbsl at the base,
123 1850 mbsl at the caldera floor and from 1320 to 1540 mbsl at the caldera rim (de Ronde et al.,
124 2019a; Fig. 2). Two neovolcanic cones occur in the southeastern part of the caldera. The
125 larger, Upper Cone reaches 1220 mbsl and is partly connected with the smaller, Lower Cone
126 to the Northeast (Fig. 2B).

127 Brothers volcano is the most hydrothermally active volcano along the Kermadec arc and hosts
128 two adjacent hydrothermal system types with contrasting fluid chemistry and rock alteration
129 characteristics (de Ronde et al., 2005; de Ronde et al., 2011; de Ronde et al., 2019d). One
130 type is characterized by discharge of high-temperature (≤ 320 °C) fluids that are moderately
131 acidic and are suggested to originate from heating of infiltrating seawater (e.g., de Ronde et
132 al., 2011). This type occurs at the W, NW, and Upper Caldera sites (Sites U1527 and U1530;
133 Fig. 2). The other type is defined by the venting of lower temperature (≤ 120 °C) fluids that
134 are highly acidic, enriched in $CO_2$ (and other gases) as well as sulfate (de Ronde et al., 2011),
135 and often associated with native sulfur-bearing chimneys. The low pH and abundance of
136 sulfur and sulfate are commonly associated with an influx of magmatic vapors rich in $SO_2$,
137 which disproportionates upon cooling to form native sulfur and sulfuric acid (e.g., Gamo et
138 al., 1997; de Ronde et al., 2011; Seewald et al, 2015). Active venting of these acid-sulfate
139 fluids occurs at the crests of the neovolcanic Upper Cone (Site U1528). However, the
140 alteration minerals in deeper sections at the NW Caldera (Hole U1530A) also indicate the
141 presence of acid-sulfate fluids at an earlier stage of hydrothermal and magmatic activity (de
142 Ronde et al., 2019c; de Ronde et al., 2019d).

## Sample Materials

*Snowcap, Manus Basin*

We investigated one unaltered plagioclase-phyric dacitic rock that was collected at Snowcap by the ROV *MARUM-QUEST* during the *RV SONNE* Expedition SO-216 (Table 1) and nine rock samples that were drilled during ODP Expedition 193 (Site 1188) and show variable extents of alteration and types of secondary mineral assemblages. Two main alteration types can be distinguished based on the secondary mineralogy: one type typically contains chlorite, illite, and magnetite while the other type (argillic alteration) produces rocks of bleached appearance with pyrophyllite as the main secondary phase, which is commonly accompanied by natroalunite. This pyrophyllite-natroalunite assemblage suggests alteration by acidic fluids at moderate temperatures. The low pH is likely related to the condensation of magmatic $SO_2$ in the shallow basement above felsic intrusions and is common in suprasubduction magma-hydrothermal systems (e.g, Gamo et al., 1997; Seewald et al., 2019; Hedenquist and Arribas, 2021). The two main alteration types can be further subdivided to five alteration subtypes, using a classification scheme based on previous work (Shipboard Scientific Party, 2002; Lackschewitz et al., 2004; Paulick et al., 2005; Lackschewitz et al. 2006; Paulick and Bach, 2006). In the following, the alteration types are described in order of their occurrence with depth (in brackets are the respective colors in Figure 3):

(1) unaltered dacite (dark gray): seafloor down to ~33.80 mbsf, the dacitic to rhyodacitic rocks are unaltered to weakly altered lava flows that are aphyric to plagioclase-clinopyroxene phyric and moderately vesicular. The groundmass is glassy to microlitic and locally shows a perlitic texture.

(2) Pyrophyllite (prl)-rich alteration (light pink): is manifested by pervasive bleaching and replacement of primary phases by pyrophyllite, accompanied by varying proportions of illite, chlorite, cristobalite, smectite, anhydrite, gypsum, barite, mixed-layer clays

and pyrite down to 116.86 mbsf, with some gaps where pyrophyllite is absent. A second bleached and pyrophyllite-rich zone appears at deeper levels (236.40 to 255.80 mbsf); it has quartz instead of cristobalite.

(3) Illite (ill)-rich alteration (blue): illite is present in most of the altered rocks and is typical for hydrothermal alteration by seawater-derived fluids (K-rich) at elevated temperatures. Besides illite, only quartz or cristobalite, anhydrite and pyrite were detected.

(4) Chlorite (chl)-rich alteration (green): several zones show significant amounts of chlorite, along with illite, quartz or cristobalite, mixed-layer clays, magnetite, anhydrite and pyrite. Especially below 275 mbsf, chlorite becomes a prominent secondary phase.

(5) Magnetite (mgt)-rich alteration (brown): two depth intervals stand out by the abundance of magnetite (154.98 to 183.87 mbsf and 318.23 mbsf to down to the bottom of the Hole 1188F at 386.7 mbsf), which occurs with illite and/or chlorite, quartz, anhydrite and pyrite as other common secondary phases. Magnetite appears in vesicles, as halos around anhydrite-pyrite veins, and disseminated in the groundmass. In the lower part of the first magnetite-rich section also the clay mineral corrensite was detected.

*Brothers Volcano, Kermadec Arc*

Brothers volcano consists of dacitic to rhyolitic lavas that are commonly plagioclase-clinopyroxene phyric and show a glassy to microlitic groundmass; as well as volcaniclastic rocks comprising mono- or polymict lapillistones and pyroclastic material (Haase et al., 2006; de Ronde et al., 2019a). At Hole U1530A, a sedimentary unit is also present from 30.70 to 59.62 mbsf, comprised of mud-, silt-, and sandstone (de Ronde et al., 2019c). In this study, we investigated four rocks from Brothers volcano that were classified as unaltered, plagioclase-clinopyroxene phyric, dacitic lavas. Two samples were collected by ROV *MARUM-QUEST*

194 during *RV Sonne* Expedition SO-253 (one at the NW Caldera and one at the Upper Cone site)
195 and two were recovered during IODP drilling Expedition 376, one from Hole U1527A at the
196 NW Caldera and one from Hole U1528D at the Upper Cone (Table 2). We also investigated
197 76 altered rock samples from Brothers volcano that were recovered during IODP Expedition
198 376: 24 samples from Site U1527, 28 samples from Site U1528, and 24 samples from Site
199 U1530 (Table 2).

200 The alteration type classification of Brothers volcano used in this study is based on secondary
201 mineralogy from observations of the IODP Expedition 376 shipboard scientists and XRD data
202 of five drill cores (de Ronde et al., 2019d; de Ronde et al., 2019e). Two of the cores studied
203 here are located at the NW Caldera, approximately 400 m horizontal distance from each other;
204 Site U1527 is located on the rim of the NW Caldera in a water depth of 1464 mbsl and
205 reaches a drilled depth of 238 mbsf, whereas Hole U1530A was drilled to 453.1 mbsf on a
206 narrow terrace along the caldera wall at 1595 mbsl (Fig. 2). Five alteration types for the NW
207 Caldera were distinguished in this study (in brackets the dedicated colors in Figure 4 are
208 given):

209 (1) stockwork zone (red): At the very top of Hole U1530A, rocks of a stockwork zone
210 consisting of bluish altered lava fragments replaced by opal-CT, smectite, chlorite and
211 pyrite were cored. The clasts are surrounded by a network of up to cm-thick veins of
212 anhydrite, barite, pyrite, sphalerite and minor chalcopyrite.
213 (2) chlorite (chl)-rich alteration (green): this alteration type underlies the stockwork zone
214 in Hole U1530A and is the only alteration type at Site U1527 underneath the unaltered
215 dacitic cap. The protoliths are lava flows, volcaniclastic, pyroclastic and sedimentary
216 rocks. The main alteration color is green but at Site U1527 some parts are brownish in
217 color. The secondary mineral assemblage comprises chlorite, quartz, illite and pyrite.
218 In Hole U1527C chalcopyrite and the Na-Ca-K-rich zeolite mordenite were detected.

In core from Hole U1530A, plagioclase is pseudomorphed by chlorite, anhydrite, quartz and smectite and vugs are commonly lined by quartz and anhydrite. At deeper levels of Hole U1530A, several intersections of chlorite-rich alteration of massive lava flows (Fig. 4D) alternate with pyrophyllite-rich (4) and pyrophyllite-diaspore-rich (5) alteration types.

(3) Illite (ill)-rich alteration (blue): In Hole U1530A between 65.65 and 185.16 mbsf, an illite-rich assemblage occurs, accompanied by quartz, pyrite and chlorite and mainly hosted in lapillistones and other volcaniclastics.

(4) Pyrophyllite (prl)-rich alteration (light orange): spatially below the illite-rich alteration and starting at 189.16 mbsf, a pyrophyllite alteration together with quartz, illite, pyrite and rutile occurs. The alteration stands out by its bleached appearance that in places affects the whole rock or occurs as halo around veins and fractures.

(5) Pyrophyllite (prl)-diaspore(dsp)-rich alteration (dark orange): starting at 227.50 mbsf and going down-core, the pyrophyllite-rich mineral assemblage already present in the overlying alteration type is accompanied by diaspore, as well as quartz, illite, pyrite, rutile and in the upper part of this alteration type the Al-rich sorosilicate zunyite is present.

Deep in Hole U1527C (220.98 to 226.49 mbsf), there is a zone of plastic deformation in which the rocks have elevated chlorite and illite contents (Fig. 4B).

In addition to the unaltered and altered rock samples, we also investigated hydrothermal quartz separates from the NW Caldera (Hole U1530A) that formed in vugs, veins or matrix.

The third studied drill core is 359-m deep and originates from Hole U1528D at the Upper Cone, situated in a water depth of 1228 mbsl. The uppermost basement of the Upper Cone site comprises unconsolidated dacitic lava fragments (purple cap, Fig. 4A) that contain aggregates of native sulfur. Below around 40 mbsf two alteration types were identified with diffuse

boundaries against each other that are strongly interlinked and mixed with each other (in brackets the dedicated colors in Figure 4 are given):

(1) Pyrophyllite (prl)-natroalunite (natro)-rich altered effusive and volcaniclastic rocks show white to light gray color due to strong bleaching. Pyrophyllite, natroalunite, anhydrite and pyrite are the main secondary phases. Veins and vugs are commonly filled with native sulfur, quartz, anhydrite and pyrite.

(2) Illite-rich alteration of lavas and volcaniclastics, show dark to grayish-blue alteration colors and a secondary mineral assemblage of illite, opal-CT, quartz, anhydrite and pyrite.

The rocks at the Upper Cone site (U1528) commonly have a strongly bleached appearance. In deeper sections of Hole U1528D, however, some of the rocks still have relatively unaltered to weakly altered patches that are closely associated with highly bleached, pyrophyllite-natroalunite-rich zones (de Ronde et al., 2019b).

# Methods

*Preparation of Rock Powders*

Geochemical analyses in this study were performed on rock powders. For the unaltered rock samples collected by ROV at Snowcap (SO-216) and at Brothers volcano (SO-253), as well as for the altered rocks from the drill-cores of Brothers volcano (IODP Exp. 376) rock powders were prepared at the University of Bremen, Germany. The outer surface of rock pieces was removed by a diamond saw and the interior was powdered by an agate-ball-bearing mill.

The rock powders of the two unaltered samples from Brothers volcano drill-cores (IODP Exp. 376) were prepared at the GEOMAR – Helmholtz Centre for Ocean Research Kiel, Germany by an agate mortar and mill.

For the altered material from the drill cores of Snowcap (ODP Leg 193), the shipboard-prepared rock powders from the core depository were used.

*Boron and Strontium Concentrations*

The B concentrations of unaltered and altered rock samples from Snowcap (Manus Basin), as well as B concentrations of the unaltered rocks recovered from Brothers volcano were determined during the course of B isotope ratio measurements using a Thermo Scientific Neptune Plus Multicollector-inductively coupled plasma-mass spectrometer (MC-ICP-MS) at the University of Bremen, following methods described in Hansen et al. (2017). Based on long-term analyses of reference material IAEA-B5 (basalt), boron concentrations are usually determined with an uncertainty of 10% (2RSD). In this study, the average B concentration of four independent sample solutions of IAEA-B-5 was 9.2 ± 1.2 µg/g (2sd), in good agreement with the range of published concentration values (8.9 to 11.3 µg/g B, GeoRem database; query January 2020; http:// georem. mpchmainz.gwdg. de).

The B concentrations of altered rocks from Brothers volcano were measured by ICP-MS at the at the PSO (Pôle Spectrométrie Océan), Brest, France. Before measurements, rock powders (120 mg) were dissolved in a mixture of concentrated HF + $HNO_3$, evaporated to dryness, subsequently dissolved in concentrated $HNO_3$ + HCl and evaporated again at 80 °C. Sample concentrations were calibrated against rock reference materials AN-G (anorthosite), IF-G (iron formation) and WS-E (dolerite) from GIT-IWG; BHVO-2 (basalt), W2 (diabase), and DN-C (dolerite) from USGS; and BR (basalt), GH (granite), UB-N (serpentinite) from CNRS-CRPG (Govindaraju, 1994). The reference material BHVO-2 yielded a B concentration of 3.0 µg/g, in agreement with the range of published concentration values (1–3.12 µg/g B) and the compiled value (2.95 µg/g B) of the GeoRem database; query December 2021; http:// georem. mpchmainz.gwdg. de. The detection limit of this method was 0.64 µg/g B and the blank concentration 0.31 µg/g B. The repeatability of values for the same standard

292 solution (BHVO-2) was always better than 4% (2RSD). The intermediate precision was ≤
293 20% (2RSD).

294 The Sr concentrations of altered rock samples from Brothers volcano were measured by ICP-
295 MS at the at the PSO (Pôle Spectrométrie Océan), Brest, France. The detection limit was 0.05
296 µg/g Sr and the blank concentration was 0.01 µg/g Sr. The repeatability of values for the same
297 standard solution (BHVO-2) was always better than 1% (2RSD).

298 The Sr concentrations of the unaltered rock samples from Brothers volcano were determined
299 by a SPECTRO Xepos Plus X-Ray fluorescence (XRF) analyzer at the GeoZentrum
300 Nordbayern, FAU Erlangen-Nürnberg. Analyses were performed from fused discs created
301 from the sample powders. The typical repeatability precision expressed as RSD was <2% for
302 high concentrations (basaltic references materials BE-N of 1370 µg/g and BR of 1320 µg/g),
303 <4% for intermediate concentrations (granitic reference material GA of 310 µg/g), and <11%
304 for low concentrations (granitic reference material AC-E of 3 µg/g). The Sr reference values
305 were taken from the GEOREM database.

306 *Boron Isotope Ratios*

307 Preparation of sample material and determination of B isotope ratios of three unaltered and 36
308 altered rock samples from Snowcap and Brothers volcano were performed in the Isotope
309 Geochemistry Laboratory at MARUM – Centre for Marine Environmental Sciences,
310 University of Bremen. Procedures for isolation and purification of B were adapted from
311 Romer et al. (2014) and are described in further detail in Hansen et al. (2017). The procedure
312 was based on alkaline fusion of rock powders (44.5 to 454.9 mg) with $K_2CO_3$ as fluxing agent
313 (1:4), followed by a two-step column separation; first with Amberlit IRA 743 and then with
314 AG 50W-X8 (mesh 200-400). An appropriate amount of mannitol was used to keep B stable
315 in solution. Isotope measurements were performed on the MC-ICP-MS using the SIS (stable
316 introduction system consisting of a low flow PFA nebulizer (50 µl) combined with a double-

pass quartz spray chamber) and a high- efficiency x-cone (same as for B concentrations). Purified sample and reference solutions were dissolved in 2% $HNO_3$, closely matched to 50ppb B, and repeatedly analyzed in the standard – sample - standard bracketing mode using unprocessed NIST SRM 951 as standard, supplemented by baseline determination. Boron isotopic compositions are given in the $\delta^{11}B$ (‰) notation: [$\delta^{11}B = \{[(^{11}B/^{10}B)_{sample}/(^{11}B/^{10}B)_{NIST\ SRM\ 951}] - 1\} \times 1000$]. The digestion and chemical separation technique was checked for B loss and contamination. The total B loss was always < 0.2 % of the total amount of B in sample solution and thus without influence on the B isotope composition. The procedural blank was less than 23 ng B with a $\delta^{11}B$ value of on average -1.7 ± 6.6 ‰ ($2sd_{mean}$). Accuracy and repeatability for the separation procedure and measurement was checked through multiple analyses of reference materials. The certified reference material NIST SRM 951 gave a $\delta^{11}B$ value of -0.1 ± 0.1 ‰ (2sd, n=4). The basaltic reference material IAEA-B-5 gave a $\delta^{11}B$ value of -4.3 ± 0.1 ‰ (2sd, n=3), in good agreement with the compiled value of -4.1 ± 2.7 ‰ from Gonfiantini et al. (2003), and also agreed with measured values of -4.3 ± 0.2 ‰ (2sd, n=3, Hansen et al., 2017) and -4.2 ± 0.2 ‰ (2sd, n=4, Wilckens et al., 2018). The granitic reference material ZGI-GM yielded a $\delta^{11}B$ value of -0.1 ± 0.2 ‰ (2sd, n=3). The uncertainty of the B isotopic composition of rock samples is given as 2sd based on multiple mass-spectrometer analyses.

*Strontium Isotope Ratios*

The Sr isotope measurements of one unaltered and 18 altered rock samples from Brothers volcano were performed at the Isotope Geochemistry Laboratory at the MARUM. The rock powders were dissolved in several successive steps. It was ensured that the samples were completely in solution; if necessary, the last two steps had to be repeated. First, the powder was dissolved in a 5:1 mixture of concentrated HF and $HNO_3$ at 140 °C for three days and dried at 80 °C. Then the sample was re-dissolved in a 2:1 mixture of concentrated HCl and $HNO_3$ for two days at 140 °C, dried at 80 °C, dissolved in 300 µl HNO3 and 150 µl $H_2O_2$,

dried at 65 °C and finally dissolved in 3 ml 2.5 M $HNO_3$ overnight at 140 °C and dried. The baryte-rich sample from the stockwork zone (376-U1530A-4R-1W, 67-69 cm) left an insoluble residue that had to be removed by centrifugation before purification. Separation and purification of Sr were conducted by column separation prepared with 70 µl Sr.spec$^{TM}$ resin, following the procedure described by Deniel and Pin (2001). Firstly, the sample material dissolved in 1 ml 2 M $HNO_3$ were loaded on the columns (in 100 µl steps). Secondly, 1.2 ml of 2 M $HNO_3$, 1 ml 7 M $HNO_3$ and 0.3 ml 2 M $HNO_3$ were added (in 100 µl, 500 µl and 100 µl steps) to remove unwanted elements. Subsequently, Sr was collected by adding 1 ml of 0.05 $HNO_3$ (in 100 µl steps), charged with 30 µl 0.1 M $H_3PO_4$ and the solution was dried at 90 °C on a hotplate. Removal of organic material was ensured by adding 40 µl of concentrated $HNO_3$, drying at 90 °C, adding of 40 µl of $H_2O_2$ and drying again.

The determination of Sr isotopes was performed by a Thermo Scientific TRITON Plus thermal ionization mass spectrometer (TIMS) in the Isotope Geochemistry Laboratory at the MARUM. The instrumental fractionation was corrected to the natural $^{87}Sr/^{86}Sr$ ratio of 0.1194. The procedural blank (< 50 pg Sr) is insignificant compared with the Sr concentration in the sample solutions (≥ 200 ng Sr). The reference material NIST SRM 987 gave a composition of 0.710247 ± 0.000004 ($2sd_{mean}$, n = 1). The analytical accuracy and long-term precision for $^{87}Sr/^{86}Sr$ of reference material NIST SRM 987 was 0.710246 ± 0.000011 ($2sd_{mean}$, n = 24; period: May 2015 to May 2017). This is within the range of published values analyzed by TIMS of 0.710250 ± 0.000034 (2SD, n = 1245, disregarding data < 0.7102 and > 0.7103) calculated from GeoRem database (query September 2017; http:// georem.mpch-mainz. gwdg. de).

In addition, Sr isotopic compositions of 16 altered rock samples from Brothers volcano drill-cores were measured by a Thermo Scientific Neptune MC-ICP-MS at the PSO, Brest, France. Prior to measurements, Sr was purified by a one stage chromatography procedure using

Sr.spec$^{TM}$ resin. The standard reference material NIST SRM 987 measured over three analytical sessions yielded $^{87}Sr/^{86}Sr$ = 0.710251 ± 0.000028 (n=10), 0.710257 ± 0.000018 (n=25), 0.710255 ± 0.000020 (n=50). The in-house seawater standard (IAPSO Standard Seawater) gave $^{87}Sr/^{86}Sr$ = 0.709133 ± 0.000034 (n=5) identical, within uncertainty, to the average of worldwide oligotrophic oceanic water (e.g., El Meknassi et al., 2020). The comparability of Sr isotope data from the two different methods and facilities was checked using rock sample 376-U1530A-39R-2W,78-80. The $^{87}Sr/^{86}Sr$ compositions from the University of Bremen (0.705990 ± 0.000006) and the PSO (0.706007 ± 0.000014) agree within analytical uncertainties.

*Oxygen Isotope Analysis of Quartz*

From drill-core of Hole U1530A at the NW Caldera of Brothers volcano, 13 quartz separates were handpicked under the binocular microscope, including vein (7) and vug fillings (4) and coarse quartz crystals replacing rock matrices (2). Selected quartz grains from each separate were mounted in epoxy, polished, coated with a thin carbon layer and imaged by cathodoluminescence (CL) to study their inner textures and crystal zoning. The CL imaging was performed using a Gatan CL detector installed on a JEOL Superprobe JXA-8230 at the Hebrew University of Jerusalem.

Oxygen isotope ratios were measured along traverses in single quartz crystals (previously imaged by CL, Appendix Table A1) using the CAMECA IMS-1280 secondary ion mass spectrometer (SIMS) at Wisc-SIMS (Wisconsin Secondary Ion Mass Spectrometer), Department of Geoscience, University of Wisconsin-Madison. Detailed descriptions of the O isotope analytical methods are given elsewhere (Kelly et al., 2007; Kita et al., 2009; Valley & Kita, 2009; Heck et al., 2011; Wang et al., 2014) and the most important points are summarized here. Oxygen isotope analyses were performed by using a primary beam of 2 nA $^{133}Cs^{+}$ ions focused to a spot diameter of approximately 10 μm (1 to 2 μm pit depth). One spot

393 analysis lasted four minutes, including pre-sputtering through the carbon layer, stabilizing of
394 the secondary beam, and centering as well as integrating of the secondary ions. The ions of
395 $^{16}O^-$ and $^{18}O^-$ were simultaneously collected in two movable Faraday cup detectors,
396 accompanied by collection of $^{16}OH^-$ ions in the axial Faraday cup to identify potential water
397 traces in the quartz. The average $^{16}O^-$ intensity was $3 \times 10^9$ counts per second (cps). A
398 nuclear magnetic resonance (NMR) probe stabilized the magnetic field strength, which was
399 readjusted every 12 hours. Analyses were performed in the standard-sample-standard
400 bracketing mode (four analyses of UWQ-1 quartz followed by up to 20 sample analyses and
401 another four analyses of UWQ-1) to evaluate the reproducibility of measurements and to
402 ensure that measurements were not affected by instrumental drift. Raw $^{18}O/^{16}O$ sample ratios
403 were corrected for the VSMOW oxygen scale based on UWQ-1 standard measurements ($\delta^{18}O$
404 $_{UWQ\text{-}1}$ = 12.33 ± 0.14 ‰, Kelly et al., 2007). Oxygen isotope ratios are given in the
405 conventional notation: $[\delta^{18}O_{VSMOW}$ (‰) = $\{[(^{18}O/^{16}O)_{sample}/ (^{18}O/^{16}O)_{VSMOW}] -1\}\times1000]$. The
406 intermediate precision of the $\delta^{18}O$ bracketing standard measurements was on average ±0.2 ‰
407 (2sd, n=27).

408 # Results

409 *Unaltered Rocks*

410 The unaltered dacite sample from Snowcap has a B concentration of 21.7 µg/g and a $\delta^{11}B$
411 value of +6.8 ± 0.1 ‰, close to the values measured for the two unaltered dacites from
412 Brothers volcano (18.7 and 19.6 µg/g B and $\delta^{11}B$ values of +4.8 ± 0.1 and +5.8 ± 0.1 ‰). The
413 unaltered rocks from Brothers volcano have a Sr isotope ratio of 0.703970 ± 0.000004 at the
414 Lower Cone and 0.704109 ± 0.000006 at the NW Caldera site and Sr contents of 202 µg/g
415 and 232 µg/g, respectively.

*Altered Rocks*

The B concentrations and $\delta^{11}B$ values of altered rocks from Snowcap (Fig. 3) range from 1.2 to 7.8 µg/g and +5.0 ± 0.1 to +23.2 ± 0.1 ‰, respectively (Table 1, Fig. 5A). The two advanced argillic altered rocks that were sampled from Snowcap have slightly higher B concentrations (4.8 and 7.8 µg/g) compared to the other altered rocks that were recovered from Snowcap (up to 3.9 µg/g). The highest $\delta^{11}B$ value at Snowcap of +23.2 ± 0.1 ‰ is reached at 174.36 mbsf for an altered rock with a magnetite-illite-(corrensite)-rich alteration mineral assemblage.

Altered rocks from the three drill sites at Brothers volcano (Fig. 4) range from 0.8 to 5.2 µg/g B (with one exceptional value of 15.6 µg/g) and from +1.2 ± 0.1 to +16.7 ± 0.1 ‰ in $\delta^{11}B$ (Table 2, Fig. 5A, B). Three altered rocks from the upper part of Hole U1527C have $\delta^{11}B$ values lower than unaltered rock, whereas two rocks from a deformed zone that appears between 220.98 and 226.49 mbsf have higher than unaltered rock $\delta^{11}B$ values (Fig. 4B). At Site U1528, altered rock samples shallower than ca. 75 m have increased $\delta^{11}B$ values compared to unaltered rock, while altered rock samples deeper than 75 m have lower than unaltered rock $\delta^{11}B$ values (Fig. 4C). At Hole U1530A $\delta^{11}B$, values of altered rocks are usually higher than fresh values, beside one sample at 127.11 mbsf with a lower value of +1.2 ± 0.1 ‰. The $\delta^{11}B$ values at Hole U1530A alternate between higher and lower values with depth (Fig. 4D).

Altered rocks at Brothers volcano have Sr concentrations between 15 µg/g and 766 µg/g. The $^{87}Sr/^{86}Sr$ values lie between 0.704190 ± 0.000005 and 0.706982 ± 0.000013 (Fig. 5B, D).

*Oxygen Isotope Ratios and $\Delta^{18}O_{Qtz\text{-}H2O}$ Thermometry*

The CL images in Figure 6 show representative microtextural features of individual quartz crystals that were separated from altered rocks of Hole U1530A at the NW Caldera of Brothers volcano. A hydrothermal origin of the investigated quartz crystals was suggested

441 because the crystals were either hand-picked from vein or vug fillings and thus were certainly
442 precipitated from solutions, or the crystals were separated from the matrix and were texturally
443 closely associated with the secondary mineral assemblage. The vug-filling quartz crystals
444 from the top part of Hole U1530A show μm-scale alternating CL-brighter and CL-darker
445 growth bands, representing progressive stages of hydrothermal precipitation or continuous
446 growth with varying fluid composition (Fig. 6B). The CL images of quartz crystals from
447 intermediate depth in Hole U1530A show healed fractures with CL-brighter or CL-darker
448 quartz compared to the surrounding quartz crystal (Fig.6), also indicative of a later stage
449 crystal growth under shifted hydrothermal precipitation conditions. The variations in the CL-
450 imaging spectrum of quartz can be explained by different intrinsic and extrinsic defects, like
451 lattice defects, poor crystallographic ordering, or incorporation of trace elements to a certain
452 extent (Götze et al., 2001). Several CL images of euhedral shaped quartz crystals separated
453 from vein or vug infills reveal concentric zoning, indicative of free growth towards open
454 spaces within the host rocks (Fig. 6).

455 The $\delta^{18}O$ values from traverses across 13 quartz grains from Hole U1530A are given in Table
456 3. Eight of the traverses, representative of six depth intervals in Hole U1530A, are shown
457 with corresponding CL images in Fig. 6. The total range in measured $\delta^{18}O$ values is +5.6 ±
458 0.1 ‰ to +9.9 ± 0.2 ‰. One quartz crystal with concentric zoning from the deeper part of
459 Hole U1530A (Fig. 6E, rightmost) shows the highest variability in $\delta^{18}O$ values of an
460 individual crystal from +6.7 ± 0.2 ‰ (crystal rim) to +9.5 ± 0.2 ‰ (crystal core).

461 Quartz precipitation temperatures were calculated using qtz-water oxygen isotope
462 thermometry, as calibrated by Sharp and Kirschner (1994): $1000 \ln \alpha_{(qtz\text{-}water)} = -2.9 + (3.65 \times 10^6/T^2)$. The calculations are based on the assumption that the measured $\delta^{18}O$ values of the
463
464 quartz crystals represent the equilibrium values with the interacting hydrothermal fluid during
465 precipitation of the quartz. The exact $\delta^{18}O$ of the interacting fluid is unknown but it is

466 assumed to be near seawater, and we calculated a temperature range for the minimum
467 ($\delta^{18}O_{water}$ = 0 ‰) and maximum ($\delta^{18}O_{water}$ = +1 ‰) values measured in fluids venting at the
468 NW Caldera (de Ronde et al., 2011). The calculated temperatures show±3 to ±8 °C (2sd) that
469 derived from $\delta^{18}O$ measurements. However, also regarding the range in $\delta^{18}O$ value of the
470 fluids from 0 to +1 ‰ an average absolute temperature difference of 31 ± 10 °C (2sd) for an
471 individual temperature has to be considered.

472 The total range of quartz precipitation temperatures is 262 to 425 °C (for $\delta^{18}O_{water}$ between 0
473 and +1 ‰). Two quartz grains from the stockwork zone at shallow levels (22.07 to 22.09
474 mbsf) of Hole U1530A yielded comparably low precipitation temperatures (of 278 to 315 °C).
475 Two quartz grains from a lava flow altered to a chlorite-rich secondary mineral assemblage
476 (61.08 to 61.11 mbsf) gave highly variable temperatures (269 to 425 °C), but mostly above
477 350 °C. Likewise, a primarily chlorite-altered lava flow in greater depth of Hole U1530A
478 (290.86 to 290.88 mbsf) gave high formation temperatures in the range of 334 to 400 °C,
479 except for one measurement very close to a crack within the grain (289 to 315 °C). Quartz
480 separates from host rocks dominated by pyrophyllite and diaspore-rich secondary mineral
481 assemblages from above and below the chlorite-rich altered lava flow show considerable
482 variation in $\delta^{18}O$ values, but a tendency towards lower precipitation temperatures (262 to 353
483 °C). Quartz separates from the deepest interval (309.83 to 309.85 mbsf) display zoning in the
484 CL images for two of the three quartz crystals (Fig. 6E) and high $\delta^{18}O$ values at the core
485 (formation temperatures as low as 262 °C), enveloped by low $\delta^{18}O$ values at the rim
486 (formation temperatures as high as 380 °C). In the third crystal low $\delta^{18}O$ values were
487 measured only at the outermost edges and these therefore may represent secondary effects.

# Discussion

*Signatures of Unaltered Rocks*

*Brothers volcano*. The B contents (18.7 and 19.6 µg/g) and $\delta^{11}B$ values (+4.8 ± 0.1 and +5.8 ± 0.1 ‰) of the two unaltered dacites from Brothers volcano lie between the published values of two seamounts to the south of Brothers volcano (Rumble III: B of 10.4 µg/g, $\delta^{11}B$ of 11.5 ± 0.4 ‰, and Rumble IV: B of 15.7 µg/g, $\delta^{11}B$ of 11.5 ± 0.4 ‰, Leeman et al., 2017) and the volcanic edifices of the Northern Kermadec arc (B > 20 µg/g and $\delta^{11}B$ of up to 7.0 ± 0.5 ‰, Leeman et al., 2017). This is in agreement with the overall increase in B concentrations and $\delta^{11}B$ values along the Tonga-Kermadec volcanic arc from New Zealand northwards that was described by Leeman et al., 2017 and was attributed by them to a steeper thermal gradient or a greater sedimentary influence in the magma source to the south.

*Snowcap, PACMANUS.* The Manus back-arc basin exhibits a complicated tectonic constellation, with the inactive Manus trench to the north and the actively subducting New Britain trench to the south (Martinez and Taylor, 1996, Fig. 1). The Southeast Rifts (SER), of which Pual Ridge with the Snowcap hydrothermal area is a part, were suggested to represent back-arc crust in an early rifting stage that shows geochemical indications of present influx from slab subduction to the south (Park et al., 2010; Beier et al., 2015). Typical evidence for slab influx is an increased abundance of fluid mobile elements, like B, in rocks from arcs and back arc basins (up to 37 µg/g B) compared to MORB (< 1 µg/g B, Hoog and Savov, 2018), and variable but tends to be higher $\delta^{11}B$ values ($\delta^{11}B \approx$ -9 to +16 ‰; Hoog and Savov, 2018; Marschall, 2018 and references therein) compared to MOR basalt average (-7.1 ± 0.9 ‰; Marschall et al., 2017). In line with these predictions, the unaltered dacitic sample from Snowcap has arelatively high B content of 21.7 µg/g and a $\delta^{11}B$ value of +6.8 ± 0.1 ‰, similar to other volcanic edifices of the SER that showed B concentrations of 11.8 to 23.7

µg/g and $\delta^{11}B$ values in a range of +6.5 to +8.3 ‰ (Wilckens et al., 2018). This indicates that the dacitic rocks at Snowcap experienced significant contribution from the subducting slab.

*Signatures of Altered Oceanic Crust*

*Boron Concentrations and Isotope Ratios*. During hydrothermal alteration of mafic and felsic rocks, B tends to partition into the fluid phase at higher temperatures (> 150 °C) and into the solid phase at lower temperatures (<150 °C, e.g., Ishikawa and Nakamura, 1992). The B isotopic fractionation during fluid-rock interaction is controlled by variations in temperature, mineralogy and w/r-ratios (Spivack and Edmond, 1987). The potential pH effect on B isotopic fractionation is negligible in hydrothermal systems that are hosted in basaltic or more felsic crust because the interacting fluids have pH values < 5 at which the $B(OH)_3$ species dominates (e.g., Kakihana et al., 1977, Spivack and Edmond, 1987, Palmer et al., 1987). Altered rocks usually show an increase in $\delta^{11}B$ values by progressive alteration compared to unaltered oceanic crust (≤ +16 ‰, also regarding unaltered crust in arc and back-arc basin settings) due to interaction with seawater-derived fluids ($\delta^{11}B$ values of initially +40 ‰).

Altered rocks from Brothers volcano and Snowcap are B-depleted relative to unaltered rocks and usually have ≤ 5 µg/g, corresponding to a B loss of ≥ 75 % (Fig. 5A) pointing to extensive alteration at elevated temperatures.

At Snowcap and Brothers volcano the alteration mineral assemblages (Paulick and Bach, 2006; de Ronde et al., 2011), fluid inclusion data (Vanko et al., 2004; de Ronde et al., 2005; Diehl et al., 2020; Lee et al., 2022), as well as temperature, acidity and gas concentrations of vent fluids (de Ronde et al., 2011; Kleint et al., 2019; Reeves et al., 2011) suggest the existence of two distinct types of hydrothermal activity. One of these types is thought to be dominated by heated seawater-rock interaction. The chlorite-, illite- and magnetite-(corrensite)-rich alteration types at Snowcap and Brothers volcano as well as the mixed alteration types that occur at Snowcap and the stockwork alteration at Brothers volcano are

thought to be part of this seawater hydrothermal type. This is because the appearance of chlorite points to hydrothermal alteration by entrained seawater (Mg-rich) at elevated temperatures (e.g., Bach et al., 2013). The other type of hydrothermal interaction is advanced argillic alteration, in which the pyrophyllite-alunite and pyrophyllite-diaspore-rich assemblages and the presence of native sulfur are attributed to the influx of a magmatic vapor rich in $SO_2$ (e.g., de Ronde et al., 2011; Seewald et al., 2019). Wilckens et al. (2018) presented B and $\delta^{11}B$ vent fluid data from Western Pacific back-arc basins that implicate a lowering in $\delta^{11}B$ fluid compositions due to the influence of magmatic fluids compared to solely seawater derived hydrothermal fluids. This shift in $\delta^{11}B$ values of the fluids might also be reflected by differences in the $\delta^{11}B$ composition of altered rocks that are either affected by seawater- or by magmatic-derived fluids. However, the B and $\delta^{11}B$ data of altered rocks from Snowcap and Brothers volcano that were investigated in this study show no systematic difference in B or $\delta^{11}B$ between the advanced argillic alteration and seawater-dominated alteration types (Fig. 5A). The missing evidence for a magmatic fluid imprint on the B and $\delta^{11}B$ values of altered rocks, can be explained by three possibilities: (1) the magmatic fluid and the seawater-derived fluid have similar $\delta^{11}B$ values, (2) overprint of the magmatic fluid signal of the altered rocks due to extensive dilution by high seawater fluxes, (3) overprint by low-temperature (< 150 °C) alteration. A seawater-like $\delta^{11}B$ value of the magmatic fluid is implausible, since lowering in $\delta^{11}B$ of fluids affected by magma degassing versus solely seawater affected fluids was previously observed (Wilckens et al., 2018) and the advanced argillic altered rocks show no noticeable lowering in $\delta^{11}B$ compared to the other altered rocks (Fig. 5A). More likely is a combination of strong dilution of the magmatic fluid by high fluxes of seawater-derived hydrothermal fluids, locally accompanied by a low-temperature alteration overprint. Low-temperature overprint is evident by the occurrence of smectite through-out all three investigated drill cores of Brothers volcano (de Ronde et al., 2019e) and by the abundance of corrensite at intermediate depth at Snowcap (Fig. 3). Nonetheless, a

563 greater extent of low-temperature overprint is unlikely due to the low B concentrations of the
564 altered rocks. One altered rock from the top-part section of Hole U1527C at the NW Caldera
565 of Brothers volcano has comparatively high B concentrations (15.6 µg/g) but the $\delta^{11}B$ value
566 points to higher retention of the unaltered signal and do not support a larger impact by a
567 seawater-derived fluid of high $\delta^{11}B$ composition (Fig. 4B).

568 The previous paragraph emphasized that secondary mineralogy and differing fluid sources
569 seem to have a minor effect on B and $\delta^{11}B$ systematics of altered rocks at Brothers volcano
570 and Snowcap. Instead, the B content and $\delta^{11}B$ composition of altered rocks are potentially
571 more strongly affected by alteration temperatures and w/r-ratios. The low B concentrations of
572 altered compared to unaltered rocks and high $\delta^{11}B$ values of altered rocks, up to +23.2 ± 0.1
573 ‰ at Snowcap and +16.7 ± 0.1 ‰ at Brothers volcano, point to extensive high-temperature
574 fluid-rock interaction with a seawater-derived fluid (Fig. 5A). The Sr isotope ratio of
575 hydrothermally altered rocks is a well-established proxy for w/r-ratios (McCulloch et al.,
576 1980; Marks et al., 2015). The $\delta^{11}B$ values show a weak positive ($R^2 = 0.3$) but nonetheless
577 significant ($F_{krit} << F$, $p < 0.05$) correlation with Sr isotope ratios of altered rocks from
578 Brothers volcano (Fig. 5B), suggesting that B isotopes are also influenced by w/r-ratios but
579 there are also other impact factors. A significant difference is that $^{11}B/^{10}B$ fractionate in
580 dependance on temperature and potentially also the secondary minerals during fluid-rock
581 interaction (Spivack and Edmond, 1987), while $^{87}Sr/^{86}Sr$ show no isotopic fractionation.
582 Further, B is strongly depleted in the altered rocks which indicates more efficient leaching of
583 B relative to Sr (Table 2). To test the impact of various w/r-ratios on the B and $\delta^{11}B$ values of
584 altered rocks for different temperatures, we modified a model calculation suggested by
585 Yamaoka et al. (2015a) to estimate the change in altered rock composition with increasing
586 reaction progress (Fig. 7). The calculation is based on reaction of multiple batches of fluids in
587 equilibrium with a progressively altered rock portion. The changing B concentration of the
588 altered rock ($C_R$) can be calculated by using the following mass balance:

589 $$C_R + (W/R)C_F = C_R^i + (W/R)C_F^i \quad (2)$$

590 where $C_R^i$ is the B concentration of the unaltered rock (20.0 µg/g, average B concentration of
591 unaltered rocks from Brothers volcano and Snowcap), $C_F^i$ is the B concentration of seawater
592 (4.5 µg/g), and *W/R* is the water/rock-ratio. Further, the distribution coefficient between rock
593 ($C_R$) and fluid B concentrations ($C_F$) of $D_B$ that is defined as $D_B=C_R/C_F$ is needed for the
594 calculation. The $D_B$ value is temperature-dependent due to the preferred B partitioning into
595 the fluid phase at elevated temperatures (e.g., Ishikawa and Nakamura, 1992). It is also
596 influenced by the nature of the secondary mineral assemblage. Yamaoka et al. (2012)
597 estimated a $D_B$ of 0.1 (and also tested 0.3) at 350 °C for their model calculations in a basalt-
598 hosted system. For later model calculations of a basalt-hosted (Yamaoka et al., 2015a) and a
599 back-arc-hosted system of more felsic rock compositions (Yamaoka et al., 2015b), a $D_B$ value
600 of 0.1 at 300 °C was assumed. In this study, $D_B$ values of 0.1 for 300 °C, 0.3 for 250 °C, 0.6
601 for 200 °C, and 1 for 150 °C were used to emphasize the enhanced partitioning of B towards
602 the fluid with increasing temperatures. The main B hosting phases in basalt-fluid as well as
603 dacite-fluid hydrothermal systems are newly formed clay minerals (e.g. chlorite, illite,
604 smectite) and therefore the approach to use similar $D_B$ values for basaltic as well as more
605 felsic hosted hydrothermal systems might be acceptable.

606 The changing B isotope ratio of the altered rock ($^{11/10}B_R$) is based on a mass balance assuming
607 a B isotopic fractionation factor, α, between the B isotope ratio of the rock and fluid ($^{11/10}B_F$)
608 that is defined as $\alpha=^{11/10}B_R/^{11/10}B_F$:

609 $$[C_R\,{}^{11/10}B_R + \left(\frac{W}{R}\right) C_F\,{}^{11/10}B_F]/[C_R + (W/R)C_F]$$

610 $$= \left[C_R^i\,{}^{\frac{11}{10}}B_R^i + \left(\frac{W}{R}\right) C_F^i\,{}^{\frac{11}{10}}B_F^i\right]/[C_F^i + \left(\frac{W}{R}\right) C_F^i] \quad (3)$$

where $^{11/10}B_R^i$ is the B isotope ratio of the unaltered rock (+5.8 ‰, deduced from the average $\delta^{11}B$ value of unaltered rocks from Brothers volcano and Snowcap), and $^{11/10}B_F^i$ is the B isotope ratio of seawater (+39.6 ‰, Foster et al., 2010). The α values for different temperature conditions (0.985 for 300°C, 0.983 for 250 °C, 0.981 for 200 °C, and 0.979 for 150 °C) were calculated based on the empirical calibration of mica-fluid B isotope fractionation by Wunder et al. (2005). This procedure is appropriate to address the $^{11/10}B$ partitioning between minerals and fluids, which is affected by the coordination of B in the interacting phases (e.g. Kakihana et al., 1977). Micas and the likely B hosting mineral phases in the altered dacites (illite, pyrophyllite, chlorite or smectites) have in common that B is tetrahedrally coordinated (e.g. Williams et al., 2001, Hervig et al., 2002).

The results of the model calculations show the potential influence of changes in the w/r-ratios and temperature on the B and $\delta^{11}B$ composition of the altered rocks (Fig. 7). In accordance to the model (Fig. 7), a fast onset of significant B loss from the rocks with increasing reaction progress can be expected that is even greater at elevated temperatures. In early stages of fluid-rock interaction when a significant portion of primary B is still retained, the $\delta^{11}B$ composition of the altered rocks is expected to decrease relative to the unaltered rocks due to the preference of $^{11}B$ for the trigonal B species that is dominant in acidic fluids that leads to a passive enrichment of $^{10}B$ in tetrahedrally coordinated silicates (Kakihana et al., 1977; Palmer et al., 1987; Spivack and Edmond, 1987). In later stages when the proportion of fluid- relative to rock-derived B becomes greater, a distinct increase in $\delta^{11}B$ values of the altered rocks with progressing fluid-rock interaction can be expected due to the high $\delta^{11}B$ values of seawater-derived fluids (Fig. 7).

For Snowcap, the model results and measured $\delta^{11}B$ values of the altered rocks indicate that the illite-magnetite-(corrensite)-altered rocks around 170 to 190 mbsf experienced very high w/r-ratios. In contrast, the $\delta^{11}B$ values of the two advanced argillic altered samples at the top-

636 part of Hole 1188A suggest moderate w/r-ratios and comparatively low alteration
637 temperatures (Fig. 3, Fig. 7). For the NW Caldera site of Brothers volcano, the $\delta^{11}B$ values of
638 altered rocks that are lower than unaltered rock $\delta^{11}B$ values of the upper part in Hole U1527C
639 point to relatively low w/r-ratios according to the model calculation results (Fig. 4B, Fig. 7).
640 The deformed zone that appears in deeper sections of Hole U1527C has higher $\delta^{11}B$ values
641 than the top section and suggests increased w/r-ratios. The more variable $\delta^{11}B$ values of
642 altered rock samples that were recovered from Hole U1530A from the NW Caldera indicate
643 higher variability of w/r-ratios based on the model (Fig. 4D). Noticeable is the decrease in
644 $\delta^{11}B$ values starting from the chlorite-rich lava flow at the top of Hole U1530A downwards to
645 the underlying illite-rich and highly altered volcaniclastics, pointing to a possible decrease in
646 w/r-ratios in this section. At the Upper Cone (Site U1528), in the part above ~75 m the $\delta^{11}B$
647 values are significantly increased relative to unaltered compositions and point to moderate to
648 high w/r-ratios, while < 75 m the lower than unaltered $\delta^{11}B$ values point to lower w/r-ratios
649 based on the model calculations.

650 The temperatures assumed in the model calculations are in accordance with estimated
651 alteration temperatures of the seawater dominated alteration (≤ 250 °C) and the advanced
652 argillic alteration potentially influenced by magma degassing (230-350 °C), constrained based
653 on secondary minerals at Brothers volcano (de Ronde et al., 2019d) and oxygen isotopes of
654 clay minerals at Snowcap (Lackschewitz et al., 2004). Indeed, the differences in resulting B
655 and $\delta^{11}B$ composition of altered rocks at differing temperatures (Fig. 7) are rather moderate
656 and insufficiently resolvable, especially due to the strong dependency on the determined $D_B$
657 value that still has to be defined for dacite-fluid interaction.

658 In general, limitations of w/r-ratio constraints based on the model calculations are: (1)
659 inappropriate assumptions of alteration temperature could lead to an underestimation of w/r-
660 ratios, (2) modification of the interacting fluid composition towards lower $\delta^{11}B$ than seawater

661 values are not regarded by the model but would also cause underestimation of w/r-ratios, and
662 (3) potential variations of the $D_B$ and α values for different alteration mineral assemblages that
663 would affect $\delta^{11}B$ compositions of altered rocks were not considered. Estimated w/r-ratios
664 based on $\delta^{11}B$ compositions must be regarded as minimal values because the model tends to
665 underestimate the effective w/r-ratios as described above. Nevertheless, the w/r-ratio
666 sensitivity interlinked with a temperature dependency of B distribution and isotopic
667 fractionation makes it a useful complement to other tracers for w/r-ratio variations, like Sr
668 isotope ratios.

669 *Oxygen Isotope Ratios and Temperature Constraints*. The $\delta^{18}O$ values of quartz crystals from
670 Hole U1530A at the NW Caldera site of Brothers volcano constrain variations of precipitation
671 temperatures with depth and over time. The stockwork zone in Hole U1530A (NW Caldera
672 site, seafloor to 31.28 mbsf), displays uniformly lower alteration temperatures (278 to 315 °C,
673 Fig. 6) than the underlying basement, likely due to infiltration of cold seawater through cracks
674 and joints close to the seafloor. Fluctuations in the relative intensity of low-T seawater ingress
675 versus pulses of hydrothermal activity with high-T fluid upflow possibly led to the wider
676 range of alteration temperatures (269 to 425 °C) in the chlorite-altered lava flow underlying
677 the stockwork zone. A deeper chloritized lava flow of Hole U1530A shows relatively high
678 and less-variable alteration temperatures (334 to 400 °C) compared to those in the
679 volcaniclastic zones above and below it (262 to 353 °C). These temperature differences may
680 reflect a permeability contrast between the more coherent lava flows and the surrounding
681 volcaniclastic units (Fig. 8). Indeed, the core-to-rim $\delta^{18}O$ zoning in quartz grains from deeper
682 levels of Hole U1530A (Fig. 6) indicates a shift from lower (minimum 262 °C) to higher
683 (maximum 380 °C) temperatures with time. The increase in temperature can be explained by
684 a sealing effect of secondary minerals that led to a decrease in seawater ingress (e.g., Dobson
685 et al., 2003; Heap et al., 2017), which is also indicated by the very few open fractures

observed in the core of Hole U1530A (de Ronde et al., 2019c) or by an increase in higher-T fluid pulses in later stages of alteration.

*Implications for Subsurface Processes in Hydrothermal Systems*

In this section, we combine B and O isotope data to set constraints on w/r-ratios and temperatures with depth and assess potential reasons for variations. Shifts in the w/r-ratios and temperatures are often linked to changes of the fluid flow in the sub-seafloor that in turn is sensitively coupled to mobilization and precipitation processes, potentially also critical for ore formation.

For Snowcap (Site 1188), the comparatively high B concentrations of two altered samples that were taken from the topmost part of the site closely below the dacitic cap indicate relatively low alteration temperatures and moderate w/r-ratios based on the model calculations (Fig. 7). In contrast, for the deeper-seated illite-magnetite-(corrensite)-rich alteration type at Snowcap the model calculation gives very high w/r-ratios (Fig. 7) and $\delta^{18}O$ measurements of clay minerals from this section (Lackschewitz et al., 2004) point to lower alteration temperatures than above and below. An increase in w/r-ratios accompanied by a decrease in alteration temperature might point to a preferred ingress of cold seawater to this domain, potentially due to higher permeability than in the overlying rocks. Indeed, reconstructions of volcanic facies at Snowcap (Paulick and Herzig, 2003; Paulick et al., 2004; Paulick and Bach, 2006) showed that the basement exhibits distinct boundaries between more coherent volcanic lavas and primary as well as re-sedimented hyaloclastites, which likely have distinctly different permeabilities. Thus, the high $\delta^{11}B$ values of the magnetite- and corrensite-rich layer may best be explained by alteration with high w/r-ratios caused by the proximity to the permeability barrier imposed by imposed by more coherent overlying lava flows.

Similar to Snowcap, altered rocks that were recovered from Hole U1530A at the NW Caldera of Brothers volcano show a high variability in $\delta^{11}B$ values with depth (Fig. 4D) that might be

711 the result of changing w/r-ratios due to permeability contrasts between the different
712 lithological units (Fig. 7, Fig. 8). This assumption is supported by $\delta^{18}O_{Qtz}$-derived
713 temperatures that indicate higher alteration temperatures within a lava flow around 291 mbsf
714 (Fig. 6D) compared to the over- and underlying volcaniclastic rocks (Fig. 6C, E), which may
715 point to reduced fluid-induced cooling within the lava flow. Furthermore, at a similar depth
716 around 291 mbsf a coherent lava flow was identified in Hole U1530A that is less affected by
717 alteration and shows a lower porosity than altered volcaniclastics based on microresistivity
718 image facies interpretation and downhole petrophysical measurements (Massiot et al., 2022).

719 At the Upper Cone (Site U1528) of Brothers volcano, the $\delta^{11}B$ values of altered rocks are high
720 in the upper sections and sharply decrease at around 75 mbsf and downwards (Fig. 4C). This
721 points to an evolution from more fluid-dominated to more rock-dominated alteration
722 conditions with depth. Downhole measurements and borehole wall imaging suggest that also
723 at Site U1528 lava flows become more abundant in deeper parts (~270 mbsf and lower) of the
724 basement (Massiot et al., 2022). The B contents and $\delta^{11}B$ values at the Upper Cone (Site
725 U1528) however show only negligible variations at depths >75 mbsf. This might point to a
726 more pervasive alteration at the Upper Cone site.

727 Estimates of w/r-ratios and temperatures as well as lithological and structural observations at
728 Snowcap and Brothers volcano suppose a large impact on the sub-seafloor fluid flow regime
729 by permeability contrasts between lithological units. The idea of sealing caps that act as traps
730 for incoming fluids was described for oceanic spreading centers before (e.g., Zierenberg et al.,
731 1998; Roberts et al., 2003). Nevertheless, particularly the shallow water depth (typical < 1000
732 mbsl) volcanic features in arc- and back-arc environments are hosted in promotes an
733 especially explosive volcanism that often results in the formation of more permeable
734 basement that is prone for entrainment of cold seawater (e.g., Fiske et al., 2001). Cooling
735 within the hydrothermal system is one of the major factors that enhances metal-sulfide

precipitation (e.g., Reed and Palandri, 2006), and following the basement structure and permeability distribution of interbedded strata are highly important for ore formation processes (e.g., Tivey, 2007).

## Summary and Conclusions

Pathways of fluid flow and the distribution of temperature are primary controls of mass transfers in subseafloor hydrothermal systems. In this study, we investigated the applicability of B concentrations and isotope ratios of altered rocks and O isotope ratios of hydrothermal quartz as tracers for water-to-rock interaction conditions, including w/r-ratios, precipitation temperatures, secondary mineralogy, and different fluid sources. The results indicate that the combination of B and O isotope systematics is a useful approach in assessing variations in w/r-ratios and temperatures of seafloor hydrothermal systems. The approach was used to determine the variability in subseafloor fluid flow intensity and temperature in two felsic rock-hosted hydrothermal systems that are variably affected by influx of magma-derived fluids: Brothers volcano in the Southern Kermadec Arc, and Snowcap vent field in the PACMANUS hydrothermal area on Pual Ridge in the Manus Basin. In both sites, ocean drilling has sampled the subseafloor of hydrothermally active areas, which provides unparalleled insights into basement alteration and mineralization.

For Brothers volcano, at the Upper Cone (Site U1528) a distinct shift from higher to lower $\delta^{11}B$ values with increasing depth occurs that is suggested to be caused by a decrease in w/r-ratios with increasing depth and probably represent a change from fluid- to rock-dominated hydrothermal conditions with depth potentially due to compaction processes. In contrast, at the NW Caldera (Site U1527) a plastically deformed zone in greater depth (220 to 225 mbsf) seems to be influenced by increased w/r-ratios compared to shallower levels of the site. At the NW Caldera (Site U1530) the high variability in $\delta^{11}B$ values of altered rocks that are suggested to be coupled to changing w/r-ratios and the results that were derived from quartz-

761 water oxygen isotope thermometry hint to a strong control of fluid flow by permeability
762 differences between more coherent lava flows and more permeable volcaniclastic rocks.
763 These results highlight that fluid flow in the seafloor can be characterized by a more fluid
764 controlled pervasive flow through the rock column that naturally decreases with depth due to
765 compaction or can be stronger controlled by lithological or structural features.

766 For Snowcap, high $\delta^{11}B$ values in -magnetite-chlorite altered rocks between 160 and 190 mbsf
767 point to rock alteration under increased w/r ratios. This peak in alteration intensity occurs
768 close to volcanic facies boundaries suggesting that (similar to Site U1530) permeability
769 contrasts between different volcanic units had a strong control on the intensity of fluid flow.

770 This study hence shows the importance of permeability contrasts on fluid pathways and
771 alteration temperatures in the subseafloor of arc and back-arc hydrothermal systems. Episodes
772 of deformation likewise caused pulses of increased flow of seawater-derived fluids. The
773 variable alteration types (in particular at Site U1530) are most plausibly explained by
774 transients in the intensity of magmatic degassing. Unfortunately, our combined B and O
775 isotopic approach did not turn out a useful tracer for identifying different sources of elements
776 (i.e., magma-derived versus rock-leached). This is because a systematic difference in B
777 isotopic composition of rocks altered by interactions with seawater-derived fluids that were
778 variably affected by magmatic fluids could not be recognized.

779 The data presented help constrain the conditions of water-rock interactions in two active felsic
780 rock-hosted hydrothermal vent systems both of which have considerable accumulation of
781 polymetallic massive sulfides at the seafloor. It is clear that the basement underneath these
782 sulfide deposits should also be mineralized to some extent, in particular in areas where hot,
783 metal-laden hydrothermal solutions mix with cold entrained seawater. Although we identified
784 zones in the basement where this mixing likely played a role in setting the water-rock
785 interactions, a relation between alteration and mineralization could not be established. This is

in part due to the generally low intensity of sulfidization throughout the basement drilled in the two work areas.

## Acknowledgements

The authors thank the shipboard participants of ODP Expedition 193, IODP Expedition 376 and of SO-216 and SO-253, including the crews and pilots of *MARUM QUEST*. We also thank P. Brandl, M. Portnyagin, D. Garbe-Schönberg, and F. Hauff for providing the rock powders and performing the Sr concentration measurements of the two unaltered drill-core samples from Brothers volcano. Further, we thank J. Valley for support conducting the oxygen isotope measurements and S. Humphris for her helpful remarks on the manuscript. We also thank R. Trumbull and one anonymous reviewer for their constructive comments. This research used samples and/or data provided by the International Ocean Discovery Program (IODP). This research was funded by the German-Israeli Foundation for Scientific Research and Development grant #I-1357-301.8/2016 to W. Bach and Y. Katzir.

## References

Audétat, A., 2019, The Metal Content of Magmatic-Hydrothermal Fluids and Its Relationship to Mineralization Potential: Economic Geology, v. 114, p. 1033–1056.

Bach, W., Jöns, N., and Klein, F., 2013, Metasomatism within the Ocean Crust, in Harlov, D., and Austrheim, H., ed., Metasomatism and the chemical transformation of rock: the role of fluids in terrestrial and extraterrestrial processes, Lecture Notes in Earth System Sciences, Springer, p. 253-288.

Balance, P.F., Ablaev, A.G., Pushchin, I.K., Pletnev, S.P., Birylina, M.G., Itaya, T., Follas, H.A., and Gibson, G.W., 1999, Morphology and history of the Kermadec trench–arc–backarc basin–remnant arc system at 30 to 32°S: Marine Geology, v. 159, p. 35–62.

Beier, C., Bach, W., Turner, S., Niedermeier, D., Woodhead, J., Erzinger, J., and Krumm, S., 2015, Origin of Silicic Magmas at Spreading Centres—an Example from the South East Rift, Manus Basin: Journal of Petrology, v. 56, p. 255–272.

Binns, R.A., and Scott, S.D., 1993, Actively forming polymetallic sulfide deposits associated with felsic volcanic rocks in the Eastern Manus back-arc basin, Papua New Guinea: Economic Geology, v. 88, p. 2226-2236.

Caratori Tontini, F., Davy, B., de Ronde, C.E.J., Embley, R.W., Leybourne, M., and Tivey, M.A., 2012, Crustal Magnetization of Brothers Volcano, New Zealand, Measured by Autonomous Underwater Vehicles: Economic Geology, v. 107, p. 1571–1581.

de Ronde, C.E.J., Hannington, M.D., Stoffers, P., Wright, I.C., Ditchburn, R.G., Reyes, A.G., Baker, E.T., Massoth, G.J., Lupton, J.E., Walker, S.L., Greene, R.R., Soong, C.W.R., Ishibashi, J., Lebon, G.T., Bray, C.J., and Resing, J.A., 2005, Evolution of a Submarine Magmatic-Hydrothermal System: Economic Geology, v. 100, p. 1097–1133.

de Ronde, C.E.J., Humphris, S.E., Höfig, T.W., Brandl, P.A., Cai, L., Cai, Y., Caratori Tontini, F., Deans, J.R., Farough, A., Jamieson, J.W., Kolandaivelu, K.P., Kutovaya, A., Labonté, J.M., Martin, A.J., Massiot, C., McDermott, J.M., McIntosh

I.M., Nozaki, T., Pellizari, V.H., Reyes, A.G., Roberts, S., Rouxel, O., Schlicht, L.E.M., Seo, J.H., Straub, S.M., Strehlow, K., Takai, K., Tanner, D., Tepley III, F.J., and Zhang, C., 2019a, Expedition 376 summary, in de Ronde, C.E.J., Humphris, S.E., Höfig, T.W. and the Expedition 376 Scientists, ed., Proceedings of the International Ocean Discovery Program, v. 376, College Station, Texas.

de Ronde, C.E.J., Humphris, S.E., Höfig, T.W., Brandl, P.A., Cai, L., Cai, Y., Caratori Tontini, F., Deans, J.R., Farough, A., Jamieson, J.W., Kolandaivelu, K.P., Kutovaya, A., Labonté, J.M., Martin, A.J., Massiot, C., McDermott, J.M., McIntosh, I.M., Nozaki, T., Pellizari, V.H., Reyes, A.G., Roberts, S., Rouxel, O., Schlicht, L.E.M., Seo, J.H., Straub, S.M., Strehlow, K., Takai, K., Tanner, D., Tepley III, F.J., and Zhang, C., 2019b, Site U1528, in de Ronde, C.E.J., Humphris, S.E., Höfig, T.W. and the Expedition 376 Scientists, ed., Proceedings of the International Ocean Discovery Program, v. 376, College Station, Texas.

de Ronde, C.E.J., Humphris, S.E., Höfig, T.W., Brandl, P.A., Cai, L., Cai, Y., Caratori Tontini, F., Deans, J.R., Farough, A., Jamieson, J.W., Kolandaivelu, K.P., Kutovaya, A., Labonté, J.M., Martin, A.J., Massiot, C., McDermott, J.M., McIntosh, I.M., Nozaki, T., Pellizari, V.H., Reyes, A.G., Roberts, S., Rouxel, O., Schlicht, L.E.M., Seo, J.H., Straub, S.M., Strehlow, K., Takai, K., Tanner, D., Tepley III, F.J., and Zhang, C., 2019c, Site U1530, in de Ronde, C.E.J., Humphris, S.E., Höfig, T.W. and the Expedition 376 Scientists, ed., Proceedings of the International Ocean Discovery Program, v. 376, College Station, Texas.

de Ronde, C.E.J., Humphris, S.E., Höfig, T.W., Reyes, A.G., and the IODP Expedition 376 Scientists, 2019d, Critical role of caldera collapse in the formation of seafloor mineralization: Geology, v. 47, p. 762–766.

de Ronde, C.E.J., Humphris, S.E., Höfig, T.W., and the Expedition 376 Scientists, 2019e, Proceedings of the International Ocean Discovery Program, v. 376, College Station, Texas.

de Ronde, C.E.J., Massoth, G.J., Butterfield, D.A., Christenson, B.W., Ishibashi, J., Ditchburn, R.G., Hannington, M.D., Brathwaite, R.L., Lupton, J.E., Kamenetsky, V.S., Graham, I.J., Zellmer, G.F., Dziak, R.P., Embley, R.W., Dekov, V.M., Munnik, F., Lahr, J., Evans, L.J., and Takai, K., 2011, Submarine hydrothermal activity and gold-rich mineralization at Brothers Volcano, Kermadec Arc, New Zealand: Mineralium Deposita, v. 46, p. 541–584.

Deniel, C., and Pin, C., 2001, Single-stage method for the simultaneous isolation of lead and strontium from silicate samples for isotopic measurements: Analytica Chimica Acta, v. 426, p. 95–103.

Diehl, A., 2019, Causes for variable hydrothermal vent fluid compositions in intraoceanic arcs : insights from fluid compositions and mineral precipitates of the South Kermadec Arc: Dissertation, Bremen, Germany, The University of Bremen, 170 p.

Diehl, A., de Ronde, C.E.J., and Bach, W., 2020, Subcritical phase separation and occurrence of deep-seated brines at the NW Caldera Vent Field, Brothers Volcano: Evidence from fluid inclusions in hydrothermal precipitates: Geofluids, v. 2020, ID 8868259, pp. 22.

Dobson, P.F., Kneafsey, T.J., Hulen, J., and Simmons, A., 2003, Porosity, permeability, and fluid flow in the Yellowstone geothermal system, Wyoming: Journal of Volcanology and Geothermal Research, v. 123, p. 313–324.

El Meknassi, S., Dera, G., De Rafélis, M., Brahmi, C., Lartaud, F., Hodel, F., Jeandel, C., Menjot, L., Mounic, S., Henry, M., Besson, P., Chavagnac, V., 2020, Seawater $^{87}Sr/^{86}Sr$ ratios along continental margins: Patterns and processes in open and restricted shelf domains: Chemical Geology, v. 558, 119874.

Embley, R.W., Ronde, C.E.J. de, Merle, S.G., Davy, B., and Tontini, F.C., 2012, Detailed Morphology and Structure of an Active Submarine Arc Caldera: Economic Geology, v. 107, p. 1557–1570.

Fiske, R.S., Nada, J., Iizasa, K., Yuasa, M., and Klaus, A., 2001, Submarine silicic caldera at the front of the Izu-Bonin arc, Japan: Voluminous seafloor eruptions of rhyolite pumice: Geological Society of America Bulletin, v. 133, p. 813-824.

Foster, G.L., Pogge von Strandmann, P.A.E., and Rae, J.W.B., 2010, Boron and magnesium isotopic composition of seawater: Geochemistry, Geophysics, Geosystems, v. 11.

Foustoukos, D.I., and Seyfried, W.E., 2007, Fluid Phase Separation Processes in Submarine Hydrothermal Systems: Reviews in Mineralogy and Geochemistry, v. 65, p. 213–239.

Gamo, T., Okamura, K., Charlou, J.-L., Urabe, T., Auzende, J.-M., Ishibashi, J., Shitashima, K., Chiba, H., and Cruise, S.S.P.o.t.M., 1997, Acidic and sulfate-rich hydrothermal fluids from the Manus back-arc basin, Papua New Guinea: Geology, v. 25, p. 139–142.

Gonfiantini, R., Tonarini, S., Gröning, M., Adorni-Braccesi, A., Al-Ammar, A.S., Astner, M., Bächler, S., Barnes, R.M., Bassett, R.L., Cocherie, A., Deyhle, A., Dini, A., Ferrara, G., Gaillardet, J., Grimm., J., Guerrot, C., Krähenbühl, U., Layne, G.D. Lemarchand, D., Meixner, A., Northington, D.J., Pennisi, M., Reitznerová, E., Rodushkin, I., Sugiura, N., Surberg, R., Tonn, S., Wiedenbeck, M., Wunderli, S., Xiao, Y., Zack, T., 2003, Intercomparison of boron isotope and

873 concentration measurements. Part II: Evaluation of results: Geostandards Newsletter: The Journal of Geostandards and
874 Geoanalysis, v. 27, p. 41-57.

875 Govindaraju, K., 1994, Compilation of working values and sample description for 383 geostandards: Geostandards and
876 Geoanalytical Research, v. 18, p. 1-158.

877 Götze, J., Plötze, M., and Habermann, D., 2001, Origin, spectral characteristics and practical applications of the
878 cathodoluminescence (CL) of quartz - a review: Mineralogy and Petrology, v. 71, p. 225-250.

879 Haase, K.M., Stroncik, N., Garbe-Schönberg, D., and Stoffers, P., 2006, Formation of island arc dacite magmas by extreme
880 crystal fractionation: Journal of Volcanology and Geothermal Research, v. 152, p. 316–330.

881 Hansen, C.T., Meixner, A., Kasemann, S.A., and Bach, W., 2017, New insight on Li and B isotope fractionation during
882 serpentinization derived from batch reaction investigations: Geochimica et Cosmochimica Acta, v. 217, p. 51–79.

883 Heap, M.J., Kennedy, B.M., Farquharson, J.I., Ashworth, J., Mayer, K., Letham-Brake, M., Reuschlé, T., Gilg, H.A., Scheu,
884 B., Lavallée, Y., Siratovich, P., Cole, J., Jolly, A.D., Baud, P., and Dingwell, D.B., 2017, A multidisciplinary approach to
885 quantify the permeability of the Whakaari/White Island volcanic hydrothermal system (Taupo Volcanic Zone, New
886 Zealand): Journal of Volcanology and Geothermal Research, v. 332, p. 88–108.

887 Heck, P.R., Huberty, J.M., Kita, N.T., Ushikubo, T., Kozdon, R., and Valley, J.W., 2011, SIMS analyses of silicon and
888 oxygen isotope ratios for quartz from Archean and Paleoproterozoic banded iron formations: Geochimica et
889 Cosmochimica Acta, v. 75, p. 5879–5891.

890 Hedenquist, J.W., and Arribas, A., 2021, Exploration implications of multiple formation environments of advanced argillic
891 minerals: Economic Geology and the Bulletin of the Society of Economic Geologists, v. 117 (3), p. 609-643.

892 Hervig, R.L., Moore, G.M., Williams, L.B., Peacock, S.M., Holloway, J.R., and Roggensack, K., 2002, Isotopic and
893 elemental partitioning of boron between hydrous fluid and silicate melt: American Mineralogist, v. 87, p. 769-774.

894 Hoog, J.C. de, and Savov, I.P., 2018, Boron Isotopes as a Tracer of Subduction Zone Processes, in Marschall, H., and Foster,
895 G., ed., Boron Isotopes, p. 217–247.

896 Ishikawa, T., and Nakamura, E., 1992, Boron isotope geochemistry of the oceanic crust from DSDP/ODP Hole 504B:
897 Geochimica et Cosmochimica Acta, v. 56, p. 1633-1639.

898 James, R.H., Allen, D.E., and Seyfried, W.E., 2003, An experimental study of alteration of oceanic crust and terrigenous
899 sediments at moderate temperatures (51 to 350°C): Geochimica et Cosmochimica Acta, v. 67, p. 681–691.

900 Kakihana, H., Kotaka, M., Satoh, S., Nomura, M., and Okamoto, M., 1977, Fundamental Studies on the Ion-Exchange
901 Separation of Boron Isotopes: Bulletin of the chemical society of Japan, v. 50(1), p. 158-163.

902 Kelly, J.L., Fu, B., Kita, N.T., and Valley, J.W., 2007, Optically continuous silcrete quartz cements of the St. Peter
903 Sandstone: Geochimica et Cosmochimica Acta, v. 71, p. 3812–3832.

904 Kesler, S.E., 2005, Ore-Forming Fluids: Elements v.1, p 13-18.

905 Kita, N.T., Ushikubo, T., Fu, B., and Valley, J.W., 2009, High precision SIMS oxygen isotope analysis and the effect of
906 sample topography: Chemical Geology, v. 264, p. 43-57.

907 Kleint, C., Bach, W., Diehl, A., Fröhberg, N., Garbe-Schönberg, D., Hartmann, J.F., de Ronde, C.E.J., Sander, S.G., Strauss,
908 H., Stucker, V.K., Thal, J., Zitoun, R., Koschinsky, A., 2019, Geochemical characterization of highly diverse
909 hydrothermal fluids from volcanic vent systems of the Kermadec intraoceanic arc: Chemical Geology, v. 528, p. 119289.

910 Lackschewitz, K.S., Asada, R., and Paulick, H., 2006, Data Report: Summary of revised alteration phases for PACMANUS
911 hydrothermal field - X-Ray Diffraction Analyses of altered felsic volcanic rocks from Holes 1188A, 1188F, 1189A, and
912 1189B, in Barriga, F.J.A.S., Binns, R.A., Miller, D.J., and Herzig, P.M., ed., Proceedings of the Ocean Drilling Program
913 Scientific Results, v. 193.

914 Lackschewitz, K.S., Devey, C.W., Stoffers, P., Botz, R., Eisenhauer, A., Kummetz, M., Schmidt, M., and Singer, A., 2004,
915 Mineralogical, geochemical and isotopic characteristics of hydrothermal alteration processes in the active, submarine,
916 felsic-hosted PACMANUS field, Manus Basin, Papua New Guinea: Geochimica et Cosmochimica Acta, v. 68, p. 4405–
917 4427.

918 Lee, H.J., Seo, J.H., de Ronde, C.E.J., and Heinrich, C.A., 2022, Fluid Inclusion Evidence for Subseafloor Magmatic-
919 Hydrothermal Processes at Brothers Volcano, Kermadec Arc, New Zealand: Economic Geology Special Issue.

920 Leeman, W.P., Tonarini, S., and Turner, S., 2017, Boron isotope variations in Tonga-Kermadec-New Zealand arc lavas:
921 Geochemistry, Geophysics, Geosystems, v. 18, p. 1126–1162.

Marks, N., Zierenberg, R.A., and Schiffman, P., 2015, Strontium and oxygen isotopic profiles through 3 km of hydrothermally altered oceanic crust in the Reykjanes Geothermal System, Iceland: Chemical Geology, v. 412, p. 34–47.

Marschall, H., 2018, Boron Isotopes in the Ocean Floor Realm and the Mantle, in Marschall H., and Foster, G., ed., Boron Isotopes, p. 189–215.

Marschall, H.R., Wanless, V.D., Shimizu, N., Pogge von Strandmann, P.A., Elliott, T., and Monteleone, B.D., 2017, The boron and lithium isotopic composition of mid-ocean ridge basalts and the mantle: Geochimica et Cosmochimica Acta, v. 207, p. 102–138.

Martinez, F., and Taylor, B., 1996, Backarc spreading, rifting, and microplate rotation, between transform faults in the Manus Basin: Marine Geophysical Research, v. 18, p. 203–224.

Massiot, C., McIntosh, I., Deans, J., Milicich, S.D., Caratori Tontini, F., de Ronde, C.E.J., Adam, L., Kolandaivelu, K., and Guerin, G., 2022, Petrophysical Facies and Inferences on Permeability at Brothers Volcano, Kermadec Arc, Using Downhole Images and Petrophysical Data: Economic Geology Special Issue.

McCulloch, M.T., Gregory, R.T., Wasserburg, G.J., and Taylor, Jr.H.P., 1980, A neodymium, strontium, and oxygen isotopic study of the Cretaceous Samail ophiolite and implications for the petrogenesis and seawater-hydrothermal alteration of oceanic crust: Earth and Planetary Science Letters, v. 46, p. 201–211.

Palmer, M.R., Spivack, A.J., and Edmond, J.M., 1987, Temperature and pH controls over isotopic fractionation during adsorption of boron on marine clay: Geochimica et Cosmochimica Acta, v. 51, p. 2319-2323.

Park, S.-H., Lee, S.-M., Kamenov, G.D., Kwon, S.-T., and Lee, K.-Y., 2010, Tracing the origin of subduction components beneath the South East rift in the Manus Basin, Papua New Guinea: Chemical Geology, v. 269, p. 339–349.

Paulick, H., and Bach,W., 2006, Phyllosilicate Alteration Mineral Assemblages in the Active Subsea-Floor Pacmanus Hydrothermal System, Papua New Guinea, ODP Leg 193: Economic Geology, v. 101, p. 633–650.

Paulick, H., and Herzig, P.M., 2003, Volcanic facies controls on mass transfer at the active, dacite-hosted Pacmanus hydrothermal system, Manus basin, Papua New Guinea (Ocean Drilling Program Leg 193), in Eliopoulos, G.D. et al., ed., Mineral exploration and sustainable development, Millpress Rotterdam, p. 167–170.

Paulick, H., Herzig, P.M., and Hoernes S., 2005, Data Report: A comprehensive geochemical, mineralogical, and isotopic data set of varibly altered dacitic volcanic rocks from the subsurface of the PACMANUS hydrothermal field (ODP Leg 193), in Barriga, F.J.A.S., Binns, R.A., Miller, D.J., and Herzig, P.M., ed., Proceedings of the Ocean Drilling Program Scientific Results, v. 193.

Paulick, H., Vanko, D.A., and Yeats, C.J., 2004, Drill core-based facies reconstruction of a deep-marine felsic volcano hosting an active hydrothermal system (Pual Ridge, Papau New Guinea, ODP Leg 193): Journal of Volcanology and Geothermal Research, v. 130, p. 31–50.

Raffone, N., Ottolini, L., Tonarini, S., Gianelli, G., and Fridleifsson, G.Ó., 2008, A SIMS study of lithium, boron and chlorine in basalts from Reykjanes (southwestern Iceland): Microchimica Acta, v. 161, p. 307-312.

Reed, M.H., and Palandri, J., 2006, Sulfide Mineral Precipitation from Hydrothermal Fluids: Reviews in Mineralogy and Geochemistry, v. 61(1), p. 609-631.

Reeves, E.P., Seewald, J.S., Saccocia, P., Bach, W., Craddock, P.R., Shanks, W.C., Sylva, S.P., Walsh, E., Pichler, T., and Rosner, M., 2011, Geochemistry of hydrothermal fluids from the PACMANUS, Northeast Pual and Vienna Woods hydrothermal fields, Manus Basin, Papua New Guinea: Geochimica et Cosmochimica Acta, v. 75, p. 1088–1123.

Roberts, S., Bach, W., Binns, R.A., Vanko, D.A., Yeats, C.J., Teagle, D., Blacklock, K., Blusztajn, J.S., Boyce, A.J., Cooper, M.J., Holland, N., and McDonald, B., 2003, Contrasting evolution of hydrothermal fluids in the PACMANUS system, Manus Basin: The Sr and S isotope evidence: Geology, v. 31, p. 805-808.

Romer, R.L., Meixner, A., and Hahne, K., 2014, Lithium and boron isotopic composition of sedimentary rocks — The role of source history and depositional environment: Gondwana Research, v. 26, p. 1093–1110.

Seewald, J.S., Reeves, E.P., Bach, W., Saccocia, P.J., Craddock, P.R., Shanks, W.C., Sylva, S.P., Pichler, T., Rosner, M., and Walsh, E, 2015, Submarine venting of magmatic volatiles in the Eastern Manus Basin, Papua New Guinea: Geochimica et Cosmochimica Acta, v. 163, p. 178–199.

Seewald, J.S., Reeves, E.P., Bach, W., Saccocia, P.J., Craddock, P.R., Walsh, E., Shanks, W.C., Sylva, S.P., Pichler, T., and Rosner, M., 2019, Geochemistry of hot-springs at the SuSu Knolls hydrothermal field, Eastern Manus Basin: Geochimica et Cosmochimica Acta, v. 255, p. 25–48.

971 Sharp, Z., and Kirschner, D., 1994, Quartz-calcite oxygen isotope thermometry: Geochimica et Cosmochimica Acta, v. 58, p.
972 4491–4501.

973 Shipboard Scientific Party, 2001, Leg 193 Preliminary Report: Anatomy of an Active Felsic-Hosted Hydrothermal System,
974 Eastern Manus Basin. ODP Preliminary Reports, 93 (online). Available from World Wide Web: <http://www-
975 odp.tamu.edu/publications/prelim/193_prel/193prel.pdf>, cited 2022-05-29.

976 Shipboard Scientific Party, 2002, Leg 193 Summary, in Binns, R.A., Barriga, F.J.A.S., and Miller, D.J., ed., Proceedings of
977 the Ocean Drilling Program Initial Reports, v. 193.

978 Smith, H.J., Spivack, A.J., Staudigel, H., and Hart, S.R., 1995, The boron isotopic composition of altered oceanic crust:
979 Chemical Geology, v. 126, p. 119-135.

980 Spivack, A., and Edmond, J., 1987, Boron isotope exchange between seawater and the oceanic crust: Geochimica et
981 Cosmochimica Acta, v. 51, p. 1033–1043.

982 Thal, J., Tivey, M., Yoerger, D., Jöns, N., and Bach, W., 2014, Geologic setting of PACManus hydrothermal area — High
983 resolution mapping and in situ observations: Marine Geology, v. 355, p. 98–114.

984 Thompson, G., and Melson, W.G., 1970, Boron contents of serpentinites and metabasalts in the oceanic crust: Implications
985 for the boron cycle in the oceans: Earth and Planetary Science Letters, v. 8, p. 61-65.

986 Tivey, M.K., 2007, Generation of seafloor hydrothermal vent fluids and associated mineral deposits: Oceanography, v. 20, p.
987 50-65.

988 Valley, J.W., and Kita, N.T., 2009, In situ Oxygen Isotope Geochemistry by Ion Microprobe, in Fayek. M., ed., MAC Short
989 Course: Secondary Ion Mass Spectrometry in the Earth Sciences, v. 41, p.19-63.

990 Vanko, D.A., Bach, W., Roberts, S., Yeats, C.J., and Scott, S.D., 2004, Fluid inclusion insights from anhydrite veins up to
991 350 meters below the seafloor at the deep-sea PACMANUS hydrothermal field. Manus Basin back-arc rift, Papua New
992 Guinea: Journal of Geophysical Research, B03201.

993 Wang, X-L., Coble, M.A., Valley, J.W., Shu, X-J., Kitajima, K., Spicuzza, M.J., Sun, T., 2014, Influence of radiation damage
994 on late Jurassic zircon from southern China: Evidence from in situ measurement of oxygen isotopes, laser Raman, U-Pb
995 ages, and trace elements: Chemical Geology, v. 389, p. 122-136.

996 Whitney, J.A., 1975, Vapor generation on a quartz monzonite magma; a synthetic model with application to porphyry copper
997 deposits: Economic Geology, v. 70, p. 346–358.

998 Wilckens, F.K., Reeves, E.P., Bach, W., Meixner, A., Seewald, J.S., Koschinsky, A., and Kasemann, S.A., 2018, The
999 influence of magmatic fluids and phase separation on B systematics in submarine hydrothermal vent fluids from back-arc
1000 basins: Geochimica et Cosmochimica Acta, v. 232, p. 140–162.

1001 Williams, L.B., Hervig, R.L., Holloway, J.R., and Hutcheon, I., 2001, Boron isotope geochemistry during diagenesis. Part I.
1002 Experimental determination of fractionation during illitization of smectite: Geochimica et Cosmochimica Acta, v. 65(11),
1003 p. 1769-1782.

1004 Wunder, B., Meixner, A., Romer, R.L., Wirth, R., and Heinrich, W., 2005, The geochemical cycle of boron: Lithos, v. 84, p.
1005 206–216.

1006 Yamaoka, K., Ishikawa, T., Matsubaya, O., Ishiyama, D., Nagaishi, K., Hiroyasu, Y., Chiba, H. and Kawahata, H., 2012,
1007 Boron and oxygen isotope systematics for a complete section of oceanic crustal rocks in the Oman ophiolite: Geochimica
1008 et Cosmochimica Acta, v. 84, p. 543–559.

1009 Yamaoka, K., Matsukura, S., Ishikawa, T., and Kawahata, H., 2015a, Boron isotope systematics of a fossil hydrothermal
1010 system from the Troodos ophiolite, Cyprus: Chemical Geology, v. 396, p. 61–73.

1011 Yamaoka, K., Hong, E., Ishikawa, T., Gamo, T., and Kawahata, H., 2015b, Boron isotope geochemistry of vent fluids from
1012 arc/back-arc seafloor hydrothermal systems in the western Pacific: Chemical Geology, v. 392, p. 9-18.

1013 Yang, K., and Scott, S.D., 1996, Possible contribution of a metal-rich magmatic fluid to a sea-floor hydrothermal system:
1014 Nature, v. 383, p. 420–423.

1015 Zierenberg, R.A., Fouquet, Y., Miller, D.J., Bahr, J.M., Baker, P.A., Bjerkgard, T., Brunner, C.A., Duckworth, R.C., Gable,
1016 R., Gieskes, J., Goodfellow, W.D., Gröschel-Becker, H.M., Guerin, G., Ishibashi, J., Iturrino, G., James, R.H.,
1017 Lackschewitz, K.S., Marquez, L.L., Nehling, P., Peter, J.M., Rigsby, C.A., Schultheiss, P., Shanks III, W.C., Simoneit,
1018 B.R.T., Summit, M., Teagle, D.A.H., Urbat, M., and Zuffa, G.G., 1998, The deep structure of a sea-floor hydrothermal
1019 deposit: Nature, v. 392, p.485-488.

1020

*Fig. 1: Geological setting of the Manus Basin. (A) Location of ODP Leg 193, PACManus in the Manus Basin (yellow star) modified after Thal et al. (2014). An overview map is inserted that shows the position of the Manus Basin in the Pacific with a red dot. (B) Rock types at Pual Ridge, sites of hydrothermal activity (red dots) and location of PACManus, modified after Shipboard Scientific Party (2001) The thick orange lines represent plate boundaries. Open-toothed lines symbolize inactive subduction, while filled-tooth lines indicate active subduction. Thin orange lines in (B) show extensional faults. WIT=Willaumez Transform; METZ=Manus Extensional Transform Zone; DT=Djaul Transform; WT=Weitin Transform; MMP=Manus Microplate; MSC=Manus Spreading Centre; SER=Southeast Ridges.*

*Fig. 2: Geological setting of the Southern Kermadec arc. (A) Location of Brothers volcano within the Southern Kermadec arc, modified after Ballance et al. (1999). (B) Bathymetric map of Brothers volcano modified from Embley et al. (2012). Light gray patches indicate zones of low magnetization intensity (Caratori Tontini et al., 2012) that are suggested to represent zones of high-temperature fluid upflow. Yellow stars mark drilling locations (IODP Expedition 376) from which samples used in this study came. The red line refers to the cross-section shown in Figure 4.*

*Fig.3: Variations in boron concentration and isotopic composition of altered rocks and alteration mineral assemblages with depth at Snowcap, ODP Site 1188 (Hole 1188A from 0 to 211.6 mbsf and Hole 1188F from 218 to 386.7 mbsf), Manus Basin. The gray vertical line represents the unaltered rock compositions. Errors of 2sd are smaller than symbol size. Half-boxes represent rocks with mixed alteration types. Mineral abbreviations: prl = pyrophyllite, ill = illite, chl=chlorite, qtz=quartz, crs=cristobalite, sm=smectite, anh=anhydrite, gp=gypsum, ba=barite, py=pyrite, mgt=magnetite, crr=corrensite.*

*Fig.4: Alteration patterns, lithostratigraphy (after de Ronde et al., 2019e) and geochemical variations with depth at Brothers volcano. (A) Cross-section (see Fig. **2**B) of Brothers*

*volcano and distribution of alteration types based on shipboard observations and XRD analyses of IODP Expedition 376, modified after de Ronde et al. (2019d). Boreholes were projected to the cross-section. (B, C, D): B concentrations and isotopic compositions of altered rocks Sites U1527, U1528 and Site U1530, respectively. The symbols are the same as in Figure 5; symbol colors match alteration type. The errors (2sd) of the B isotopic compositions are smaller than the symbol sizes. The range of unaltered rock compositions is illustrated as light gray vertical line, with the average in dark gray. Mineral abbreviations: plg = plagioclase, px = pyroxene.*

*Fig.5: Chemical and isotopic compositions of unaltered and variably altered rocks from Snowcap and Brothers volcano. Errors (2sd) of B and Sr isotopes are smaller than symbol size. (A) B concentrations versus $\delta^{11}B$ compositions. (B) Sr versus B isotopic compositions. Inset shows the relation of the B and Sr isotope composition of unaltered and altered rocks relative to seawater. Mineral abbreviations are given in Fig.3.*

*Fig.6: O isotope values ($\delta^{18}O_{VSMOW}$) and calculated formation temperatures (pink shaded) of quartz grains from different depth intervals and alteration types in Hole U1530A, NW Caldera, Brothers volcano. Temperatures are based on oxygen isotope quartz-water thermometry calibrated by Sharp and Kirschner (1994). The pink shades give the range of minimum and maximum temperatures. (A) $\delta^{18}O_{VSMOW}$ and temperatures versus depth, alteration types also included; (B), (C), (D), and (E) show CL images of single quartz grains, including the locations of SIMS analyses, the measured $\delta^{18}O_{Qtz}$ values and the corresponding temperatures.*

*Fig.7: Model calculations of B contents and isotopic ratio during progressive fluid-rock interaction for varies temperatures, adapted from Yamaoka et al. (2015a). The italic numbers mark the w/r-ratios. An initial rock composition based on average unaltered rock from Brothers volcano and Snowcap (20.0 µg/g and +5.8 ‰), and an initial fluid composition*

*based on unaltered bottom seawater (4.5 µg/g and +39.6 ‰) were assumed. The observed B and $\delta^{11}B$ compositions of Brothers volcano and Snowcap are shown with the same symbols as in Figure 5. Estimates (see text for details): for 300 °C ($D_B$=0.1, α=0.985), for 250 °C ($D_B$=0.3, α=0.983), for 200 °C ($D_B$=0.6, α=0.981), and for 150 °C ($D_B$=1.0, α=0.979).*

*Fig.8: Summary sketch of the alteration evolution at Brothers volcano. Alteration types are the same as in Figure 4. The formation steps (A) Pre-caldera, (B) Caldera collapse and (C) resurgent cone were adapted from de Ronde et al. (2019d). In the pre-caldera stage (A), advanced argillic alteration due to magmatic fluid upflow took place. After collapse of the caldera (B and C), increased seawater ingress was initiated and chlorite- and/or illite-rich alteration occurred. A more detailed section of Hole U1530A at the NW Caldera (D) shows that the more coherent lava-flows act as permeability barriers and exhibit low extents of seawater ingress and increased alteration temperatures (up to 425 °C) compared to the surrounding volcaniclastics that experienced increased seawater ingress and lower alteration temperatures (262 to 353 °C). At the Upper Cone site (C), increased seawater ingress occurs at the topmost part and decreasing with depth, probably due to compaction and sealing of the crust by secondary minerals.*

*Table 1: Alteration types, secondary mineral assemblages, B concentrations and isotopic compositions of unaltered and altered rocks from Snowcap, Manus Basin.*

*Table 2: Alteration types, and B and Sr concentrations and isotopic compositions of altered and unaltered classified rocks from Brothers volcano, Kermadec arc.*

*Table 3: Oxygen isotope ratios ($\delta^{18}O_{VSMOW}$) measured by SIMS of quartz single crystal domains from Hole U1530A, NW Caldera, Brothers volcano.*

*Appendix Table A1: Oxygen isotope measurements by SIMS on quartz from sample material (IODP Exp. 376, Brothers volcano) and reference material UWQ-1. The position of the measured points is projected to the CL images of the quartz separates.*

Fig. 1

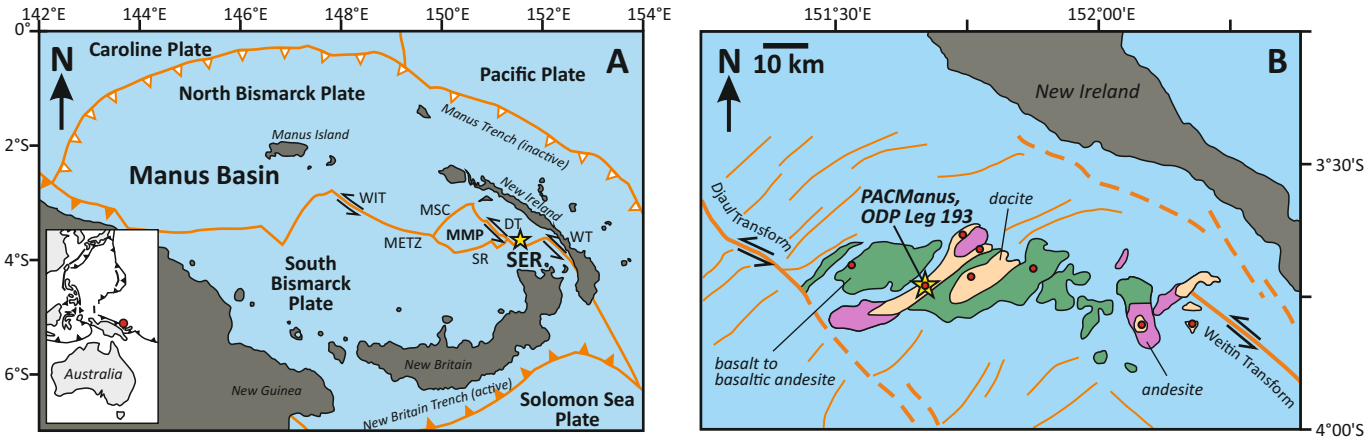
142°E
144°E
146°E
148°E
150°E
152°E
154°E
0°
2°S
4°S
6°S
N
Caroline Plate
North Bismarck Plate
Pacific Plate
A
Manus Island
Manus Trench (inactive)
Manus Basin
New Ireland
WIT
MSC
DT
METZ
MMP
SR
SER
WT
South
Bismarck
Plate
Australia
New Britain
New Guinea
New Britain Trench (active)
Solomon Sea
Plate
151°30'E
152°00'E
3°30'S
4°00'S
N
10 km
B
New Ireland
Djaul Transform
PACManus,
ODP Leg 193
dacite
basalt to
basaltic andesite
andesite
Weitin Transform

Fig. 2

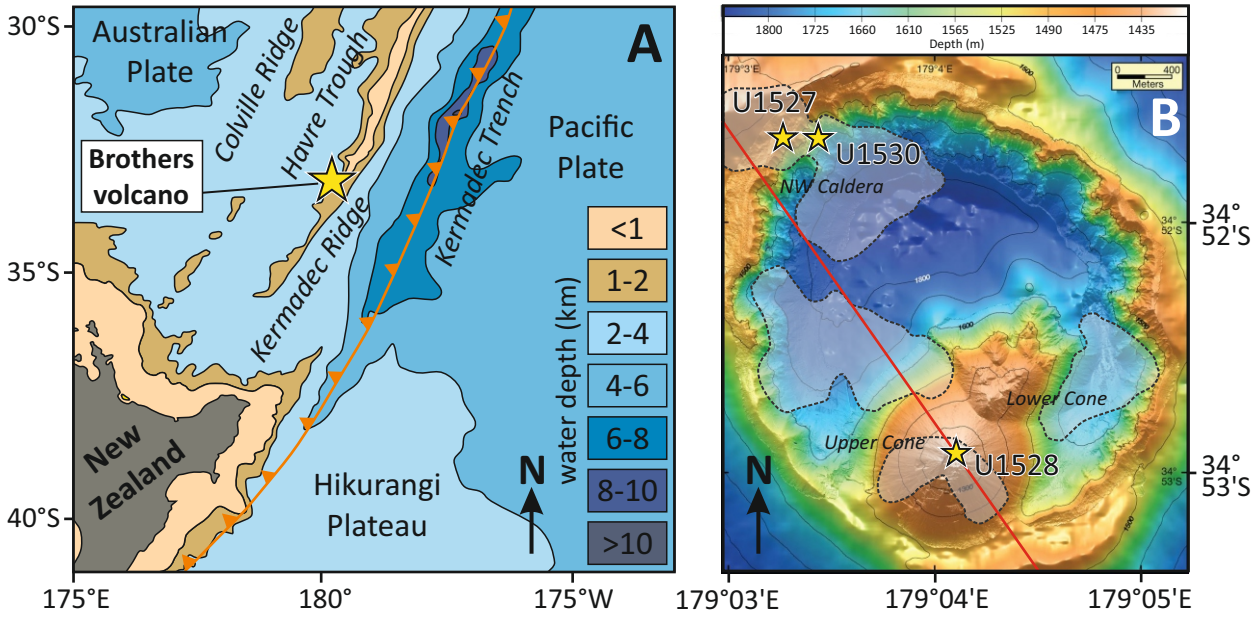
A
Australian Plate
Colville Ridge
Havre Trough
Brothers volcano
Kermadec Ridge
Kermadec Trench
Pacific Plate
New Zealand
Hikurangi Plateau
N
water depth (km)
<1
1-2
2-4
4-6
6-8
8-10
>10
30°S
35°S
40°S
175°E
180°
175°W
B
U1527
U1530
NW Caldera
Lower Cone
Upper Cone
U1528
N
34° 52'S
34° 53'S
179°03'E
179°04'E
179°05'E

Fig. 3

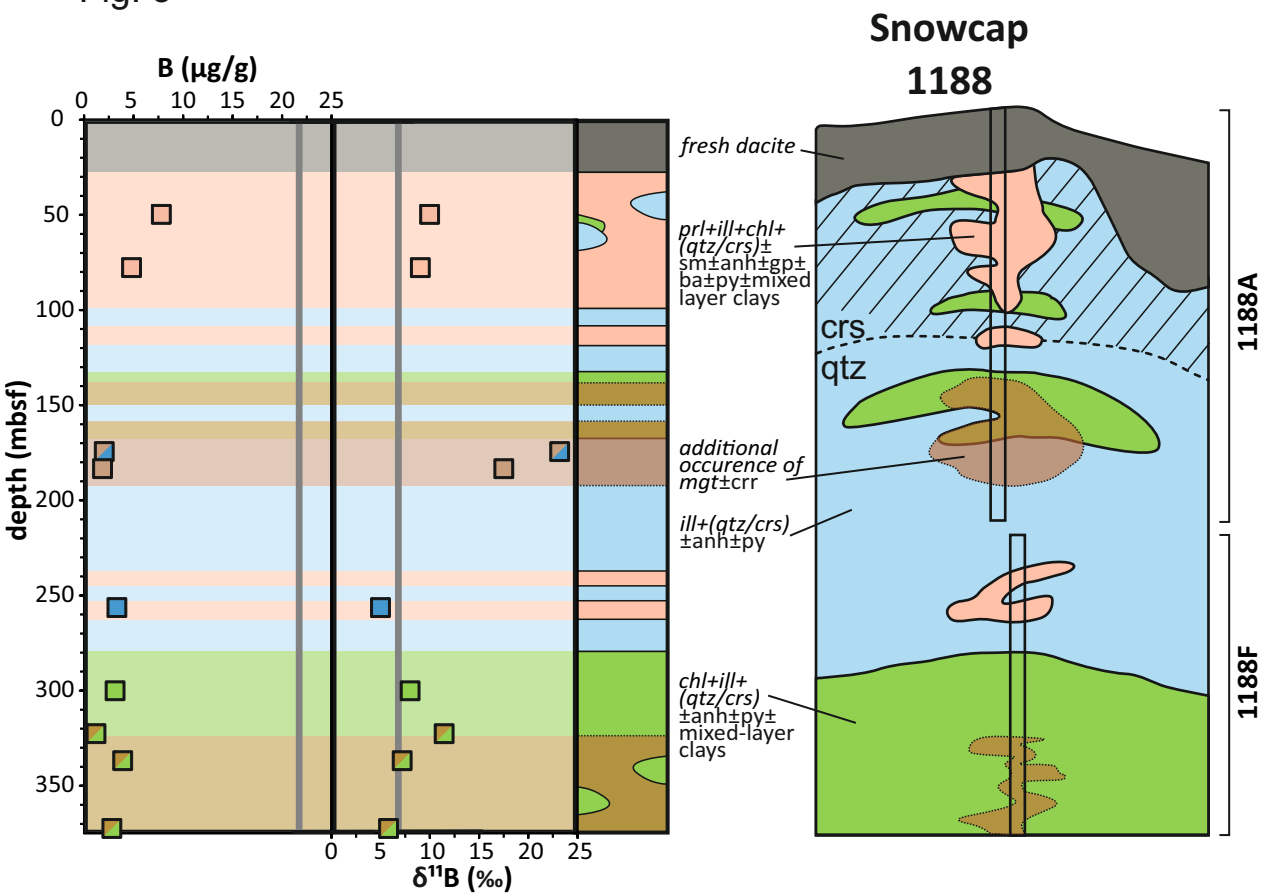
B (µg/g)
0
5
10
15
20
25
depth (mbsf)
0
50
100
150
200
250
300
350
δ11B (‰)
Snowcap
1188
fresh dacite
prl+ill+chl+
(qtz/crs)±
sm±anh±gp±
ba±py±mixed
layer clays
crs
qtz
additional
occurence of
mgt±crr
ill+(qtz/crs)
±anh±py
chl+ill+
(qtz/crs)
±anh±py±
mixed-layer
clays
1188A
1188F

Fig. 4

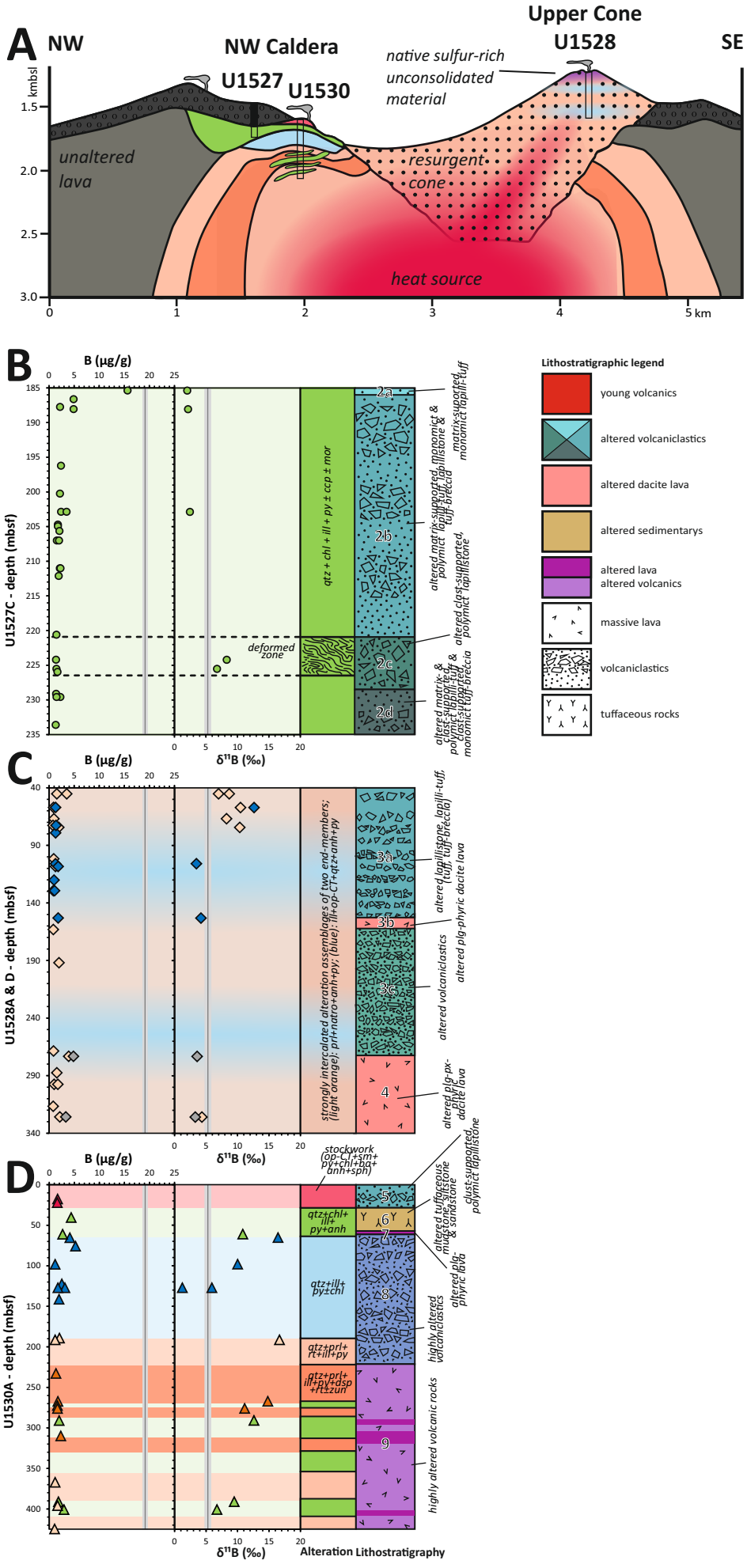
A
NW
NW Caldera
U1527
U1530
Upper Cone
U1528
SE
native sulfur-rich unconsolidated material
unaltered lava
resurgent cone
heat source
kmbsl
1.5
2.0
2.5
3.0
0
1
2
3
4
5 km
B
B (µg/g)
U1527C - depth (mbsf)
qtz + chl + ill + py ± ccp ± mor
deformed zone
2a
2b
2c
2d
δ11B (‰)
C
B (µg/g)
U1528A & D - depth (mbsf)
strongly intercalated alteration assemblages of two end-members; (light orange): prl+natro+anh+py; (blue): ill+op-CT+qtz+anh+py
3a
3b
3c
4
δ11B (‰)
D
B (µg/g)
U1530A - depth (mbsf)
stockwork (op-CT+sm+ py+chl+bq+ anh+sph)
qtz+chl+ ill+ py+anh
qtz+ill+ py±chl
qtz+prl+ rt+ill+py
qtz+prl+ ill+py+dsp +rt±zun
5
6
7
8
9
δ11B (‰)
Alteration Lithostratigraphy
Lithostratigraphic legend
young volcanics
altered volcaniclastics
altered dacite lava
altered sedimentarys
altered lava
altered volcanics
massive lava
volcaniclastics
tuffaceous rocks

Fig. 5

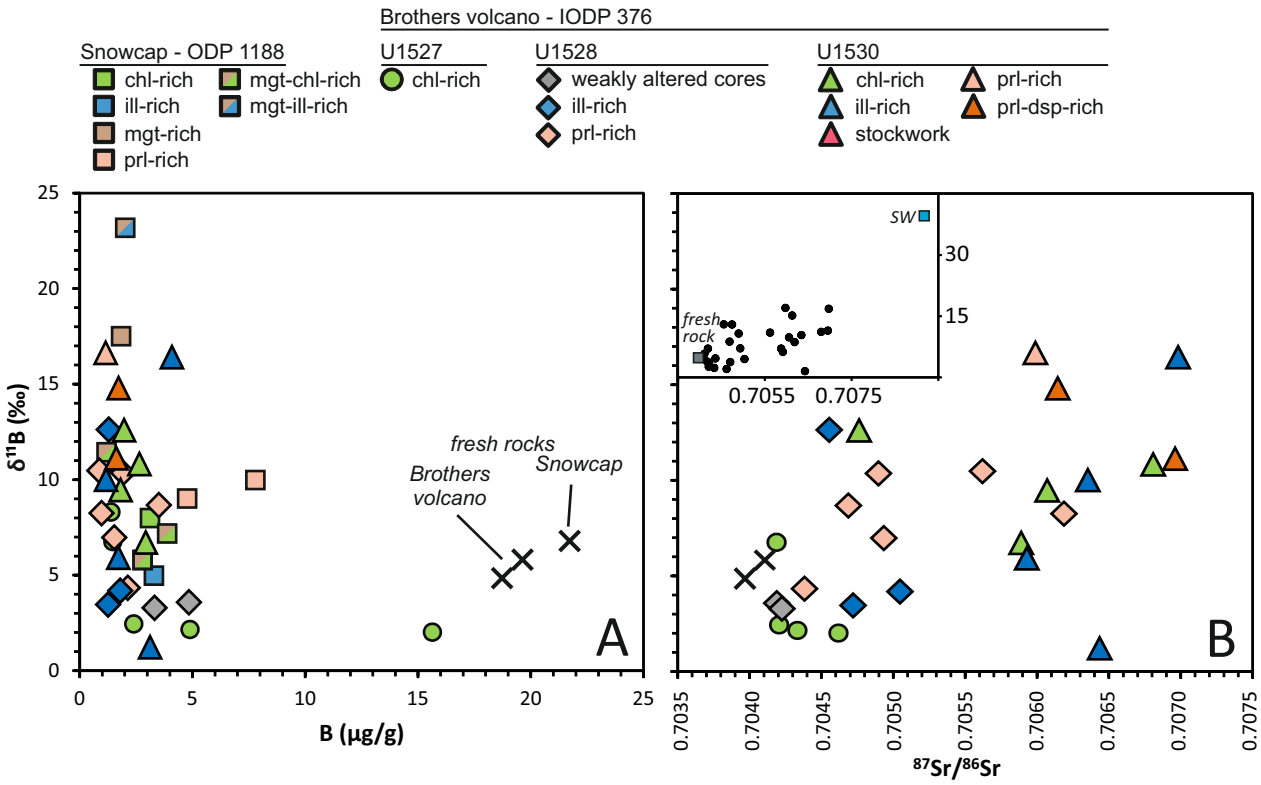
Brothers volcano - IODP 376
Snowcap - ODP 1188
chl-rich
mgt-chl-rich
ill-rich
mgt-ill-rich
mgt-rich
prl-rich
U1527
chl-rich
U1528
weakly altered cores
ill-rich
prl-rich
U1530
chl-rich
prl-rich
ill-rich
prl-dsp-rich
stockwork
δ11B (‰)
B (µg/g)
fresh rocks
Brothers volcano
Snowcap
A
sw
fresh rock
0.7055
0.7075
30
15
B
87Sr/86Sr

Fig. 6

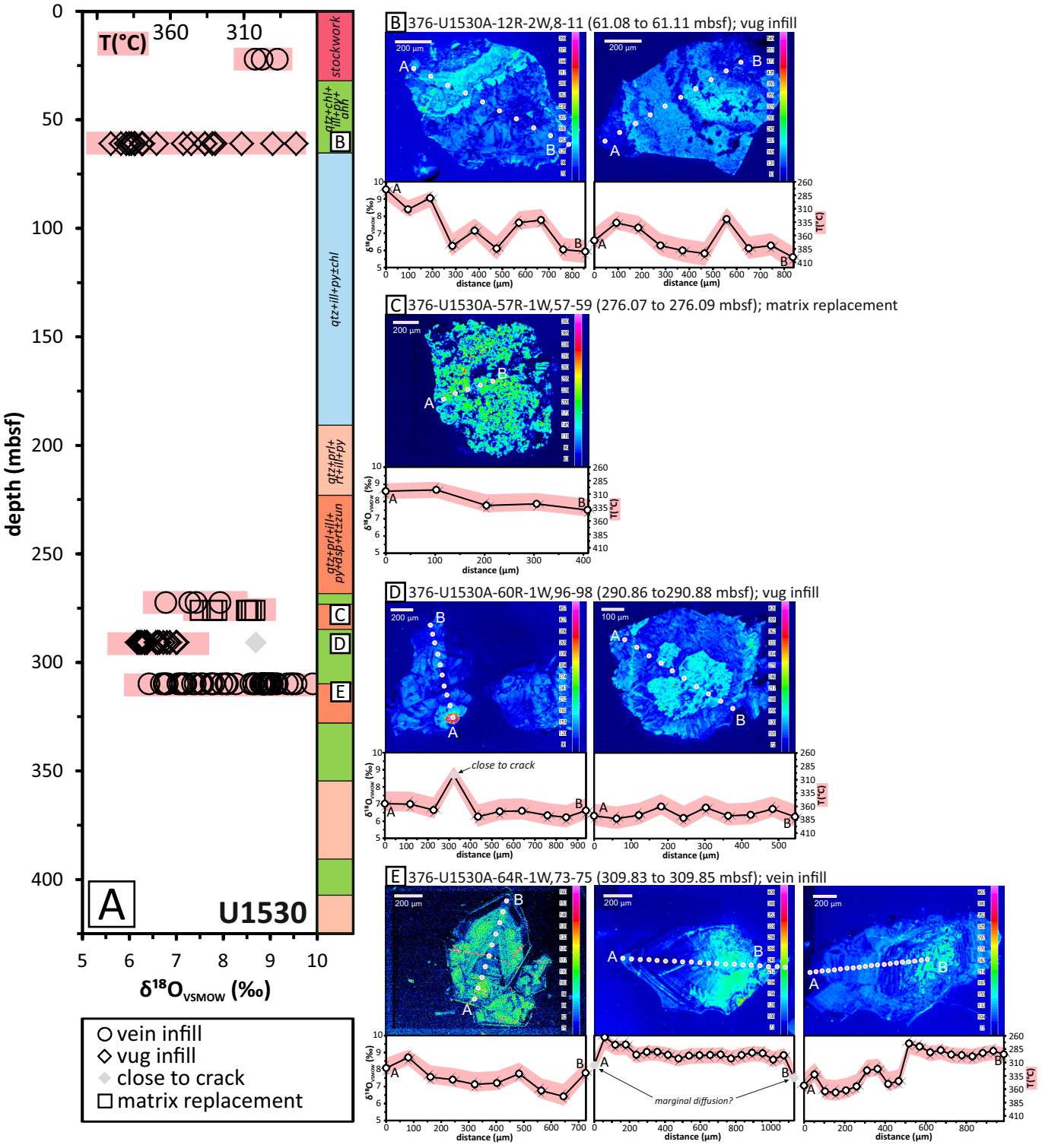
A
U1530
T(°C)
360
310
depth (mbsf)
δ18OVSMOW (‰)
stockwork
qtz+chl+ill+py+anh
qtz+ill+py±chl
qtz±prl+ill±py
qtz±prl+ill+py±sp±rt±zun
B
C
D
E
vein infill
vug infill
close to crack
matrix replacement
B 376-U1530A-12R-2W,8-11 (61.08 to 61.11 mbsf); vug infill
C 376-U1530A-57R-1W,57-59 (276.07 to 276.09 mbsf); matrix replacement
D 376-U1530A-60R-1W,96-98 (290.86 to290.88 mbsf); vug infill
close to crack
E 376-U1530A-64R-1W,73-75 (309.83 to 309.85 mbsf); vein infill
marginal diffusion?
distance (µm)
T(°C)

Fig. 7

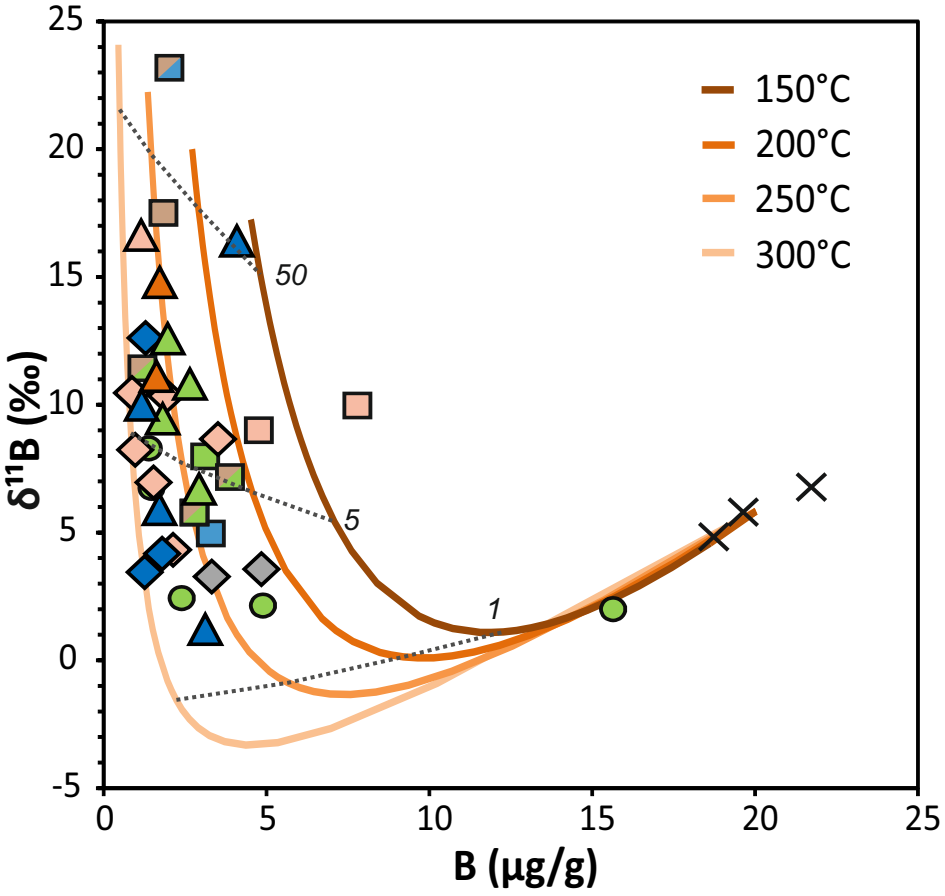

Fig. 8

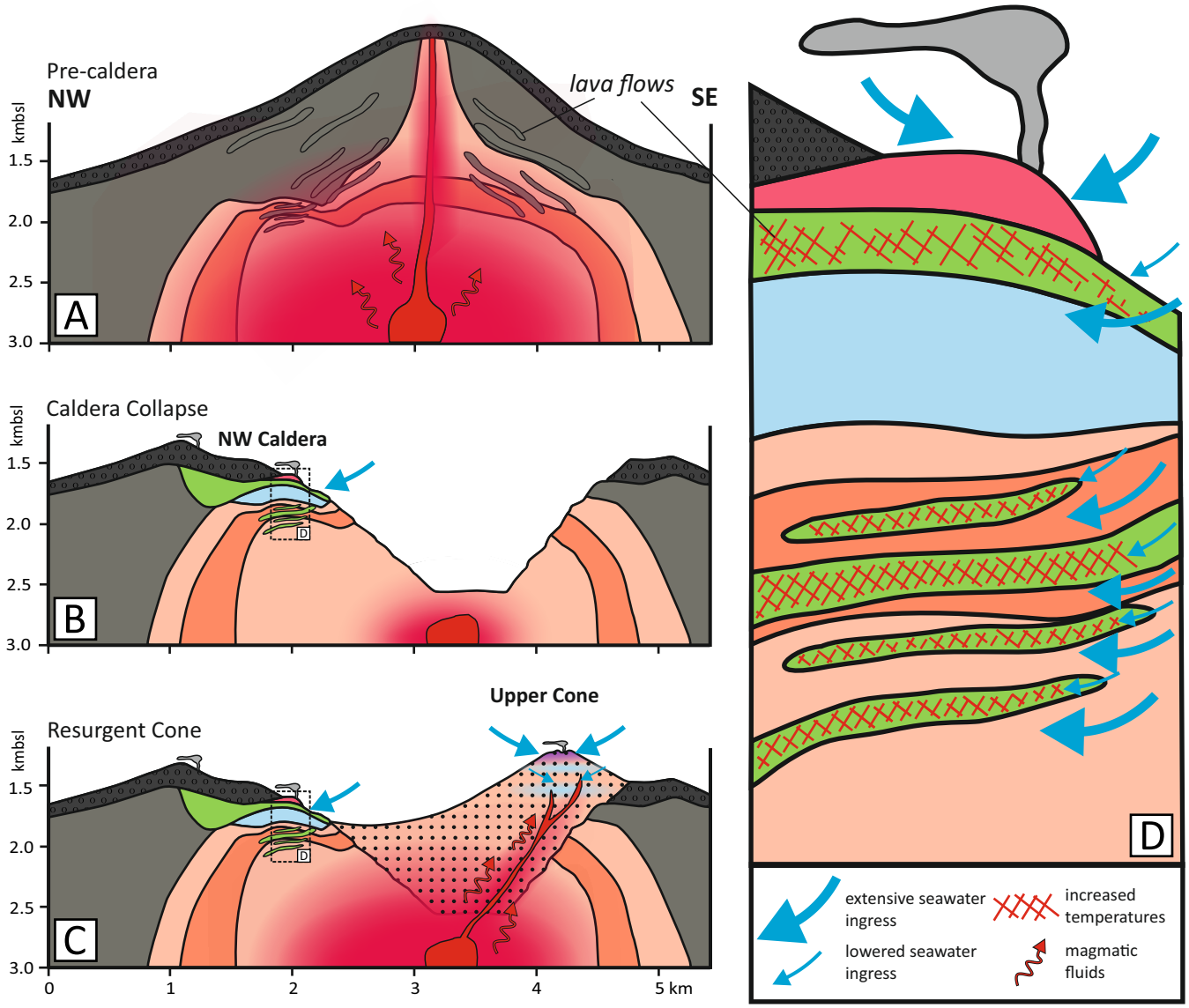
Pre-caldera
NW
lava flows
SE
kmbsl
1.5
2.0
2.5
3.0
A
Caldera Collapse
NW Caldera
D
B
Upper Cone
Resurgent Cone
C
0
1
2
3
4
5 km
D
extensive seawater ingress
lowered seawater ingress
increased temperatures
magmatic fluids

Table 1: Alteration types, secondary mineral assemblages, B concentrations and isotopic compositions of unaltered and altered rocks from Snowcap, Manus Basin.

| sample name | alteration type* | depth (mbsf) top | depth (mbsf) bottom | secondary mineral assemblage** | B µg/g | $\delta^{11}B$ ‰ | 2sd ‰ |
|---|---|---|---|---|---|---|---|
| 193-U1188A-7R-1W, 145-147 | prl-rich | 49.65 | 49.67 | anh (crs, py, prl, qtz) | 7.8 | 10.0 | 0.1 |
| 193-U1188A-10R-1W, 35-37 | prl-rich | 77.65 | 77.67 | qtz, crs (prl, ba, py) | 4.8 | 9.0 | 0.1 |
| 193-U1188A-20R-1W, 46-47 | mgt-ill-rich | 174.36 | 174.37 | qtz (plg, anh, crr, mgt, ill, py) | 2.0 | 23.2 | 0.1 |
| 193-U1188A-21R-1W, 20-21 | mgt-rich | 183.30 | 183.31 | qtz (plg, mgt, crr, py) | 1.9 | 17.5 | 0.1 |
| 193-U1188F-16Z-1W, 139-141 | ill-rich | 256.29 | 256.31 | qtz (py, ill, brittle mica, anh) | 3.3 | 5.0 | 0.1 |
| 193-U1188F-26Z-1W, 20-23 | chl-rich | 300.03 | 300.06 | qtz (anh, py, ill, chl, chl-mixed-layer, smc) | 3.1 | 8.0 | 0.1 |
| 193-U1188F-31Z-1W, 1-3 | mgt-chl-rich | 322.61 | 322.63 | qtz, plg (chl, mgt, py, anh) | 1.2 | 11.4 | 0.1 |
| 193-U1188F-34Z-1W, 40-41 | mgt-chl-rich | 336.80 | 336.81 | plg, qtz (ill, chl, py, mgt, ill-mixed-layer) | 3.9 | 7.2 | 0.1 |
| 193-U1188F-43Z-1W, 90-91 | mgt-chl-rich | 372.40 | 372.41 | qtz, plg (chl, anh, py, mgt) | 2.8 | 5.8 | 0.1 |
| SO-216-043-ROV10 | | | | fresh dacitic cap rock | 21.7 | 6.8 | 0.1 |

* alteration types are described in the chapter "Sample Material", subchapter "Snowcap, Manus Basin".

**secondary mineral assemblages were identified by XRD and taken from Lackschewitz et al. (2006).

anh=anhydrite; ba=barite; chl=chlorite; crr=corrensite; crs=cristobalite; ill=illite; mgt=magnetite; plg=plagioclase; prl=pyrophyllite; py=pyrite; qtz=quartz; smc=smectite

Table 1: Alteration types, secondary mineral assemblages, B concentratio

| sample name | alteration type* | depth (mbsf) top | depth (mbsf) bottom |
|---|---|---|---|
| 193-U1188A-7R-1W, 145-147 | prl-rich | 49.65 | 49.67 |
| 193-U1188A-10R-1W, 35-37 | prl-rich | 77.65 | 77.67 |
| 193-U1188A-20R-1W, 46-47 | mgt-ill-rich | 174.36 | 174.37 |
| 193-U1188A-21R-1W, 20-21 | mgt-rich | 183.30 | 183.31 |
| 193-U1188F-16Z-1W, 139-141 | ill-rich | 256.29 | 256.31 |
| 193-U1188F-26Z-1W, 20-23 | chl-rich | 300.03 | 300.06 |
| 193-U1188F-31Z-1W, 1-3 | mgt-chl-rich | 322.61 | 322.63 |
| 193-U1188F-34Z-1W, 40-41 | mgt-chl-rich | 336.80 | 336.81 |
| 193-U1188F-43Z-1W, 90-91 | mgt-chl-rich | 372.40 | 372.41 |
| SO-216-043-ROV10 | | | |

* alteration types are described in the chapter "Sample Material", subcha
**secondary mineral assemblages were identified by XRD and taken from

anh=anhydrite; ba=barite; chl=chlorite; crr=corrensite; crs=cristobalite; i

ns and isotopic compositions of fresh and altered rocks from Snowcap, Manus Basin.

| secondary mineral assemblage** | B µg/g | $\delta^{11}B$ ‰ | 2sd ‰ |
|---|---|---|---|
| anh (crs, py, prl, qtz) | 7.8 | 10.0 | 0.1 |
| qtz, crs (prl, ba, py) | 4.8 | 9.0 | 0.1 |
| qtz (plg, anh, crr, mgt, ill, py) | 2.0 | 23.2 | 0.1 |
| qtz (plg, mgt, crr, py) | 1.9 | 17.5 | 0.1 |
| qtz (py, ill, brittle mica, anh) | 3.3 | 5.0 | 0.1 |
| qtz (anh, py, ill, chl, chl-mixed-layer, smc) | 3.1 | 8.0 | 0.1 |
| qtz, plg (chl, mgt, py, anh) | 1.2 | 11.4 | 0.1 |
| plg, qtz (ill, chl, py, mgt, ill-mixed-layer) | 3.9 | 7.2 | 0.1 |
| qtz, plg (chl, anh, py, mgt) | 2.8 | 5.8 | 0.1 |
| fresh dacitic cap rock | 21.7 | 6.8 | 0.1 |

ɔter "Snowcap, Manus Basin"
Lackschewitz et al. (2006)

ll=illite; mgt=magnetite; plg=plagioclase; prl=pyrophyllite; py=pyrite; qtz=quartz; smc=smectite

Table 2: Alteration types, and B and Sr concentrations and isotopic compositions of altered and unaltered classified rocks from Brothers volcano, Kermadec arc.

| sample name | alteration type* | depth (mbsf) top | bottom | B† µg/g | Sr† µg/g | $\delta^{11}B$ ‰ | 2sd ‰ | $^{87}Sr/^{86}Sr$ ($2sd_{mean}$) |
|---|---|---|---|---|---|---|---|---|
| *altered rock samples* | | | | | | | | |
| 376-U1527C- | | | | | | | | |
| 11R-1W, 17-18 | chl-rich | 185.37 | 185.38 | 15.6 | 191 | 2.0 | 0.1 | 0.704621(9)† |
| 11R-1W, 143-145 | chl-rich | 186.63 | 186.65 | 4.9 | 179 | | | |
| 11R-2W, 108-110 | chl-rich | 187.74 | 187.76 | 2.2 | 187 | | | |
| 11R-3W, 8-12 | chl-rich | 188.06 | 188.10 | 4.9 | 204 | 2.1 | 0.1 | 0.704336(4) |
| 12R-1W, 142-144 | chl-rich | 196.22 | 196.24 | 2.4 | 222 | | | 0.704286(15)† |
| 13R-1W, 65-68 | chl-rich | 200.25 | 200.28 | 2.2 | 205 | | | |
| 13R-3W, 50-52 GREEN | chl-rich | 202.87 | 202.89 | 2.4 | 254 | 2.4 | 0.1 | 0.704208(4) |
| 13R-3W, 50-52 YELLOW | chl-rich | 202.87 | 202.89 | 3.5 | 216 | | | 0.704202(6) |
| 14R-1W, 32-34 | chl-rich | 204.72 | 204.74 | 1.8 | 241 | | | |
| 14R-1W, 55-58 | chl-rich | 204.95 | 204.98 | 1.8 | 234 | | | |
| 14R-2W, 47-50 | chl-rich | 205.64 | 205.67 | 2.1 | 247 | | | |
| 14R-3W, 45-49 CLAST | chl-rich | 207.01 | 207.05 | 1.6 | 242 | | | |
| 14R-3W, 45-49 MATRIX | chl-rich | 207.01 | 207.05 | 2.0 | 223 | | | |
| 15R-2W, 43-50 MIX | chl-rich | 211.02 | 211.09 | 2.2 | 222 | | | |
| 15R-2W, 43-50 CLAST | chl-rich | 211.02 | 211.09 | 2.3 | 249 | | | |
| 15R-3W, 3-6 | chl-rich | 212.12 | 212.15 | 1.9 | 240 | | | |
| 17R-2W, 45-49 | chl-rich | 220.60 | 220.64 | 1.5 | 213 | | | |
| 18R-1W,60-63 | chl-rich | 224.20 | 224.23 | 1.4 | | 8.3 | 0.1 | |
| 18R-2W, 52-56 | chl-rich | 225.51 | 225.55 | 1.5 | 200 | 6.8 | 0.1 | 0.704190(5) |
| 18R-2W, 97-99 | chl-rich | 225.96 | 225.98 | 1.7 | 188 | | | |
| 19R-1W, 71-75 | chl-rich | 229.11 | 229.15 | 1.4 | 72 | | | 0.704536(13)† |
| 19R-1W, 117-120 CLAST | chl-rich | 229.57 | 229.60 | 2.3 | 209 | | | |
| 19R-1W, 117-120 MATRIX | chl-rich | 229.57 | 229.60 | 1.5 | 121 | | | |
| 20R-1W, 40-43 | chl-rich | 233.60 | 233.63 | 1.4 | 210 | | | |
| 376-U1528A- | | | | | | | | |
| 7R-1W, 21-23 CLAST | prl-rich | 45.21 | 45.23 | 3.5 | 127 | 8.7 | 0.1 | 0.704688(9)† |
| 7R-1W, 21-23 MATRIX | prl-rich | 45.21 | 45.23 | 1.5 | 189 | 7.0 | 0.1 | 0.704935(18)† |
| 9R-2W, 97-99 CORE | ill-rich | 57.07 | 57.09 | 1.3 | 147 | 12.6 | 0.1 | 0.704555(9)† |
| 9R-2W, 97-99 HALO | prl-rich | 57.07 | 57.09 | 0.9 | 430 | 10.5 | 0.1 | 0.705622(11)† |
| 13R-1W, 57-59 | prl-rich | 74.37 | 74.39 | 1.9 | 138 | 10.4 | 0.1 | 0.704898(5) |
| 14R-1W, 53-56 CORE | ill-rich | 79.13 | 79.16 | 1.3 | 169 | | | |
| 376-U1528D- | | | | | | | | |
| 3R-1W, 75-77 | prl-rich | 66.85 | 66.87 | 1.0 | 215 | 8.3 | 0.1 | 0.706188(6) |
| 4R-2W, 28-31 CLAST | prl-rich | 72.64 | 72.75 | 0.8 | 222 | | | |
| 4R-2W, 28-31 MATRIX | ill-rich | 72.64 | 72.75 | 1.4 | 213 | | | |
| 10R-2W, 16-18 HALO | prl-rich | 101.72 | 101.74 | 0.9 | 424 | | | |
| 11R-1W, 100-102 | ill-rich | 105.90 | 105.92 | 1.3 | 220 | 3.5 | 0.1 | 0.704721(5) |
| 11R-3W, 44-46 CORE | ill-rich | 108.33 | 108.35 | 1.8 | 340 | | | |
| 11R-3W, 44-46 HALO | prl-rich | 108.33 | 108.35 | 1.3 | 206 | | | |
| 14R-1W, 80-82 | ill-rich | 120.10 | 120.12 | 1.0 | 226 | | | |
| 16R-1W, 48-50 MATRIX | ill-rich | 129.38 | 129.40 | 1.1 | 196 | | | |
| 16R-1W, 48-50 CLAST | prl-rich | 129.38 | 129.40 | 0.8 | 235 | | | |
| 21R-1W, 16-18 | ill-rich | 153.06 | 153.08 | 1.8 | 148 | 4.2 | 0.1 | 0.705048(5) |
| 23R-1W, 61-63 | prl-rich | 163.11 | 163.13 | 0.8 | 232 | | | |
| 29R-1W, 65-67 | prl-rich | 191.95 | 191.97 | 2.0 | 150 | | | |
| 45R-1W, 52-54 | prl-rich | 268.62 | 268.64 | 0.9 | 271 | | | |
| 46R-1W, 32-34 CORE | weakly altered | 273.22 | 273.24 | 4.8 | 189 | 3.6 | 0.1 | 0.704191(19)† |
| 46R-1W, 32-34 HALO | prl-rich | 273.22 | 273.24 | 3.9 | 190 | | | |
| 49R-1W, 19-21 | prl-rich | 287.49 | 287.51 | 1.5 | 174 | | | |
| 51R-1W, 60-62 | prl-rich | 297.50 | 297.52 | 1.0 | 213 | | | |
| 51R-1W, 60-62 (replicate) | prl-rich | 297.50 | 297.52 | 1.8 | 194 | | | |
| 55R-1W, 51-53 | prl-rich | 316.61 | 316.63 | 0.8 | 169 | | | |
| 57R-1W, 15-18 CORE | weakly altered | 325.85 | 325.88 | 3.3 | 192 | 3.3 | 0.1 | 0.704227(14)† |
| 57R-1W, 15-18 HALO | prl-rich | 325.85 | 325.88 | 2.1 | 203 | 4.3 | 0.1 | 0.704383(6) |
| 376-U1530A- | | | | | | | | |
| 3R-1W, 60-62 | stockwork | 17.50 | 17.52 | 1.6 | 297 | | | |
| 4R-1W, 67-69 | stockwork | 22.07 | 22.09 | 1.6 | 766 | | | 0.706376(5) |
| 8R-1W, 19-21 | chl-rich (sandstone) | 40.49 | 40.51 | 4.4 | 15 | | | 0.705059(7) |
| 12R-2W, 8-11 | chl-rich (lava flow) | 61.08 | 61.11 | 2.7 | 87 | 10.8 | 0.1 | 0.706809(7) |
| 13R-1W, 100-102 | ill-rich | 65.30 | 65.32 | 4.1 | 84 | 16.4 | 0.1 | 0.706982(13)† |
| 15R-2W, 43-45 | ill-rich | 75.78 | 75.85 | 5.2 | 124 | | | |
| 20R-1W, 24-26 | ill-rich | 98.14 | 98.16 | 1.2 | 29 | 10.0 | 0.1 | 0.706354(8) |

| | | | | | | | | |
|---|---|---|---|---|---|---|---|---|
| 25R-1W, 43-45 | ill-rich | 122.33 | 122.35 | 2.5 | 21 | | | |
| 26R-1W, 41-43 CLAST | ill-rich | 127.11 | 127.13 | 3.1 | 39 | 1.2 | 0.1 | 0.706436(14)† |
| 26R-1W, 41-43 MATRIX | ill-rich | 127.11 | 127.13 | 1.7 | 19 | 5.9 | 0.1 | 0.705929(17)† |
| 29R-1W, 22-24 | ill-rich | 141.32 | 141.34 | 1.9 | 42 | | | |
| 39R-1W, 6-8 | prl-rich | 189.16 | 189.18 | 2.0 | 58 | | | |
| 39R-2W, 78-80 | prl-rich | 191.38 | 191.40 | 1.2 | 45 | 16.7 | 0.1 | 0.705990(6) |
| 39R-2W, 78-80 (replicate) | prl-rich | 191.38 | 191.40 | | | | | 0.706007(14)† |
| 48R-1W, 45-47 | prl-dsp-rich | 232.75 | 232.77 | 1.3 | 214 | | | 0.706301(7) |
| 55R-1W, 137-139 | prl-dsp-rich | 267.27 | 267.29 | 1.7 | 91 | 14.8 | 0.1 | 0.706145(3) |
| 56R-2W, 40-42 | prl-dsp-rich | 272.40 | 272.42 | 1.6 | 240 | | | |
| 57R-1W, 57-59 | prl-dsp-rich | 276.07 | 276.09 | 1.6 | 284 | 11.1 | 0.1 | 0.706962(14) |
| 60R-1W, 96-98 | chl-rich (lava flow) | 290.86 | 290.88 | 2.0 | 16 | 12.6 | 0.1 | 0.704763(7) |
| 64R-1W, 73-75 | prl-dsp-rich | 309.83 | 309.85 | 2.3 | 79 | | | |
| 76R-1W, 36-38 | prl-rich | 367.06 | 367.08 | 1.2 | 170 | | | 0.706326(15)† |
| 81R-1W, 41-44 | chl-rich (lava flow) | 391.11 | 391.14 | 1.8 | 77 | 9.5 | 0.1 | 0.706072(25)† |
| 82R-1W, 38-40 | prl-rich | 395.88 | 395.90 | 1.7 | 81 | | | |
| 83R-1W, 49-51 | chl-rich (lava flow) | 400.79 | 400.81 | 2.9 | 68 | 6.7 | 0.1 | 0.705891(17)† |
| 88R-1W, 42-45 | prl-rich | 424.72 | 424.75 | 1.1 | 20 | | | |

| *petrographic unaltered rock samples* | | | | **B** µg/g | **Sr** µg/g | **$\delta^{11}B$** ‰ | **2sd** ‰ | **$^{87}Sr/^{86}Sr(2sd_{mean})$** |
|---|---|---|---|---|---|---|---|---|
| 376-U1527A-6R-1W,71-78 | | 49.21 | 49.28 | | 215◊ | | | |
| 376-U1528D-21R-1W,75-79 | | 153.65 | 153.69 | | 202◊ | | | |
| | **water depth [m]** | **Latitude** | **Longitude** | | | | | |
| SO-253-045-7R (Lower Cone) | 1317 | 34° 52.730' S | 179° 04.266' E | 18.7 | 232Δ | 4.8 | 0.1 | 0.703970(4) |
| SO-253-081-10B (NW Caldera) | 1580 | 34° 51.659' S | 179° 03.438' E | 19.6 | 229Δ | 5.8 | 0.1 | 0.704109(6)Δ |

*alteration types are described in the chapter "Sample Material", subchapter "Brothers volcano, Kermadec Arc".

†measurements were performed at the PSO, Brest.

◊measurements were performed at the GEOMAR, Kiel.

Δdata were taken from Diehl (2019).

all measurements without special indications were performed at the MARUM, University of Bremen

mineral abbreviations: chl=chlorite; prl=pyrophyllite; ill=illite; dsp=diaspore

Table 2: Alteration types, B and Sr concentrations and B and Sr isotopic compositions of alte

| sample name | alteration type* | depth (mbsf) top | bottom |
|---|---|---|---|
| *altered rock samples* | | | |
| 376-U1527C- | | | |
| 11R-1W, 17-18 | chl-rich | 185.37 | 185.38 |
| 11R-1W, 143-145 | chl-rich | 186.63 | 186.65 |
| 11R-2W, 108-110 | chl-rich | 187.74 | 187.76 |
| 11R-3W, 8-12 | chl-rich | 188.06 | 188.10 |
| 12R-1W, 142-144 | chl-rich | 196.22 | 196.24 |
| 13R-1W, 65-68 | chl-rich | 200.25 | 200.28 |
| 13R-3W, 50-52 GREEN | chl-rich | 202.87 | 202.89 |
| 13R-3W, 50-52 YELLOW | chl-rich | 202.87 | 202.89 |
| 14R-1W, 32-34 | chl-rich | 204.72 | 204.74 |
| 14R-1W, 55-58 | chl-rich | 204.95 | 204.98 |
| 14R-2W, 47-50 | chl-rich | 205.64 | 205.67 |
| 14R-3W, 45-49 CLAST | chl-rich | 207.01 | 207.05 |
| 14R-3W, 45-49 MATRIX | chl-rich | 207.01 | 207.05 |
| 15R-2W, 43-50 MIX | chl-rich | 211.02 | 211.09 |
| 15R-2W, 43-50 CLAST | chl-rich | 211.02 | 211.09 |
| 15R-3W, 3-6 | chl-rich | 212.12 | 212.15 |
| 17R-2W, 45-49 | chl-rich | 220.60 | 220.64 |
| 18R-1W,60-63 | chl-rich | 224.20 | 224.23 |
| 18R-2W, 52-56 | chl-rich | 225.51 | 225.55 |
| 18R-2W, 97-99 | chl-rich | 225.96 | 225.98 |
| 19R-1W, 71-75 | chl-rich | 229.11 | 229.15 |
| 19R-1W, 117-120 CLAST | chl-rich | 229.57 | 229.60 |
| 19R-1W, 117-120 MATRIX | chl-rich | 229.57 | 229.60 |
| 20R-1W, 40-43 | chl-rich | 233.60 | 233.63 |
| 376-U1528A- | | | |
| 7R-1W, 21-23 CLAST | prl-rich | 45.21 | 45.23 |
| 7R-1W, 21-23 MATRIX | prl-rich | 45.21 | 45.23 |
| 9R-2W, 97-99 CORE | ill-rich | 57.07 | 57.09 |
| 9R-2W, 97-99 HALO | prl-rich | 57.07 | 57.09 |
| 13R-1W, 57-59 | prl-rich | 74.37 | 74.39 |
| 14R-1W, 53-56 CORE | ill-rich | 79.13 | 79.16 |
| 376-U1528D- | | | |
| 3R-1W, 75-77 | prl-rich | 66.85 | 66.87 |
| 4R-2W, 28-31 CLAST | prl-rich | 72.64 | 72.75 |
| 4R-2W, 28-31 MATRIX | ill-rich | 72.64 | 72.75 |
| 10R-2W, 16-18 HALO | prl-rich | 101.72 | 101.74 |

| | | | | |
|---|---|---|---|---|
| | 11R-1W, 100-102 | ill-rich | 105.90 | 105.92 |
| | 11R-3W, 44-46 CORE | ill-rich | 108.33 | 108.35 |
| | 11R-3W, 44-46 HALO | prl-rich | 108.33 | 108.35 |
| | 14R-1W, 80-82 | ill-rich | 120.10 | 120.12 |
| | 16R-1W, 48-50 MATRIX | ill-rich | 129.38 | 129.40 |
| | 16R-1W, 48-50 CLAST | prl-rich | 129.38 | 129.40 |
| | 21R-1W, 16-18 | ill-rich | 153.06 | 153.08 |
| | 23R-1W, 61-63 | prl-rich | 163.11 | 163.13 |
| | 29R-1W, 65-67 | prl-rich | 191.95 | 191.97 |
| | 45R-1W, 52-54 | prl-rich | 268.62 | 268.64 |
| | 46R-1W, 32-34 CORE | weakly altered | 273.22 | 273.24 |
| | 46R-1W, 32-34 HALO | prl-rich | 273.22 | 273.24 |
| | 49R-1W, 19-21 | prl-rich | 287.49 | 287.51 |
| | 51R-1W, 60-62 | prl-rich | 297.50 | 297.52 |
| | 51R-1W, 60-62 (replicate) | prl-rich | 297.50 | 297.52 |
| | 55R-1W, 51-53 | prl-rich | 316.61 | 316.63 |
| | 57R-1W, 15-18 CORE | weakly altered | 325.85 | 325.88 |
| | 57R-1W, 15-18 HALO | prl-rich | 325.85 | 325.88 |
| | | | | |
| | 376-U1530A- | | | |
| 58 | 3R-1W, 60-62 | stockwork | 17.50 | 17.52 |
| 59 | 4R-1W, 67-69 | stockwork | 22.07 | 22.09 |
| 60 | 8R-1W, 19-21 | chl-rich (sandstone) | 40.49 | 40.51 |
| 61 | 12R-2W, 8-11 | chl-rich (lava flow) | 61.08 | 61.11 |
| 62 | 13R-1W, 100-102 | ill-rich | 65.30 | 65.32 |
| 63 | 15R-2W, 43-45 | ill-rich | 75.78 | 75.85 |
| 64 | 20R-1W, 24-26 | ill-rich | 98.14 | 98.16 |
| 65 | 25R-1W, 43-45 | ill-rich | 122.33 | 122.35 |
| 66 | 26R-1W, 41-43 CLAST | ill-rich | 127.11 | 127.13 |
| 67 | 26R-1W, 41-43 MATRIX | ill-rich | 127.11 | 127.13 |
| 68 | 29R-1W, 22-24 | ill-rich | 141.32 | 141.34 |
| 69 | 39R-1W, 6-8 | prl-rich | 189.16 | 189.18 |
| 70 | 39R-2W, 78-80 | prl-rich | 191.38 | 191.40 |
| 70 | 39R-2W, 78-80 (replicate) | prl-rich | 191.38 | 191.40 |
| 71 | 48R-1W, 45-47 | prl-dsp-rich | 232.75 | 232.77 |
| 72 | 55R-1W, 137-139 | prl-dsp-rich | 267.27 | 267.29 |
| 73 | 56R-2W, 40-42 | prl-dsp-rich | 272.40 | 272.42 |
| 74 | 57R-1W, 57-59 | prl-dsp-rich | 276.07 | 276.09 |
| 75 | 60R-1W, 96-98 | chl-rich (lava flow) | 290.86 | 290.88 |
| 76 | 64R-1W, 73-75 | prl-dsp-rich | 309.83 | 309.85 |
| 77 | 76R-1W, 36-38 | prl-rich | 367.06 | 367.08 |
| 78 | 81R-1W, 41-44 | chl-rich (lava flow) | 391.11 | 391.14 |
| 79 | 82R-1W, 38-40 | prl-rich | 395.88 | 395.90 |
| 80 | 83R-1W, 49-51 | chl-rich (lava flow) | 400.79 | 400.81 |

| | | | | |
|---|---|---|---|---|
| 81 | 88R-1W, 42-45 | prl-rich | 424.72 | 424.75 |

*petrographic unaltered rock samples*

| | | | |
|---|---|---|---|
| 376-U1527A-6R-1W,71-78 | | 49.21 | 49.28 |
| 376-U1528D-21R-1W,75-79 | | 153.65 | 153.69 |
| | **water depth [m]** | **Latitude** | **Longitude** |
| SO-253-045-7R (Lower Cone) | 1317 | 34° 52.730' S | 179° 04.266' E |
| SO-253-081-10B (NW Caldera) | 1580 | 34° 51.659' S | 179° 03.438' E |

*alteration types are described in the chapter "Sample Material", subchapter "Brothers volca

†measurements were performed at the PSO, Brest

◊measurements were performed at the GEOMAR, Kiel

Δdata were taken from Diehl (2019)

all measurements without special indications were performed at the MARUM, University of

mineral abbreviations: chl=chlorite; prl=pyrophyllite; ill=illite; dsp=diaspore

ered and unaltered classified rocks based on petrographic characteristics from Brothers volcano, Kerr

| B[†] µg/g | Sr[†] µg/g | $\delta^{11}B$ ‰ | 2sd ‰ | $^{87}Sr/^{86}Sr$ (2sd) |
|---|---|---|---|---|
| 15.6 | 191 | 2.0 | 0.1 | 0.704621(9)[†] |
| 4.9 | 179 | | | |
| 2.2 | 187 | | | |
| 4.9 | 204 | 2.1 | 0.1 | 0.704336(4) |
| 2.4 | 222 | | | 0.704286(15)[†] |
| 2.2 | 205 | | | |
| 2.4 | 254 | 2.4 | 0.1 | 0.704208(4) |
| 3.5 | 216 | | | 0.704202(6) |
| 1.8 | 241 | | | |
| 1.8 | 234 | | | |
| 2.1 | 247 | | | |
| 1.6 | 242 | | | |
| 2.0 | 223 | | | |
| 2.2 | 222 | | | |
| 2.3 | 249 | | | |
| 1.9 | 240 | | | |
| 1.5 | 213 | | | |
| 1.4 | | 8.3 | 0.1 | |
| 1.5 | 200 | 6.8 | 0.1 | 0.704190(5) |
| 1.7 | 188 | | | |
| 1.4 | 72 | | | 0.704536(13)[†] |
| 2.3 | 209 | | | |
| 1.5 | 121 | | | |
| 1.4 | 210 | | | |
| 3.5 | 127 | 8.7 | 0.1 | 0.704688(9)[†] |
| 1.5 | 189 | 7.0 | 0.1 | 0.704935(18)[†] |
| 1.3 | 147 | 12.6 | 0.1 | 0.704555(9)[†] |
| 0.9 | 430 | 10.5 | 0.1 | 0.705622(11)[†] |
| 1.9 | 138 | 10.4 | 0.1 | 0.704898(5) |
| 1.3 | 169 | | | |
| 1.0 | 215 | 8.3 | 0.1 | 0.706188(6) |
| 0.8 | 222 | | | |
| 1.4 | 213 | | | |
| 0.9 | 424 | | | |

| | | | | |
|---|---|---|---|---|
| 1.3 | 220 | 3.5 | 0.1 | 0.704721(5) |
| 1.8 | 340 | | | |
| 1.3 | 206 | | | |
| 1.0 | 226 | | | |
| 1.1 | 196 | | | |
| 0.8 | 235 | | | |
| 1.8 | 148 | 4.2 | 0.1 | 0.705048(5) |
| 0.8 | 232 | | | |
| 2.0 | 150 | | | |
| 0.9 | 271 | | | |
| 4.8 | 189 | 3.6 | 0.1 | 0.704191(19)† |
| 3.9 | 190 | | | |
| 1.5 | 174 | | | |
| 1.0 | 213 | | | |
| 1.8 | 194 | | | |
| 0.8 | 169 | | | |
| 3.3 | 192 | 3.3 | 0.1 | 0.704227(14)† |
| 2.1 | 203 | 4.3 | 0.1 | 0.704383(6) |

---

| | | | | |
|---|---|---|---|---|
| 1.6 | 297 | | | |
| 1.6 | 766 | | | 0.706376(5) |
| 4.4 | 15 | | | 0.705059(7) |
| 2.7 | 87 | 10.8 | 0.1 | 0.706809(7) |
| 4.1 | 84 | 16.4 | 0.1 | 0.706982(13)† |
| 5.2 | 124 | | | |
| 1.2 | 29 | 10.0 | 0.1 | 0.706354(8) |
| 2.5 | 21 | | | |
| 3.1 | 39 | 1.2 | 0.1 | 0.706436(14)† |
| 1.7 | 19 | 5.9 | 0.1 | 0.705929(17)† |
| 1.9 | 42 | | | |
| 2.0 | 58 | | | |
| 1.2 | 45 | 16.7 | 0.1 | 0.705990(6) |
| | | | | 0.706007(14)† |
| 1.3 | 214 | | | 0.706301(7) |
| 1.7 | 91 | 14.8 | 0.1 | 0.706145(3) |
| 1.6 | 240 | | | |
| 1.6 | 284 | 11.1 | 0.1 | 0.706962(14) |
| 2.0 | 16 | 12.6 | 0.1 | 0.704763(7) |
| 2.3 | 79 | | | |
| 1.2 | 170 | | | 0.706326(15)† |
| 1.8 | 77 | 9.5 | 0.1 | 0.706072(25)† |
| 1.7 | 81 | | | |
| 2.9 | 68 | 6.7 | 0.1 | 0.705891(17)† |

1.1 20

| B<br>µg/g | Sr<br>µg/g | $\delta^{11}B$<br>‰ | 2sd<br>‰ | $^{87}Sr/^{86}Sr$(2sd) |
|---|---|---|---|---|
| | 215[◊] | | | |
| | 202[◊] | | | |
| 18.7 | 232[Δ] | 4.8 | 0.1 | 0.703970(4) |
| 19.6 | 229[Δ] | 5.8 | 0.1 | 0.704109(6)[Δ] |

ano, Kermadec Arc"

Bremen

nadec arc.

Table 3: Oxygen isotope ratios ($\delta^{18}O_{VSMOW}$) measured by SIMS of quartz single crystal domains from Hole U1530A, NW Caldera, Brothers volcano.

| Host rock | | depth (mbsf) | | quartz separate | | | $\delta^{18}O_{VSMOW}$ | 2sd | temperature (°C)† | |
|---|---|---|---|---|---|---|---|---|---|---|
| sample name | alteration type* | top | bottom | grain No. | point No. | description | (‰) | (‰) | $\delta^{18}O_{water}$ = 0 ‰◊ | = +1 ‰◊ |
| *376-U1530A-* | | | | | | | | | | |
| 4R-1W, 67-69 | stockwork | 22.07 | 22.09 | LSM1-17 | 1 | vein infill | 9.2 | 0.2 | 278 | 303 |
| 4R-1W, 67-69 | stockwork | 22.07 | 22.09 | LSM1-17 | 2 | vein infill | 8.8 | 0.2 | 286 | 311 |
| 4R-1W, 67-69 | stockwork | 22.07 | 22.09 | LSM1-18 | 1 | vein infill | 8.7 | 0.2 | 289 | 315 |
| 12R-2W, 8-11 | chl-rich (lava flow) | 61.08 | 61.11 | LSM1-14 | 1 | vug infill | 9.6 | 0.2 | 269 | 292 |
| 12R-2W, 8-11 | chl-rich (lava flow) | 61.08 | 61.11 | LSM1-14 | 2 | vug infill | 8.4 | 0.2 | 296 | 323 |
| 12R-2W, 8-11 | chl-rich (lava flow) | 61.08 | 61.11 | LSM1-14 | 3 | vug infill | 9.1 | 0.2 | 280 | 305 |
| 12R-2W, 8-11 | chl-rich (lava flow) | 61.08 | 61.11 | LSM1-14 | 4 | vug infill | 6.3 | 0.2 | 359 | 396 |
| 12R-2W, 8-11 | chl-rich (lava flow) | 61.08 | 61.11 | LSM1-14 | 5 | vug infill | 7.1 | 0.2 | 330 | 363 |
| 12R-2W, 8-11 | chl-rich (lava flow) | 61.08 | 61.11 | LSM1-14 | 6 | vug infill | 6.1 | 0.2 | 364 | 403 |
| 12R-2W, 8-11 | chl-rich (lava flow) | 61.08 | 61.11 | LSM1-14 | 7 | vug infill | 7.6 | 0.2 | 317 | 347 |
| 12R-2W, 8-11 | chl-rich (lava flow) | 61.08 | 61.11 | LSM1-14 | 8 | vug infill | 7.8 | 0.2 | 313 | 342 |
| 12R-2W, 8-11 | chl-rich (lava flow) | 61.08 | 61.11 | LSM1-14 | 9 | vug infill | 6.0 | 0.2 | 366 | 405 |
| 12R-2W, 8-11 | chl-rich (lava flow) | 61.08 | 61.11 | LSM1-14 | 10 | vug infill | 5.9 | 0.2 | 370 | 410 |
| 12R-2W, 8-11 | chl-rich (lava flow) | 61.08 | 61.11 | LSM1-16 | 1 | vug infill | 5.6 | 0.1 | 383 | 425 |
| 12R-2W, 8-11 | chl-rich (lava flow) | 61.08 | 61.11 | LSM1-16 | 2 | vug infill | 6.3 | 0.1 | 358 | 395 |
| 12R-2W, 8-11 | chl-rich (lava flow) | 61.08 | 61.11 | LSM1-16 | 3 | vug infill | 6.1 | 0.1 | 363 | 402 |
| 12R-2W, 8-11 | chl-rich (lava flow) | 61.08 | 61.11 | LSM1-16 | 4 | vug infill | 7.8 | 0.1 | 311 | 340 |
| 12R-2W, 8-11 | chl-rich (lava flow) | 61.08 | 61.11 | LSM1-16 | 5 | vug infill | 5.8 | 0.1 | 374 | 415 |
| 12R-2W, 8-11 | chl-rich (lava flow) | 61.08 | 61.11 | LSM1-16 | 6 | vug infill | 6.0 | 0.1 | 368 | 407 |
| 12R-2W, 8-11 | chl-rich (lava flow) | 61.08 | 61.11 | LSM1-16 | 7 | vug infill | 6.3 | 0.1 | 358 | 395 |
| 12R-2W, 8-11 | chl-rich (lava flow) | 61.08 | 61.11 | LSM1-16 | 8 | vug infill | 7.3 | 0.1 | 325 | 357 |
| 12R-2W, 8-11 | chl-rich (lava flow) | 61.08 | 61.11 | LSM1-16 | 9 | vug infill | 7.6 | 0.1 | 317 | 347 |
| 12R-2W, 8-11 | chl-rich (lava flow) | 61.08 | 61.11 | LSM1-16 | 10 | vug infill | 6.6 | 0.2 | 348 | 384 |
| 56R-2W, 40-42 | prl-dsp-rich | 272.40 | 272.42 | LSM1-3 | 1 | vein infill | 7.4 | 0.1 | 322 | 354 |
| 56R-2W, 40-42 | prl-dsp-rich | 272.40 | 272.42 | LSM1-3 | 2 | vein infill | 7.3 | 0.1 | 326 | 358 |
| 56R-2W, 40-42 | prl-dsp-rich | 272.40 | 272.42 | LSM1-10 | 1 | vein infill | 6.8 | 0.1 | 342 | 376 |
| 56R-2W, 40-42 | prl-dsp-rich | 272.40 | 272.42 | LSM1-10 | 2 | vein infill | 7.9 | 0.1 | 308 | 337 |
| 57R-1W, 57-59 | prl-dsp-rich | 276.07 | 276.09 | LSM1-1 | 1 | matrix replacement | 8.5 | 0.1 | 294 | 320 |
| 57R-1W, 57-59 | prl-dsp-rich | 276.07 | 276.09 | LSM1-1 | 2 | matrix replacement | 8.5 | 0.1 | 293 | 320 |
| 57R-1W, 57-59 | prl-dsp-rich | 276.07 | 276.09 | LSM1-2 | 1 | matrix replacement | 7.5 | 0.1 | 320 | 351 |
| 57R-1W, 57-59 | prl-dsp-rich | 276.07 | 276.09 | LSM1-2 | 2 | matrix replacement | 7.9 | 0.1 | 310 | 339 |
| 57R-1W, 57-59 | prl-dsp-rich | 276.07 | 276.09 | LSM1-2 | 3 | matrix replacement | 7.8 | 0.1 | 313 | 342 |
| 57R-1W, 57-59 | prl-dsp-rich | 276.07 | 276.09 | LSM1-2 | 4 | matrix replacement | 8.7 | 0.1 | 289 | 315 |
| 57R-1W, 57-59 | prl-dsp-rich | 276.07 | 276.09 | LSM1-2 | 5 | matrix replacement | 8.6 | 0.1 | 291 | 317 |
| 60R-1W, 96-98 | chl-rich (lava flow) | 290.86 | 290.88 | LSM1-4 | 1 | vug infill | 7.0 | 0.1 | 334 | 367 |
| 60R-1W, 96-98 | chl-rich (lava flow) | 290.86 | 290.88 | LSM1-4 | 2 | vug infill | 7.0 | 0.1 | 335 | 368 |
| 60R-1W, 96-98 | chl-rich (lava flow) | 290.86 | 290.88 | LSM1-4 | 3 | vug infill | 6.6 | 0.1 | 346 | 381 |
| 60R-1W, 96-98 | chl-rich (lava flow) | 290.86 | 290.88 | LSM1-4 | 4 | vug infill; point close to crack | 8.7 | 0.1 | 289 | 315 |
| 60R-1W, 96-98 | chl-rich (lava flow) | 290.86 | 290.88 | LSM1-4 | 5 | vug infill | 6.3 | 0.1 | 359 | 397 |
| 60R-1W, 96-98 | chl-rich (lava flow) | 290.86 | 290.88 | LSM1-4 | 6 | vug infill | 6.6 | 0.1 | 348 | 384 |
| 60R-1W, 96-98 | chl-rich (lava flow) | 290.86 | 290.88 | LSM1-4 | 7 | vug infill | 6.6 | 0.1 | 347 | 383 |
| 60R-1W, 96-98 | chl-rich (lava flow) | 290.86 | 290.88 | LSM1-4 | 8 | vug infill | 6.3 | 0.1 | 356 | 393 |
| 60R-1W, 96-98 | chl-rich (lava flow) | 290.86 | 290.88 | LSM1-4 | 9 | vug infill | 6.2 | 0.1 | 360 | 398 |
| 60R-1W, 96-98 | chl-rich (lava flow) | 290.86 | 290.88 | LSM1-4 | 10 | vug infill | 6.6 | 0.1 | 347 | 383 |
| 60R-1W, 96-98 | chl-rich (lava flow) | 290.86 | 290.88 | LSM1-5 | 1 | vug infill | 6.3 | 0.1 | 358 | 396 |
| 60R-1W, 96-98 | chl-rich (lava flow) | 290.86 | 290.88 | LSM1-5 | 2 | vug infill | 6.7 | 0.1 | 343 | 378 |
| 60R-1W, 96-98 | chl-rich (lava flow) | 290.86 | 290.88 | LSM1-5 | 3 | vug infill | 6.4 | 0.1 | 355 | 391 |
| 60R-1W, 96-98 | chl-rich (lava flow) | 290.86 | 290.88 | LSM1-5 | 4 | vug infill | 6.3 | 0.1 | 356 | 394 |
| 60R-1W, 96-98 | chl-rich (lava flow) | 290.86 | 290.88 | LSM1-5 | 5 | vug infill | 6.8 | 0.1 | 341 | 375 |
| 60R-1W, 96-98 | chl-rich (lava flow) | 290.86 | 290.88 | LSM1-5 | 6 | vug infill | 6.2 | 0.1 | 361 | 399 |
| 60R-1W, 96-98 | chl-rich (lava flow) | 290.86 | 290.88 | LSM1-5 | 7 | vug infill | 6.9 | 0.1 | 339 | 373 |
| 60R-1W, 96-98 | chl-rich (lava flow) | 290.86 | 290.88 | LSM1-5 | 8 | vug infill | 6.4 | 0.1 | 355 | 392 |
| 60R-1W, 96-98 | chl-rich (lava flow) | 290.86 | 290.88 | LSM1-5 | 9 | vug infill | 6.2 | 0.1 | 362 | 400 |
| 60R-1W, 96-98 | chl-rich (lava flow) | 290.86 | 290.88 | LSM1-5 | 10 | vug infill | 6.3 | 0.1 | 357 | 394 |
| 64R-1W, 73-75 | prl-dsp-rich | 309.83 | 309.85 | LSM1-11 | 1 | vein infill | 8.1 | 0.2 | 304 | 332 |
| 64R-1W, 73-75 | prl-dsp-rich | 309.83 | 309.85 | LSM1-11 | 2 | vein infill | 8.7 | 0.2 | 288 | 314 |
| 64R-1W, 73-75 | prl-dsp-rich | 309.83 | 309.85 | LSM1-11 | 3 | vein infill | 7.6 | 0.2 | 318 | 349 |
| 64R-1W, 73-75 | prl-dsp-rich | 309.83 | 309.85 | LSM1-11 | 4 | vein infill | 7.4 | 0.2 | 323 | 354 |
| 64R-1W, 73-75 | prl-dsp-rich | 309.83 | 309.85 | LSM1-11 | 5 | vein infill | 7.1 | 0.2 | 331 | 363 |
| 64R-1W, 73-75 | prl-dsp-rich | 309.83 | 309.85 | LSM1-11 | 6 | vein infill | 7.2 | 0.2 | 329 | 361 |
| 64R-1W, 73-75 | prl-dsp-rich | 309.83 | 309.85 | LSM1-11 | 7 | vein infill | 7.8 | 0.2 | 313 | 343 |
| 64R-1W, 73-75 | prl-dsp-rich | 309.83 | 309.85 | LSM1-11 | 8 | vein infill | 6.8 | 0.2 | 342 | 377 |
| 64R-1W, 73-75 | prl-dsp-rich | 309.83 | 309.85 | LSM1-11 | 9 | vein infill | 6.4 | 0.2 | 353 | 390 |
| 64R-1W, 73-75 | prl-dsp-rich | 309.83 | 309.85 | LSM1-11 | 10 | vein infill | 7.8 | 0.2 | 312 | 341 |
| 64R-1W, 73-75 | prl-dsp-rich | 309.83 | 309.85 | LSM1-12 | 1 | vein infill; marginal diffusion? | 7.5 | 0.2 | 319 | 350 |
| 64R-1W, 73-75 | prl-dsp-rich | 309.83 | 309.85 | LSM1-12 | 2 | vein infill | 8.8 | 0.2 | 285 | 311 |
| 64R-1W, 73-75 | prl-dsp-rich | 309.83 | 309.85 | LSM1-12 | 3 | vein infill | 8.6 | 0.2 | 291 | 318 |
| 64R-1W, 73-75 | prl-dsp-rich | 309.83 | 309.85 | LSM1-12 | 4 | vein infill | 9.0 | 0.2 | 283 | 308 |
| 64R-1W, 73-75 | prl-dsp-rich | 309.83 | 309.85 | LSM1-12 | 5 | vein infill | 9.0 | 0.2 | 282 | 307 |
| 64R-1W, 73-75 | prl-dsp-rich | 309.83 | 309.85 | LSM1-12 | 6 | vein infill | 8.9 | 0.2 | 285 | 311 |
| 64R-1W, 73-75 | prl-dsp-rich | 309.83 | 309.85 | LSM1-12 | 7 | vein infill | 8.6 | 0.2 | 290 | 316 |
| 64R-1W, 73-75 | prl-dsp-rich | 309.83 | 309.85 | LSM1-12 | 8 | vein infill | 8.9 | 0.2 | 284 | 310 |
| 64R-1W, 73-75 | prl-dsp-rich | 309.83 | 309.85 | LSM1-12 | 9 | vein infill | 8.9 | 0.2 | 285 | 310 |
| 64R-1W, 73-75 | prl-dsp-rich | 309.83 | 309.85 | LSM1-12 | 10 | vein infill | 8.8 | 0.2 | 285 | 311 |

| | | | | | | | | | | |
|---|---|---|---|---|---|---|---|---|---|---|
| 64R-1W, 73-75 | prl-dsp-rich | 309.83 | 309.85 | LSM1-12 | 11 | vein infill | 8.8 | 0.2 | 286 | 312 |
| 64R-1W, 73-75 | prl-dsp-rich | 309.83 | 309.85 | LSM1-12 | 12 | vein infill | 8.6 | 0.2 | 290 | 316 |
| 64R-1W, 73-75 | prl-dsp-rich | 309.83 | 309.85 | LSM1-12 | 13 | vein infill | 8.9 | 0.2 | 285 | 310 |
| 64R-1W, 73-75 | prl-dsp-rich | 309.83 | 309.85 | LSM1-12 | 14 | vein infill | 9.0 | 0.2 | 281 | 305 |
| 64R-1W, 73-75 | prl-dsp-rich | 309.83 | 309.85 | LSM1-12 | 15 | vein infill | 9.0 | 0.2 | 281 | 306 |
| 64R-1W, 73-75 | prl-dsp-rich | 309.83 | 309.85 | LSM1-12 | 16 | vein infill | 8.9 | 0.2 | 285 | 310 |
| 64R-1W, 73-75 | prl-dsp-rich | 309.83 | 309.85 | LSM1-12 | 17 | vein infill | 9.5 | 0.2 | 271 | 295 |
| 64R-1W, 73-75 | prl-dsp-rich | 309.83 | 309.85 | LSM1-12 | 18 | vein infill | 9.5 | 0.2 | 271 | 295 |
| 64R-1W, 73-75 | prl-dsp-rich | 309.83 | 309.85 | LSM1-12 | 19 | vein infill | 9.9 | 0.2 | 262 | 284 |
| 64R-1W, 73-75 | prl-dsp-rich | 309.83 | 309.85 | LSM1-12 | 20 | vein infill; marginal diffusion? | 8.3 | 0.2 | 300 | 327 |
| 64R-1W, 73-75 | prl-dsp-rich | 309.83 | 309.85 | LSM1-13 | 1 | vein infill | 8.9 | 0.2 | 284 | 309 |
| 64R-1W, 73-75 | prl-dsp-rich | 309.83 | 309.85 | LSM1-13 | 2 | vein infill | 9.1 | 0.2 | 279 | 304 |
| 64R-1W, 73-75 | prl-dsp-rich | 309.83 | 309.85 | LSM1-13 | 3 | vein infill | 9.0 | 0.2 | 282 | 307 |
| 64R-1W, 73-75 | prl-dsp-rich | 309.83 | 309.85 | LSM1-13 | 4 | vein infill | 8.8 | 0.2 | 286 | 312 |
| 64R-1W, 73-75 | prl-dsp-rich | 309.83 | 309.85 | LSM1-13 | 5 | vein infill | 8.9 | 0.2 | 285 | 310 |
| 64R-1W, 73-75 | prl-dsp-rich | 309.83 | 309.85 | LSM1-13 | 6 | vein infill | 8.9 | 0.2 | 284 | 309 |
| 64R-1W, 73-75 | prl-dsp-rich | 309.83 | 309.85 | LSM1-13 | 7 | vein infill | 9.2 | 0.2 | 278 | 303 |
| 64R-1W, 73-75 | prl-dsp-rich | 309.83 | 309.85 | LSM1-13 | 8 | vein infill | 9.0 | 0.2 | 281 | 306 |
| 64R-1W, 73-75 | prl-dsp-rich | 309.83 | 309.85 | LSM1-13 | 9 | vein infill | 9.4 | 0.2 | 273 | 297 |
| 64R-1W, 73-75 | prl-dsp-rich | 309.83 | 309.85 | LSM1-13 | 10 | vein infill | 9.5 | 0.2 | 269 | 293 |
| 64R-1W, 73-75 | prl-dsp-rich | 309.83 | 309.85 | LSM1-13 | 11 | vein infill | 7.3 | 0.2 | 325 | 356 |
| 64R-1W, 73-75 | prl-dsp-rich | 309.83 | 309.85 | LSM1-13 | 12 | vein infill | 7.2 | 0.2 | 329 | 362 |
| 64R-1W, 73-75 | prl-dsp-rich | 309.83 | 309.85 | LSM1-13 | 13 | vein infill | 8.1 | 0.2 | 305 | 333 |
| 64R-1W, 73-75 | prl-dsp-rich | 309.83 | 309.85 | LSM1-13 | 14 | vein infill | 8.0 | 0.2 | 307 | 336 |
| 64R-1W, 73-75 | prl-dsp-rich | 309.83 | 309.85 | LSM1-13 | 15 | vein infill | 7.0 | 0.2 | 334 | 367 |
| 64R-1W, 73-75 | prl-dsp-rich | 309.83 | 309.85 | LSM1-13 | 16 | vein infill | 6.8 | 0.2 | 341 | 375 |
| 64R-1W, 73-75 | prl-dsp-rich | 309.83 | 309.85 | LSM1-13 | 17 | vein infill | 6.7 | 0.2 | 345 | 380 |
| 64R-1W, 73-75 | prl-dsp-rich | 309.83 | 309.85 | LSM1-13 | 18 | vein infill | 6.7 | 0.2 | 343 | 378 |
| 64R-1W, 73-75 | prl-dsp-rich | 309.83 | 309.85 | LSM1-13 | 19 | vein infill | 7.7 | 0.2 | 313 | 343 |
| 64R-1W, 73-75 | prl-dsp-rich | 309.83 | 309.85 | LSM1-13 | 20 | vein infill | 7.1 | 0.2 | 332 | 365 |

*alteration types are described in the chapter "Sample Material", subchapter "Brothers volcano, Kermdec Arc".

†temperatures were calculated based on the equation given by Sharp & Kirschner (1994).

◊minimum and maximum measured $\delta^{18}O$ hydrothermal fluid compositions at the NW Caldera of Brothers volcano after deRonde et al. (2011).

Table 3: Oxygen isotope measurements ($\delta^{18}O_{VSMOW}$) for quartz separates of Hole U1530A, NW C

| Host rock | | depth (mbsf) | | quartz separate | |
|---|---|---|---|---|---|
| sample name | alteration type* | top | bottom | grain No. | point No. |
| *376-U1530A-* | | | | | |
| 4R-1W, 67-69 | stockwork | 22.07 | 22.09 | LSM1-17 | 1 |
| 4R-1W, 67-69 | stockwork | 22.07 | 22.09 | LSM1-17 | 2 |
| 4R-1W, 67-69 | stockwork | 22.07 | 22.09 | LSM1-18 | 1 |
| 12R-2W, 8-11 | chl-rich (lava flow) | 61.08 | 61.11 | LSM1-14 | 1 |
| 12R-2W, 8-11 | chl-rich (lava flow) | 61.08 | 61.11 | LSM1-14 | 2 |
| 12R-2W, 8-11 | chl-rich (lava flow) | 61.08 | 61.11 | LSM1-14 | 3 |
| 12R-2W, 8-11 | chl-rich (lava flow) | 61.08 | 61.11 | LSM1-14 | 4 |
| 12R-2W, 8-11 | chl-rich (lava flow) | 61.08 | 61.11 | LSM1-14 | 5 |
| 12R-2W, 8-11 | chl-rich (lava flow) | 61.08 | 61.11 | LSM1-14 | 6 |
| 12R-2W, 8-11 | chl-rich (lava flow) | 61.08 | 61.11 | LSM1-14 | 7 |
| 12R-2W, 8-11 | chl-rich (lava flow) | 61.08 | 61.11 | LSM1-14 | 8 |
| 12R-2W, 8-11 | chl-rich (lava flow) | 61.08 | 61.11 | LSM1-14 | 9 |
| 12R-2W, 8-11 | chl-rich (lava flow) | 61.08 | 61.11 | LSM1-14 | 10 |
| 12R-2W, 8-11 | chl-rich (lava flow) | 61.08 | 61.11 | LSM1-16 | 1 |
| 12R-2W, 8-11 | chl-rich (lava flow) | 61.08 | 61.11 | LSM1-16 | 2 |
| 12R-2W, 8-11 | chl-rich (lava flow) | 61.08 | 61.11 | LSM1-16 | 3 |
| 12R-2W, 8-11 | chl-rich (lava flow) | 61.08 | 61.11 | LSM1-16 | 4 |
| 12R-2W, 8-11 | chl-rich (lava flow) | 61.08 | 61.11 | LSM1-16 | 5 |
| 12R-2W, 8-11 | chl-rich (lava flow) | 61.08 | 61.11 | LSM1-16 | 6 |
| 12R-2W, 8-11 | chl-rich (lava flow) | 61.08 | 61.11 | LSM1-16 | 7 |
| 12R-2W, 8-11 | chl-rich (lava flow) | 61.08 | 61.11 | LSM1-16 | 8 |
| 12R-2W, 8-11 | chl-rich (lava flow) | 61.08 | 61.11 | LSM1-16 | 9 |
| 12R-2W, 8-11 | chl-rich (lava flow) | 61.08 | 61.11 | LSM1-16 | 10 |
| 56R-2W, 40-42 | prl-dsp-rich | 272.40 | 272.42 | LSM1-3 | 1 |
| 56R-2W, 40-42 | prl-dsp-rich | 272.40 | 272.42 | LSM1-3 | 2 |
| 56R-2W, 40-42 | prl-dsp-rich | 272.40 | 272.42 | LSM1-10 | 1 |
| 56R-2W, 40-42 | prl-dsp-rich | 272.40 | 272.42 | LSM1-10 | 2 |
| 57R-1W, 57-59 | prl-dsp-rich | 276.07 | 276.09 | LSM1-1 | 1 |
| 57R-1W, 57-59 | prl-dsp-rich | 276.07 | 276.09 | LSM1-1 | 2 |
| 57R-1W, 57-59 | prl-dsp-rich | 276.07 | 276.09 | LSM1-2 | 1 |
| 57R-1W, 57-59 | prl-dsp-rich | 276.07 | 276.09 | LSM1-2 | 2 |
| 57R-1W, 57-59 | prl-dsp-rich | 276.07 | 276.09 | LSM1-2 | 3 |
| 57R-1W, 57-59 | prl-dsp-rich | 276.07 | 276.09 | LSM1-2 | 4 |
| 57R-1W, 57-59 | prl-dsp-rich | 276.07 | 276.09 | LSM1-2 | 5 |
| 60R-1W, 96-98 | chl-rich (lava flow) | 290.86 | 290.88 | LSM1-4 | 1 |
| 60R-1W, 96-98 | chl-rich (lava flow) | 290.86 | 290.88 | LSM1-4 | 2 |
| 60R-1W, 96-98 | chl-rich (lava flow) | 290.86 | 290.88 | LSM1-4 | 3 |
| 60R-1W, 96-98 | chl-rich (lava flow) | 290.86 | 290.88 | LSM1-4 | 4 |
| 60R-1W, 96-98 | chl-rich (lava flow) | 290.86 | 290.88 | LSM1-4 | 5 |

| | | | | | |
|---|---|---|---|---|---|
| 60R-1W, 96-98 | chl-rich (lava flow) | 290.86 | 290.88 | LSM1-4 | 6 |
| 60R-1W, 96-98 | chl-rich (lava flow) | 290.86 | 290.88 | LSM1-4 | 7 |
| 60R-1W, 96-98 | chl-rich (lava flow) | 290.86 | 290.88 | LSM1-4 | 8 |
| 60R-1W, 96-98 | chl-rich (lava flow) | 290.86 | 290.88 | LSM1-4 | 9 |
| 60R-1W, 96-98 | chl-rich (lava flow) | 290.86 | 290.88 | LSM1-4 | 10 |
| 60R-1W, 96-98 | chl-rich (lava flow) | 290.86 | 290.88 | LSM1-5 | 1 |
| 60R-1W, 96-98 | chl-rich (lava flow) | 290.86 | 290.88 | LSM1-5 | 2 |
| 60R-1W, 96-98 | chl-rich (lava flow) | 290.86 | 290.88 | LSM1-5 | 3 |
| 60R-1W, 96-98 | chl-rich (lava flow) | 290.86 | 290.88 | LSM1-5 | 4 |
| 60R-1W, 96-98 | chl-rich (lava flow) | 290.86 | 290.88 | LSM1-5 | 5 |
| 60R-1W, 96-98 | chl-rich (lava flow) | 290.86 | 290.88 | LSM1-5 | 6 |
| 60R-1W, 96-98 | chl-rich (lava flow) | 290.86 | 290.88 | LSM1-5 | 7 |
| 60R-1W, 96-98 | chl-rich (lava flow) | 290.86 | 290.88 | LSM1-5 | 8 |
| 60R-1W, 96-98 | chl-rich (lava flow) | 290.86 | 290.88 | LSM1-5 | 9 |
| 60R-1W, 96-98 | chl-rich (lava flow) | 290.86 | 290.88 | LSM1-5 | 10 |
| 64R-1W, 73-75 | prl-dsp-rich | 309.83 | 309.85 | LSM1-11 | 1 |
| 64R-1W, 73-75 | prl-dsp-rich | 309.83 | 309.85 | LSM1-11 | 2 |
| 64R-1W, 73-75 | prl-dsp-rich | 309.83 | 309.85 | LSM1-11 | 3 |
| 64R-1W, 73-75 | prl-dsp-rich | 309.83 | 309.85 | LSM1-11 | 4 |
| 64R-1W, 73-75 | prl-dsp-rich | 309.83 | 309.85 | LSM1-11 | 5 |
| 64R-1W, 73-75 | prl-dsp-rich | 309.83 | 309.85 | LSM1-11 | 6 |
| 64R-1W, 73-75 | prl-dsp-rich | 309.83 | 309.85 | LSM1-11 | 7 |
| 64R-1W, 73-75 | prl-dsp-rich | 309.83 | 309.85 | LSM1-11 | 8 |
| 64R-1W, 73-75 | prl-dsp-rich | 309.83 | 309.85 | LSM1-11 | 9 |
| 64R-1W, 73-75 | prl-dsp-rich | 309.83 | 309.85 | LSM1-11 | 10 |
| 64R-1W, 73-75 | prl-dsp-rich | 309.83 | 309.85 | LSM1-12 | 1 |
| 64R-1W, 73-75 | prl-dsp-rich | 309.83 | 309.85 | LSM1-12 | 2 |
| 64R-1W, 73-75 | prl-dsp-rich | 309.83 | 309.85 | LSM1-12 | 3 |
| 64R-1W, 73-75 | prl-dsp-rich | 309.83 | 309.85 | LSM1-12 | 4 |
| 64R-1W, 73-75 | prl-dsp-rich | 309.83 | 309.85 | LSM1-12 | 5 |
| 64R-1W, 73-75 | prl-dsp-rich | 309.83 | 309.85 | LSM1-12 | 6 |
| 64R-1W, 73-75 | prl-dsp-rich | 309.83 | 309.85 | LSM1-12 | 7 |
| 64R-1W, 73-75 | prl-dsp-rich | 309.83 | 309.85 | LSM1-12 | 8 |
| 64R-1W, 73-75 | prl-dsp-rich | 309.83 | 309.85 | LSM1-12 | 9 |
| 64R-1W, 73-75 | prl-dsp-rich | 309.83 | 309.85 | LSM1-12 | 10 |
| 64R-1W, 73-75 | prl-dsp-rich | 309.83 | 309.85 | LSM1-12 | 11 |
| 64R-1W, 73-75 | prl-dsp-rich | 309.83 | 309.85 | LSM1-12 | 12 |
| 64R-1W, 73-75 | prl-dsp-rich | 309.83 | 309.85 | LSM1-12 | 13 |
| 64R-1W, 73-75 | prl-dsp-rich | 309.83 | 309.85 | LSM1-12 | 14 |
| 64R-1W, 73-75 | prl-dsp-rich | 309.83 | 309.85 | LSM1-12 | 15 |
| 64R-1W, 73-75 | prl-dsp-rich | 309.83 | 309.85 | LSM1-12 | 16 |
| 64R-1W, 73-75 | prl-dsp-rich | 309.83 | 309.85 | LSM1-12 | 17 |
| 64R-1W, 73-75 | prl-dsp-rich | 309.83 | 309.85 | LSM1-12 | 18 |
| 64R-1W, 73-75 | prl-dsp-rich | 309.83 | 309.85 | LSM1-12 | 19 |
| 64R-1W, 73-75 | prl-dsp-rich | 309.83 | 309.85 | LSM1-12 | 20 |

| | | | | | |
|---|---|---|---|---|---|
| 64R-1W, 73-75 | prl-dsp-rich | 309.83 | 309.85 | LSM1-13 | 1 |
| 64R-1W, 73-75 | prl-dsp-rich | 309.83 | 309.85 | LSM1-13 | 2 |
| 64R-1W, 73-75 | prl-dsp-rich | 309.83 | 309.85 | LSM1-13 | 3 |
| 64R-1W, 73-75 | prl-dsp-rich | 309.83 | 309.85 | LSM1-13 | 4 |
| 64R-1W, 73-75 | prl-dsp-rich | 309.83 | 309.85 | LSM1-13 | 5 |
| 64R-1W, 73-75 | prl-dsp-rich | 309.83 | 309.85 | LSM1-13 | 6 |
| 64R-1W, 73-75 | prl-dsp-rich | 309.83 | 309.85 | LSM1-13 | 7 |
| 64R-1W, 73-75 | prl-dsp-rich | 309.83 | 309.85 | LSM1-13 | 8 |
| 64R-1W, 73-75 | prl-dsp-rich | 309.83 | 309.85 | LSM1-13 | 9 |
| 64R-1W, 73-75 | prl-dsp-rich | 309.83 | 309.85 | LSM1-13 | 10 |
| 64R-1W, 73-75 | prl-dsp-rich | 309.83 | 309.85 | LSM1-13 | 11 |
| 64R-1W, 73-75 | prl-dsp-rich | 309.83 | 309.85 | LSM1-13 | 12 |
| 64R-1W, 73-75 | prl-dsp-rich | 309.83 | 309.85 | LSM1-13 | 13 |
| 64R-1W, 73-75 | prl-dsp-rich | 309.83 | 309.85 | LSM1-13 | 14 |
| 64R-1W, 73-75 | prl-dsp-rich | 309.83 | 309.85 | LSM1-13 | 15 |
| 64R-1W, 73-75 | prl-dsp-rich | 309.83 | 309.85 | LSM1-13 | 16 |
| 64R-1W, 73-75 | prl-dsp-rich | 309.83 | 309.85 | LSM1-13 | 17 |
| 64R-1W, 73-75 | prl-dsp-rich | 309.83 | 309.85 | LSM1-13 | 18 |
| 64R-1W, 73-75 | prl-dsp-rich | 309.83 | 309.85 | LSM1-13 | 19 |
| 64R-1W, 73-75 | prl-dsp-rich | 309.83 | 309.85 | LSM1-13 | 20 |

*alteration types are described in the chapter "Sample Material", subchapter "Brothers volcano

†temperatures were calculated based on the equation given by Sharp & Kirschner (1994)

◊minimum and maximum measured $\delta^{18}O$ hydrothermal fluid compositions at the NW Caldera

aldera, Brothers volcano (point positions are given in the Appendix, Table A. 3-8).

| description | $\delta^{18}O_{VSMOW}$ (‰) | 2sd (‰) | temperature (°C)† $\delta^{18}O_{water}$ = 0 ‰◊ | $\delta^{18}O_{water}$ = +1 ‰◊ |
|---|---|---|---|---|
| vein infill | 9.2 | 0.2 | 278 | 303 |
| vein infill | 8.8 | 0.2 | 286 | 311 |
| vein infill | 8.7 | 0.2 | 289 | 315 |
| vug infill | 9.6 | 0.2 | 269 | 292 |
| vug infill | 8.4 | 0.2 | 296 | 323 |
| vug infill | 9.1 | 0.2 | 280 | 305 |
| vug infill | 6.3 | 0.2 | 359 | 396 |
| vug infill | 7.1 | 0.2 | 330 | 363 |
| vug infill | 6.1 | 0.2 | 364 | 403 |
| vug infill | 7.6 | 0.2 | 317 | 347 |
| vug infill | 7.8 | 0.2 | 313 | 342 |
| vug infill | 6.0 | 0.2 | 366 | 405 |
| vug infill | 5.9 | 0.2 | 370 | 410 |
| vug infill | 5.6 | 0.1 | 383 | 425 |
| vug infill | 6.3 | 0.1 | 358 | 395 |
| vug infill | 6.1 | 0.1 | 363 | 402 |
| vug infill | 7.8 | 0.1 | 311 | 340 |
| vug infill | 5.8 | 0.1 | 374 | 415 |
| vug infill | 6.0 | 0.1 | 368 | 407 |
| vug infill | 6.3 | 0.1 | 358 | 395 |
| vug infill | 7.3 | 0.1 | 325 | 357 |
| vug infill | 7.6 | 0.1 | 317 | 347 |
| vug infill | 6.6 | 0.2 | 348 | 384 |
| vein infill | 7.4 | 0.1 | 322 | 354 |
| vein infill | 7.3 | 0.1 | 326 | 358 |
| vein infill | 6.8 | 0.1 | 342 | 376 |
| vein infill | 7.9 | 0.1 | 308 | 337 |
| matrix replacement | 8.5 | 0.1 | 294 | 320 |
| matrix replacement | 8.5 | 0.1 | 293 | 320 |
| matrix replacement | 7.5 | 0.1 | 320 | 351 |
| matrix replacement | 7.9 | 0.1 | 310 | 339 |
| matrix replacement | 7.8 | 0.1 | 313 | 342 |
| matrix replacement | 8.7 | 0.1 | 289 | 315 |
| matrix replacement | 8.6 | 0.1 | 291 | 317 |
| vug infill | 7.0 | 0.1 | 334 | 367 |
| vug infill | 7.0 | 0.1 | 335 | 368 |
| vug infill | 6.6 | 0.1 | 346 | 381 |
| vug infill; point close to crack | 8.7 | 0.1 | 289 | 315 |
| vug infill | 6.3 | 0.1 | 359 | 397 |

| | | | | |
|---|---|---|---|---|
| vug infill | 6.6 | 0.1 | 348 | 384 |
| vug infill | 6.6 | 0.1 | 347 | 383 |
| vug infill | 6.3 | 0.1 | 356 | 393 |
| vug infill | 6.2 | 0.1 | 360 | 398 |
| vug infill | 6.6 | 0.1 | 347 | 383 |
| vug infill | 6.3 | 0.1 | 358 | 396 |
| vug infill | 6.7 | 0.1 | 343 | 378 |
| vug infill | 6.4 | 0.1 | 355 | 391 |
| vug infill | 6.3 | 0.1 | 356 | 394 |
| vug infill | 6.8 | 0.1 | 341 | 375 |
| vug infill | 6.2 | 0.1 | 361 | 399 |
| vug infill | 6.9 | 0.1 | 339 | 373 |
| vug infill | 6.4 | 0.1 | 355 | 392 |
| vug infill | 6.2 | 0.1 | 362 | 400 |
| vug infill | 6.3 | 0.1 | 357 | 394 |
| vein infill | 8.1 | 0.2 | 304 | 332 |
| vein infill | 8.7 | 0.2 | 288 | 314 |
| vein infill | 7.6 | 0.2 | 318 | 349 |
| vein infill | 7.4 | 0.2 | 323 | 354 |
| vein infill | 7.1 | 0.2 | 331 | 363 |
| vein infill | 7.2 | 0.2 | 329 | 361 |
| vein infill | 7.8 | 0.2 | 313 | 343 |
| vein infill | 6.8 | 0.2 | 342 | 377 |
| vein infill | 6.4 | 0.2 | 353 | 390 |
| vein infill | 7.8 | 0.2 | 312 | 341 |
| vein infill; marginal diffusion? | 7.5 | 0.2 | 319 | 350 |
| vein infill | 8.8 | 0.2 | 285 | 311 |
| vein infill | 8.6 | 0.2 | 291 | 318 |
| vein infill | 9.0 | 0.2 | 283 | 308 |
| vein infill | 9.0 | 0.2 | 282 | 307 |
| vein infill | 8.9 | 0.2 | 285 | 311 |
| vein infill | 8.6 | 0.2 | 290 | 316 |
| vein infill | 8.9 | 0.2 | 284 | 310 |
| vein infill | 8.9 | 0.2 | 285 | 310 |
| vein infill | 8.8 | 0.2 | 285 | 311 |
| vein infill | 8.8 | 0.2 | 286 | 312 |
| vein infill | 8.6 | 0.2 | 290 | 316 |
| vein infill | 8.9 | 0.2 | 285 | 310 |
| vein infill | 9.0 | 0.2 | 281 | 305 |
| vein infill | 9.0 | 0.2 | 281 | 306 |
| vein infill | 8.9 | 0.2 | 285 | 310 |
| vein infill | 9.5 | 0.2 | 271 | 295 |
| vein infill | 9.5 | 0.2 | 271 | 295 |
| vein infill | 9.9 | 0.2 | 262 | 284 |
| vein infill; marginal diffusion? | 8.3 | 0.2 | 300 | 327 |

| | | | | |
|---|---|---|---|---|
| vein infill | 8.9 | 0.2 | 284 | 309 |
| vein infill | 9.1 | 0.2 | 279 | 304 |
| vein infill | 9.0 | 0.2 | 282 | 307 |
| vein infill | 8.8 | 0.2 | 286 | 312 |
| vein infill | 8.9 | 0.2 | 285 | 310 |
| vein infill | 8.9 | 0.2 | 284 | 309 |
| vein infill | 9.2 | 0.2 | 278 | 303 |
| vein infill | 9.0 | 0.2 | 281 | 306 |
| vein infill | 9.4 | 0.2 | 273 | 297 |
| vein infill | 9.5 | 0.2 | 269 | 293 |
| vein infill | 7.3 | 0.2 | 325 | 356 |
| vein infill | 7.2 | 0.2 | 329 | 362 |
| vein infill | 8.1 | 0.2 | 305 | 333 |
| vein infill | 8.0 | 0.2 | 307 | 336 |
| vein infill | 7.0 | 0.2 | 334 | 367 |
| vein infill | 6.8 | 0.2 | 341 | 375 |
| vein infill | 6.7 | 0.2 | 345 | 380 |
| vein infill | 6.7 | 0.2 | 343 | 378 |
| vein infill | 7.7 | 0.2 | 313 | 343 |
| vein infill | 7.1 | 0.2 | 332 | 365 |

ɔ, Kermdec Arc"

of Brothers volcano after deRonde et al. (2011)

Table A1: Oxygen isotope measurements on quartz that were conducted by SIMS on sample m

| spot number | spot name | host rock sample name |
|---|---|---|
| 20200302@787.asc | LSM1 UWQ-1 g1 | |
| 20200302@788.asc | LSM1 UWQ-1 g1 | |
| 20200302@789.asc | LSM1 UWQ-1 g1 | |
| 20200302@790.asc | LSM1 UWQ-1 g1 | |
| | **average and 2SD** | |
| 20200302@791.asc | LSM1_4 spot-1 | 376-U1530A-60R-1W, 96-98 |
| 20200302@792.asc | LSM1_4 spot-2 | 376-U1530A-60R-1W, 96-98 |
| 20200302@793.asc | LSM1_4 spot-3 | 376-U1530A-60R-1W, 96-98 |
| 20200302@794.asc | LSM1_4 spot-4 | 376-U1530A-60R-1W, 96-98 |
| 20200302@795.asc | LSM1_4 spot-5 | 376-U1530A-60R-1W, 96-98 |
| 20200302@796.asc | LSM1_4 spot-6 | 376-U1530A-60R-1W, 96-98 |
| 20200302@797.asc | LSM1_4 spot-7 | 376-U1530A-60R-1W, 96-98 |
| 20200302@798.asc | LSM1_4 spot-8 | 376-U1530A-60R-1W, 96-98 |
| 20200302@799.asc | LSM1_4 spot-9 | 376-U1530A-60R-1W, 96-98 |
| 20200302@800.asc | LSM1_4 spot-10 | 376-U1530A-60R-1W, 96-98 |
| 20200302@801.asc | LSM1_5 spot-1 | 376-U1530A-60R-1W, 96-98 |
| 20200302@802.asc | LSM1_5 spot-2 | 376-U1530A-60R-1W, 96-98 |
| 20200302@803.asc | LSM1_5 spot-3 | 376-U1530A-60R-1W, 96-98 |
| 20200302@804.asc | LSM1_5 spot-4 | 376-U1530A-60R-1W, 96-98 |
| 20200302@805.asc | LSM1_5 spot-5 | 376-U1530A-60R-1W, 96-98 |
| 20200302@806.asc | LSM1_5 spot-6 | 376-U1530A-60R-1W, 96-98 |
| 20200302@807.asc | LSM1_5 spot-7 | 376-U1530A-60R-1W, 96-98 |
| 20200302@808.asc | LSM1_5 spot-8 | 376-U1530A-60R-1W, 96-98 |
| 20200302@809.asc | LSM1_5 spot-9 | 376-U1530A-60R-1W, 96-98 |
| 20200302@810.asc | LSM1_5 spot-10 | 376-U1530A-60R-1W, 96-98 |
| 20200302@811.asc | LSM1 UWQ-1 g1 CsRes=143 | |
| 20200302@812.asc | LSM1 UWQ-1 g1 | |
| 20200302@813.asc | LSM1 UWQ-1 g1 | |
| 20200302@814.asc | LSM1 UWQ-1 g1 | |
| | **average and 2SD** | |
| | **bracket average and 2SD** | |
| 20200302@815.asc | LSM1_11 spot-1 | 376-U1530A-64R-1W, 73-75 |
| 20200302@816.asc | LSM1_11 spot-2 | 376-U1530A-64R-1W, 73-75 |
| 20200302@817.asc | LSM1_11 spot-3 | 376-U1530A-64R-1W, 73-75 |
| 20200302@818.asc | LSM1_11 spot-4 | 376-U1530A-64R-1W, 73-75 |
| 20200302@819.asc | LSM1_11 spot-5 | 376-U1530A-64R-1W, 73-75 |
| 20200302@820.asc | LSM1_11 spot-6 | 376-U1530A-64R-1W, 73-75 |
| 20200302@821.asc | LSM1_11 spot-7 | 376-U1530A-64R-1W, 73-75 |
| 20200302@822.asc | LSM1_11 spot-8 | 376-U1530A-64R-1W, 73-75 |
| 20200302@823.asc | LSM1_11 spot-9 | 376-U1530A-64R-1W, 73-75 |
| 20200302@824.asc | LSM1_11 spot-10 | 376-U1530A-64R-1W, 73-75 |

| | | |
|---|---|---|
| 20200302@825.asc | LSM1_14 spot-1 | 376-U1530A-12R-2W, 8-11 |
| 20200302@826.asc | LSM1_14 spot-2 | 376-U1530A-12R-2W, 8-11 |
| 20200302@827.asc | LSM1_14 spot-3 | 376-U1530A-12R-2W, 8-11 |
| 20200302@828.asc | LSM1_14 spot-4 | 376-U1530A-12R-2W, 8-11 |
| 20200302@829.asc | LSM1_14 spot-5 | 376-U1530A-12R-2W, 8-11 |
| 20200302@830.asc | LSM1_14 spot-6 | 376-U1530A-12R-2W, 8-11 |
| 20200302@831.asc | LSM1_14 spot-7 | 376-U1530A-12R-2W, 8-11 |
| 20200302@832.asc | LSM1_14 spot-8 | 376-U1530A-12R-2W, 8-11 |
| 20200302@833.asc | LSM1_14 spot-9 | 376-U1530A-12R-2W, 8-11 |
| 20200302@834.asc | LSM1_14 spot-10 | 376-U1530A-12R-2W, 8-11 |
| | | |
| 20200302@835.asc | LSM1 UWQ-1 g1 | |
| 20200302@836.asc | LSM1 UWQ-1 g1 | |
| 20200302@837.asc | LSM1 UWQ-1 g1 | |
| 20200302@838.asc | LSM1 UWQ-1 g1 | |
| | **average and 2SD** | |
| | **bracket average and 2SD** | |
| | | |
| 20200302@839.asc | LSM1_1 spot-1 | 376-U1530A-57R-1W, 57-59 |
| 20200302@840.asc | LSM1_1 spot-2 | 376-U1530A-57R-1W, 57-59 |
| 20200302@841.asc | LSM1_2 spot-1 | 376-U1530A-57R-1W, 57-59 |
| 20200302@842.asc | LSM1_2 spot-2 | 376-U1530A-57R-1W, 57-59 |
| 20200302@843.asc | LSM1_2 spot-3 | 376-U1530A-57R-1W, 57-59 |
| 20200302@844.asc | LSM1_2 spot-4 | 376-U1530A-57R-1W, 57-59 |
| 20200302@845.asc | LSM1_2 spot-5 CsRes=144 | 376-U1530A-57R-1W, 57-59 |
| 20200302@846.asc | LSM1_3 spot-1 | 376-U1530A-56R-2W, 40-42 |
| 20200302@847.asc | LSM1_3 spot-2 | 376-U1530A-56R-2W, 40-42 |
| 20200302@848.asc | LSM1_10 spot-1 | 376-U1530A-56R-2W, 40-42 |
| 20200302@849.asc | LSM1_10 spot-2 | 376-U1530A-56R-2W, 40-42 |
| 20200302@850.asc | LSM1_16 spot-1 | 376-U1530A-12R-2W, 8-11 |
| 20200302@851.asc | LSM1_16 spot-2 | 376-U1530A-12R-2W, 8-11 |
| 20200302@852.asc | LSM1_16 spot-3 | 376-U1530A-12R-2W, 8-11 |
| 20200302@853.asc | LSM1_16 spot-4 | 376-U1530A-12R-2W, 8-11 |
| 20200302@854.asc | LSM1_16 spot-5 | 376-U1530A-12R-2W, 8-11 |
| 20200302@855.asc | LSM1_16 spot-6 | 376-U1530A-12R-2W, 8-11 |
| 20200302@856.asc | LSM1_16 spot-7 | 376-U1530A-12R-2W, 8-11 |
| 20200302@857.asc | LSM1_16 spot-8 | 376-U1530A-12R-2W, 8-11 |
| 20200302@858.asc | LSM1_16 spot-9 | 376-U1530A-12R-2W, 8-11 |
| | | |
| 20200302@859.asc | LSM1 UWQ-1 g1 | |
| 20200302@860.asc | LSM1 UWQ-1 g1 | |
| 20200302@861.asc | LSM1 UWQ-1 g1 | |
| 20200302@862.asc | LSM1 UWQ-1 g1 | |
| | **average and 2SD** | |
| | **bracket average and 2SD** | |
| | | |
| 20200302@863.asc | LSM1_16 spot-10 | 376-U1530A-12R-2W, 8-11 |
| 20200302@864.asc | LSM1_17 spot-1 | 376-U1530A-4R-1W, 67-69 |

| | | |
|---|---|---|
| 20200302@865.asc | LSM1_17 spot-2 | 376-U1530A-4R-1W, 67-69 |
| 20200302@866.asc | LSM1_18 spot-1 | 376-U1530A-4R-1W, 67-69 |
| 20200302@867.asc | LSM1_12 spot-1 | 376-U1530A-64R-1W, 73-75 |
| 20200302@868.asc | LSM1_12 spot-2 | 376-U1530A-64R-1W, 73-75 |
| 20200302@869.asc | LSM1_12 spot-3 CsRes=145 | 376-U1530A-64R-1W, 73-75 |
| 20200302@870.asc | LSM1_12 spot-4 | 376-U1530A-64R-1W, 73-75 |
| 20200302@871.asc | LSM1_12 spot-5 | 376-U1530A-64R-1W, 73-75 |
| 20200302@872.asc | LSM1_12 spot-6 | 376-U1530A-64R-1W, 73-75 |
| 20200302@873.asc | LSM1_12 spot-7 | 376-U1530A-64R-1W, 73-75 |
| 20200302@874.asc | LSM1_12 spot-8 | 376-U1530A-64R-1W, 73-75 |
| 20200302@875.asc | LSM1_12 spot-9 | 376-U1530A-64R-1W, 73-75 |
| 20200302@876.asc | LSM1_12 spot-10 | 376-U1530A-64R-1W, 73-75 |
| 20200302@877.asc | LSM1_12 spot-11 | 376-U1530A-64R-1W, 73-75 |
| 20200302@878.asc | LSM1_12 spot-12 | 376-U1530A-64R-1W, 73-75 |
| 20200302@879.asc | LSM1_12 spot-13 | 376-U1530A-64R-1W, 73-75 |
| 20200302@880.asc | LSM1_12 spot-14 | 376-U1530A-64R-1W, 73-75 |
| 20200302@881.asc | LSM1_12 spot-15 | 376-U1530A-64R-1W, 73-75 |
| 20200302@882.asc | LSM1_12 spot-16 | 376-U1530A-64R-1W, 73-75 |
| | | |
| 20200302@883.asc | LSM1 UWQ-1 g1 | |
| 20200302@884.asc | LSM1 UWQ-1 g1 | |
| 20200302@885.asc | LSM1 UWQ-1 g1 | |
| 20200302@886.asc | LSM1 UWQ-1 g1 | |
| | **average and 2SD** | |
| | **bracket average and 2SD** | |
| | | |
| 20200302@887.asc | LSM1_12 spot-17 | 376-U1530A-64R-1W, 73-75 |
| 20200302@888.asc | LSM1_12 spot-18 | 376-U1530A-64R-1W, 73-75 |
| 20200302@889.asc | LSM1_12 spot-19 | 376-U1530A-64R-1W, 73-75 |
| 20200302@890.asc | LSM1_12 spot-20 | 376-U1530A-64R-1W, 73-75 |
| 20200302@891.asc | LSM1_13 spot-1 | 376-U1530A-64R-1W, 73-75 |
| 20200302@892.asc | LSM1_13 spot-2 | 376-U1530A-64R-1W, 73-75 |
| 20200302@893.asc | LSM1_13 spot-3 | 376-U1530A-64R-1W, 73-75 |
| 20200302@894.asc | LSM1_13 spot-4 | 376-U1530A-64R-1W, 73-75 |
| 20200302@895.asc | LSM1_13 spot-5 | 376-U1530A-64R-1W, 73-75 |
| 20200302@896.asc | LSM1_13 spot-6 | 376-U1530A-64R-1W, 73-75 |
| 20200302@897.asc | LSM1_13 spot-7 | 376-U1530A-64R-1W, 73-75 |
| 20200302@898.asc | LSM1_13 spot-8 | 376-U1530A-64R-1W, 73-75 |
| 20200302@899.asc | LSM1_13 spot-9 | 376-U1530A-64R-1W, 73-75 |
| 20200302@900.asc | LSM1_13 spot-10 | 376-U1530A-64R-1W, 73-75 |
| 20200302@901.asc | LSM1_13 spot-11 | 376-U1530A-64R-1W, 73-75 |
| 20200302@902.asc | LSM1_13 spot-12 | 376-U1530A-64R-1W, 73-75 |
| 20200302@903.asc | LSM1_13 spot-13 CsRes=146 | 376-U1530A-64R-1W, 73-75 |
| 20200302@904.asc | LSM1_13 spot-14 | 376-U1530A-64R-1W, 73-75 |
| 20200302@905.asc | LSM1_13 spot-15 | 376-U1530A-64R-1W, 73-75 |
| 20200302@906.asc | LSM1_13 spot-16 | 376-U1530A-64R-1W, 73-75 |
| | | |
| 20200302@907.asc | LSM1 UWQ-1 g1 | |

| | | |
|---|---|---|
| 20200302@908.asc | LSM1 UWQ-1 g1 | |
| 20200302@909.asc | LSM1 UWQ-1 g1 | |
| 20200302@910.asc | LSM1 UWQ-1 g1 | |
| | **average and 2SD** | |
| | **bracket average and 2SD** | |
| | | |
| 20200302@911.asc | LSM1_13 spot-17 | 376-U1530A-64R-1W, 73-75 |
| 20200302@912.asc | LSM1_13 spot-18 | 376-U1530A-64R-1W, 73-75 |
| 20200302@913.asc | LSM1_13 spot-19 | 376-U1530A-64R-1W, 73-75 |
| 20200302@914.asc | LSM1_13 spot-20 | 376-U1530A-64R-1W, 73-75 |
| | | |
| 20200302@915.asc | LSM1 UWQ-1 g1 | |
| 20200302@916.asc | LSM1 UWQ-1 g1 | |
| **20200302@917.asc** | **LSM1 UWQ-1 g1** | |
| 20200302@918.asc | LSM1 UWQ-1 g1 | |
| | **average and 2SD** | |
| | **bracket average and 2SD** | |

*External error is given as 2 standard deviations (2SD) of the quartz standard values for a particu
#Uncorrected value measured on the ion probe.
†Internal error is reported as 2 standard error of an individual spot (2SE) during measurement.
**$^{16}O^{1}H/^{16}O$ was measured to monitor potential contamination by water.

ıaterial (IODP Exp. 376, Brothers volcano) and the reference material UWQ-1. The position of the measuri

| quartz replacement type | $\delta^{18}O$ ‰ VSMOW | 2SD (external error)* | Mass Bias (‰) | $\delta^{18}O$ ‰ raw# |
|---|---|---|---|---|
| | | | | 3.24 |
| | | | | 3.27 |
| | | | | 3.26 |
| | | | | 3.23 |
| | | | | **3.25** |
| vug infill | 7.02 | 0.12 | -8.97 | -2.01 |
| vug infill | 6.99 | 0.12 | -8.97 | -2.04 |
| vug infill | 6.65 | 0.12 | -8.97 | -2.38 |
| vug infill | 8.69 | 0.12 | -8.97 | -0.35 |
| vug infill | 6.26 | 0.12 | -8.97 | -2.77 |
| vug infill | 6.57 | 0.12 | -8.97 | -2.46 |
| vug infill | 6.60 | 0.12 | -8.97 | -2.43 |
| vug infill | 6.34 | 0.12 | -8.97 | -2.69 |
| vug infill | 6.22 | 0.12 | -8.97 | -2.80 |
| vug infill | 6.61 | 0.12 | -8.97 | -2.42 |
| vug infill | 6.27 | 0.12 | -8.97 | -2.76 |
| vug infill | 6.73 | 0.12 | -8.97 | -2.30 |
| vug infill | 6.38 | 0.12 | -8.97 | -2.64 |
| vug infill | 6.33 | 0.12 | -8.97 | -2.70 |
| vug infill | 6.80 | 0.12 | -8.97 | -2.23 |
| vug infill | 6.20 | 0.12 | -8.97 | -2.83 |
| vug infill | 6.86 | 0.12 | -8.97 | -2.17 |
| vug infill | 6.36 | 0.12 | -8.97 | -2.66 |
| vug infill | 6.17 | 0.12 | -8.97 | -2.86 |
| vug infill | 6.32 | 0.12 | -8.97 | -2.70 |
| | | | | 3.38 |
| | | | | 3.24 |
| | | | | 3.22 |
| | | | | 3.16 |
| | | | | **3.25** |
| | **12.33** | | **-8.97** | **3.25** |
| vein infill | 8.09 | 0.18 | -8.91 | -0.90 |
| vein infill | 8.71 | 0.18 | -8.91 | -0.28 |
| vein infill | 7.56 | 0.18 | -8.91 | -1.42 |
| vein infill | 7.41 | 0.18 | -8.91 | -1.57 |
| vein infill | 7.13 | 0.18 | -8.91 | -1.84 |
| vein infill | 7.20 | 0.18 | -8.91 | -1.77 |
| vein infill | 7.76 | 0.18 | -8.91 | -1.22 |
| vein infill | 6.76 | 0.18 | -8.91 | -2.21 |
| vein infill | 6.42 | 0.18 | -8.91 | -2.55 |
| vein infill | 7.80 | 0.18 | -8.91 | -1.18 |

| | | | | |
|---|---|---|---|---|
| vug infill | 9.55 | 0.18 | -8.91 | 0.56 |
| vug infill | 8.39 | 0.18 | -8.91 | -0.59 |
| vug infill | 9.05 | 0.18 | -8.91 | 0.06 |
| vug infill | 6.26 | 0.18 | -8.91 | -2.70 |
| vug infill | 7.15 | 0.18 | -8.91 | -1.82 |
| vug infill | 6.11 | 0.18 | -8.91 | -2.85 |
| vug infill | 7.61 | 0.18 | -8.91 | -1.36 |
| vug infill | 7.77 | 0.18 | -8.91 | -1.21 |
| vug infill | 6.05 | 0.18 | -8.91 | -2.92 |
| vug infill | 5.93 | 0.18 | -8.91 | -3.03 |
| | | | | 3.31 |
| | | | | 3.37 |
| | | | | 3.39 |
| | | | | 3.41 |
| | | | | **3.37** |
| | **12.33** | | **-8.91** | **3.31** |
| matrix replacement | 8.50 | 0.11 | -8.84 | -0.42 |
| matrix replacement | 8.52 | 0.11 | -8.84 | -0.39 |
| matrix replacement | 7.51 | 0.11 | -8.84 | -1.40 |
| matrix replacement | 7.86 | 0.11 | -8.84 | -1.04 |
| matrix replacement | 7.77 | 0.11 | -8.84 | -1.14 |
| matrix replacement | 8.67 | 0.11 | -8.84 | -0.24 |
| matrix replacement | 8.60 | 0.11 | -8.84 | -0.32 |
| vein infill | 7.42 | 0.11 | -8.84 | -1.48 |
| vein infill | 7.29 | 0.11 | -8.84 | -1.62 |
| vein infill | 6.78 | 0.11 | -8.84 | -2.12 |
| vein infill | 7.93 | 0.11 | -8.84 | -0.98 |
| vug infill | 5.61 | 0.11 | -8.84 | -3.28 |
| vug infill | 6.29 | 0.11 | -8.84 | -2.60 |
| vug infill | 6.13 | 0.11 | -8.84 | -2.77 |
| vug infill | 7.83 | 0.11 | -8.84 | -1.08 |
| vug infill | 5.82 | 0.11 | -8.84 | -3.07 |
| vug infill | 6.00 | 0.11 | -8.84 | -2.89 |
| vug infill | 6.29 | 0.11 | -8.84 | -2.61 |
| vug infill | 7.32 | 0.11 | -8.84 | -1.58 |
| vug infill | 7.61 | 0.11 | -8.84 | -1.30 |
| | | | | 3.42 |
| | | | | 3.48 |
| | | | | 3.36 |
| | | | | 3.33 |
| | | | | **3.40** |
| | **12.33** | | **-8.84** | **3.38** |
| vug infill | 6.58 | 0.15 | -8.85 | -2.33 |
| vein infill | 9.15 | 0.15 | -8.85 | 0.22 |

| | | | | |
|---|---|---|---|---|
| vein infill | 8.83 | 0.15 | -8.85 | -0.11 |
| vein infill | 8.68 | 0.15 | -8.85 | -0.25 |
| vein infill | 7.52 | 0.15 | -8.85 | -1.40 |
| vein infill | 8.85 | 0.15 | -8.85 | -0.08 |
| vein infill | 8.59 | 0.15 | -8.85 | -0.34 |
| vein infill | 8.96 | 0.15 | -8.85 | 0.02 |
| vein infill | 8.99 | 0.15 | -8.85 | 0.06 |
| vein infill | 8.85 | 0.15 | -8.85 | -0.08 |
| vein infill | 8.64 | 0.15 | -8.85 | -0.29 |
| vein infill | 8.88 | 0.15 | -8.85 | -0.05 |
| vein infill | 8.85 | 0.15 | -8.85 | -0.08 |
| vein infill | 8.84 | 0.15 | -8.85 | -0.09 |
| vein infill | 8.81 | 0.15 | -8.85 | -0.12 |
| vein infill | 8.65 | 0.15 | -8.85 | -0.28 |
| vein infill | 8.86 | 0.15 | -8.85 | -0.07 |
| vein infill | 9.04 | 0.15 | -8.85 | 0.11 |
| vein infill | 9.04 | 0.15 | -8.85 | 0.10 |
| vein infill | 8.87 | 0.15 | -8.85 | -0.06 |
| | | | | 3.33 |
| | | | | 3.29 |
| | | | | 3.45 |
| | | | | 3.27 |
| | | | | **3.34** |
| | **12.33** | | **-8.85** | **3.37** |
| vein infill | 9.47 | 0.15 | -8.87 | 0.52 |
| vein infill | 9.46 | 0.15 | -8.87 | 0.51 |
| vein infill | 9.90 | 0.15 | -8.87 | 0.95 |
| vein infill | 8.26 | 0.15 | -8.87 | -0.68 |
| vein infill | 8.92 | 0.15 | -8.87 | -0.03 |
| vein infill | 9.11 | 0.15 | -8.87 | 0.16 |
| vein infill | 8.99 | 0.15 | -8.87 | 0.04 |
| vein infill | 8.79 | 0.15 | -8.87 | -0.15 |
| vein infill | 8.86 | 0.15 | -8.87 | -0.09 |
| vein infill | 8.90 | 0.15 | -8.87 | -0.05 |
| vein infill | 9.15 | 0.15 | -8.87 | 0.20 |
| vein infill | 9.03 | 0.15 | -8.87 | 0.09 |
| vein infill | 9.36 | 0.15 | -8.87 | 0.41 |
| vein infill | 9.55 | 0.15 | -8.87 | 0.60 |
| vein infill | 7.35 | 0.15 | -8.87 | -1.59 |
| vein infill | 7.18 | 0.15 | -8.87 | -1.76 |
| vein infill | 8.06 | 0.15 | -8.87 | -0.88 |
| vein infill | 7.97 | 0.15 | -8.87 | -0.97 |
| vein infill | 7.03 | 0.15 | -8.87 | -1.90 |
| vein infill | 6.81 | 0.15 | -8.87 | -2.12 |
| | | | | 3.46 |

| | | | |
|---|---|---|---|
| | | | 3.40 |
| | | | 3.34 |
| | | | 3.28 |
| | | | **3.37** |
| **12.33** | | **-8.87** | **3.35** |
| | | | |
| 6.68 | 0.20 | -8.86 | -2.24 |
| 6.74 | 0.20 | -8.86 | -2.18 |
| 7.74 | 0.20 | -8.86 | -1.19 |
| 7.08 | 0.20 | -8.86 | -1.84 |
| | | | |
| | | | 3.38 |
| | | | 3.47 |
| | | | **0.34** |
| | | | 3.18 |
| | | | **3.35** |
| **12.33** | | **-8.86** | **3.36** |

ılar bracket.

ng points is projected to the CL images (F level) of the quartz separates.

| 2SE (internal error)† | $^{16}O$ (Gcps) | Primary beam intensity (nA) | Yield (Gcps/nA) | X |
|---|---|---|---|---|
| 0.29 | 3.09 | 1.96 | 1.58 | 2660 |
| 0.28 | 3.10 | 1.97 | 1.58 | 2685 |
| 0.32 | 3.12 | 1.97 | 1.58 | 2710 |
| 0.32 | 3.12 | 1.97 | 1.58 | 2735 |
| **0.04** | | | | |
| | | | | |
| 0.28 | 2.98 | 1.97 | 1.51 | 201 |
| 0.34 | 3.10 | 1.97 | 1.57 | 182 |
| 0.33 | 3.10 | 1.96 | 1.58 | 160 |
| 0.38 | 3.10 | 1.96 | 1.58 | 147 |
| 0.27 | 3.10 | 1.95 | 1.59 | 139 |
| 0.35 | 3.10 | 1.95 | 1.59 | 129 |
| 0.33 | 3.11 | 1.94 | 1.60 | 116 |
| 0.35 | 3.09 | 1.93 | 1.60 | 101 |
| 0.32 | 3.08 | 1.93 | 1.60 | 86 |
| 0.36 | 3.01 | 1.92 | 1.56 | 71 |
| 0.24 | 2.97 | 1.92 | 1.55 | 2374 |
| 0.30 | 2.96 | 1.91 | 1.55 | 2324 |
| 0.30 | 2.98 | 1.90 | 1.57 | 2274 |
| 0.31 | 2.98 | 1.89 | 1.58 | 2224 |
| 0.31 | 2.99 | 1.89 | 1.59 | 2174 |
| 0.28 | 2.97 | 1.88 | 1.58 | 2124 |
| 0.35 | 2.97 | 1.87 | 1.59 | 2074 |
| 0.31 | 2.93 | 1.86 | 1.58 | 2024 |
| 0.34 | 2.90 | 1.85 | 1.57 | 1975 |
| 0.30 | 2.87 | 1.84 | 1.55 | 1925 |
| | | | | |
| 0.37 | 3.08 | 1.96 | 1.57 | 2660 |
| 0.32 | 3.14 | 2.00 | 1.57 | 2685 |
| 0.34 | 3.16 | 2.01 | 1.57 | 2710 |
| 0.32 | 3.18 | 2.02 | 1.57 | 2735 |
| **0.18** | | | | |
| **0.12** | | | **1.58** | |
| | | | | |
| 0.30 | 2.78 | 2.01 | 1.38 | -3068 |
| 0.22 | 2.99 | 2.02 | 1.48 | -3036 |
| 0.28 | 3.02 | 2.02 | 1.50 | -3004 |
| 0.35 | 3.09 | 2.02 | 1.53 | -2972 |
| 0.32 | 3.10 | 2.01 | 1.54 | -2941 |
| 0.26 | 3.15 | 2.01 | 1.57 | -2909 |
| 0.35 | 3.16 | 2.00 | 1.58 | -2877 |
| 0.32 | 3.20 | 2.00 | 1.60 | -2845 |
| 0.30 | 3.22 | 2.00 | 1.61 | -2813 |
| 0.36 | 3.19 | 2.00 | 1.60 | -2781 |

| | | | | |
|---|---|---|---|---|
| 0.35 | 2.93 | 1.99 | 1.47 | -2714 |
| 0.32 | 3.05 | 1.99 | 1.54 | -2636 |
| 0.37 | 3.02 | 1.98 | 1.52 | -2558 |
| 0.23 | 3.02 | 1.97 | 1.53 | -2479 |
| 0.34 | 3.04 | 1.96 | 1.55 | -2401 |
| 0.32 | 3.00 | 1.96 | 1.53 | -2323 |
| 0.29 | 3.03 | 1.95 | 1.55 | -2244 |
| 0.42 | 3.01 | 1.95 | 1.55 | -2166 |
| 0.24 | 2.98 | 1.93 | 1.54 | -2088 |
| 0.25 | 2.96 | 1.92 | 1.54 | -2010 |
| | | | | |
| 0.29 | 3.00 | 1.92 | 1.56 | 2660 |
| 0.30 | 2.98 | 1.91 | 1.56 | 2685 |
| 0.26 | 3.00 | 1.91 | 1.57 | 2710 |
| 0.29 | 2.99 | 1.90 | 1.57 | 2735 |
| **0.08** | | | | |
| **0.18** | | | **1.57** | |
| | | | | |
| 0.31 | 2.99 | 1.89 | 1.58 | -932 |
| 0.22 | 2.75 | 1.89 | 1.46 | -1054 |
| 0.41 | 3.02 | 1.88 | 1.61 | 1653 |
| 0.33 | 2.99 | 1.87 | 1.60 | 1553 |
| 0.33 | 2.92 | 1.86 | 1.57 | 1454 |
| 0.36 | 2.85 | 1.83 | 1.56 | 1355 |
| 0.27 | 2.75 | 1.94 | 1.42 | 1258 |
| 0.33 | 3.17 | 1.97 | 1.60 | 3875 |
| 0.32 | 3.19 | 1.98 | 1.61 | 4217 |
| 0.24 | 3.20 | 1.99 | 1.61 | 4322 |
| 0.25 | 3.13 | 1.99 | 1.58 | 4736 |
| 0.32 | 3.18 | 1.98 | 1.60 | 123 |
| 0.35 | 3.13 | 1.98 | 1.58 | 37 |
| 0.34 | 3.12 | 1.98 | 1.58 | -48 |
| 0.26 | 3.09 | 1.98 | 1.57 | -134 |
| 0.33 | 3.10 | 1.97 | 1.57 | -220 |
| 0.32 | 3.07 | 1.96 | 1.56 | -305 |
| 0.30 | 2.99 | 1.95 | 1.53 | -391 |
| 0.25 | 2.88 | 1.94 | 1.49 | -477 |
| 0.27 | 2.67 | 1.93 | 1.38 | -563 |
| | | | | |
| 0.33 | 3.01 | 1.92 | 1.56 | 2660 |
| 0.37 | 2.98 | 1.91 | 1.56 | 2685 |
| 0.31 | 2.99 | 1.91 | 1.57 | 2710 |
| 0.30 | 2.99 | 1.90 | 1.57 | 2735 |
| **0.13** | | | | |
| **0.11** | | | **1.57** | |
| | | | | |
| 0.29 | 2.54 | 1.89 | 1.35 | -648 |
| 0.25 | 2.86 | 1.88 | 1.52 | 1624 |

| | | | | |
|---|---|---|---|---|
| 0.30 | 2.98 | 1.88 | 1.59 | 1898 |
| 0.29 | 2.92 | 1.87 | 1.56 | 2270 |
| 0.26 | 3.06 | 1.86 | 1.65 | -1185 |
| 0.33 | 2.91 | 1.85 | 1.57 | -1244 |
| 0.34 | 3.16 | 1.97 | 1.60 | -1303 |
| 0.34 | 3.21 | 2.00 | 1.60 | -1362 |
| 0.31 | 3.21 | 2.01 | 1.59 | -1421 |
| 0.39 | 3.20 | 2.02 | 1.59 | -1480 |
| 0.32 | 3.22 | 2.02 | 1.59 | -1539 |
| 0.28 | 3.22 | 2.02 | 1.59 | -1598 |
| 0.33 | 3.21 | 2.02 | 1.59 | -1657 |
| 0.37 | 3.17 | 2.01 | 1.58 | -1716 |
| 0.33 | 3.16 | 2.00 | 1.58 | -1775 |
| 0.28 | 3.15 | 2.00 | 1.58 | -1834 |
| 0.34 | 3.13 | 1.99 | 1.57 | -1893 |
| 0.34 | 3.12 | 1.99 | 1.57 | -1951 |
| 0.35 | 3.12 | 1.98 | 1.57 | -2010 |
| 0.32 | 3.08 | 1.98 | 1.56 | -2069 |
| | | | | |
| 0.33 | 3.09 | 1.98 | 1.56 | 2660 |
| 0.31 | 3.09 | 1.98 | 1.56 | 2685 |
| 0.35 | 3.09 | 1.97 | 1.56 | 2710 |
| 0.31 | 3.10 | 1.97 | 1.57 | 2735 |
| **0.16** | | | | |
| **0.15** | | | **1.57** | |
| | | | | |
| 0.36 | 3.02 | 1.96 | 1.54 | -2128 |
| 0.32 | 2.97 | 1.95 | 1.52 | -2187 |
| 0.38 | 2.87 | 1.95 | 1.48 | -2246 |
| 0.29 | 2.74 | 1.94 | 1.41 | -2304 |
| 0.27 | 3.07 | 1.94 | 1.58 | -203 |
| 0.34 | 3.04 | 1.94 | 1.57 | -255 |
| 0.31 | 3.04 | 1.93 | 1.58 | -307 |
| 0.34 | 3.02 | 1.92 | 1.57 | -359 |
| 0.29 | 2.99 | 1.91 | 1.57 | -410 |
| 0.30 | 2.97 | 1.89 | 1.57 | -462 |
| 0.35 | 2.96 | 1.88 | 1.57 | -514 |
| 0.39 | 2.95 | 1.87 | 1.57 | -566 |
| 0.34 | 2.93 | 1.87 | 1.57 | -618 |
| 0.31 | 2.92 | 1.86 | 1.57 | -670 |
| 0.30 | 2.90 | 1.85 | 1.56 | -721 |
| 0.33 | 2.90 | 1.85 | 1.57 | -773 |
| 0.20 | 3.10 | 1.97 | 1.57 | -825 |
| 0.35 | 3.15 | 2.01 | 1.57 | -877 |
| 0.37 | 3.14 | 2.02 | 1.56 | -929 |
| 0.33 | 3.14 | 2.02 | 1.55 | -981 |
| | | | | |
| 0.33 | 3.15 | 2.02 | 1.56 | 2660 |

| | | | | |
|---|---|---|---|---|
| 0.30 | 3.17 | 2.03 | 1.56 | 2685 |
| 0.30 | 3.18 | 2.02 | 1.57 | 2710 |
| 0.33 | 3.19 | 2.02 | 1.58 | 2735 |
| **0.16** | | | | |
| **0.15** | | | **1.57** | |
| | | | | |
| 0.29 | 3.13 | 2.02 | 1.55 | -1033 |
| 0.34 | 3.08 | 2.02 | 1.53 | -1084 |
| 0.48 | 3.04 | 2.02 | 1.51 | -1136 |
| 0.31 | 2.84 | 2.01 | 1.41 | -1188 |
| | | | | |
| 0.27 | 3.14 | 2.01 | 1.56 | 2660 |
| 0.37 | 3.14 | 2.01 | 1.56 | 2685 |
| ~~**0.43**~~ | ~~**3.00**~~ | ~~**2.01**~~ | ~~**1.49**~~ | ~~**2710**~~ |
| 0.32 | 3.15 | 2.01 | 1.57 | 2735 |
| **0.29** | | | | |
| **0.20** | | | **1.57** | |

| Y | DTFA-X | DTFA-Y | $^{16}O^{1}H/^{16}O$** | reasons for rejection |
|---|---|---|---|---|
| -1291 | -21 | -18 | 0.000433151 | |
| -1291 | -21 | -18 | 0.000432442 | |
| -1291 | -21 | -18 | 0.000428615 | |
| -1291 | -21 | -17 | 0.000434105 | |
| | | | | |
| 603 | -16 | -16 | 0.000631247 | |
| 720 | -17 | -13 | 0.000605429 | |
| 827 | -17 | -12 | 0.000646146 | |
| 920 | -17 | -11 | 0.000700863 | |
| 1033 | -17 | -9 | 0.000495338 | |
| 1134 | -17 | -8 | 0.000533974 | |
| 1237 | -15 | -6 | 0.000621931 | |
| 1355 | -14 | -5 | 0.000771374 | |
| 1441 | -14 | -5 | 0.00065283 | |
| 1532 | -14 | -6 | 0.000612831 | |
| 294 | -18 | -14 | 0.000432296 | |
| 329 | -18 | -13 | 0.000741974 | |
| 363 | -19 | -13 | 0.000658627 | |
| 397 | -19 | -13 | 0.000683699 | |
| 431 | -20 | -12 | 0.000636441 | |
| 465 | -19 | -11 | 0.000511395 | |
| 499 | -19 | -10 | 0.000592954 | |
| 534 | -18 | -9 | 0.000760161 | |
| 568 | -18 | -8 | 0.000702317 | |
| 602 | -19 | -9 | 0.000714963 | |
| | | | | |
| -1311 | -20 | -18 | 0.000427062 | |
| -1311 | -20 | -18 | 0.00043297 | |
| -1311 | -20 | -18 | 0.000435911 | |
| -1311 | -20 | -18 | 0.000432281 | |
| | | | | |
| | | | **0.000432067** | |
| | | | | |
| -1380 | -7 | -20 | 0.000498536 | |
| -1306 | -8 | -18 | 0.000504841 | |
| -1232 | -8 | -17 | 0.000539515 | |
| -1158 | -9 | -16 | 0.000559826 | |
| -1084 | -9 | -14 | 0.000542666 | |
| -1010 | -10 | -12 | 0.000527462 | |
| -936 | -11 | -11 | 0.000454647 | |
| -862 | -11 | -9 | 0.000503291 | |
| -788 | -10 | -8 | 0.000483451 | |
| -714 | -7 | -11 | 0.000434279 | |

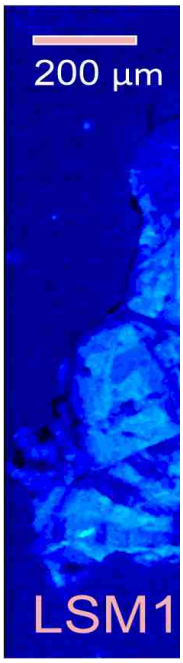


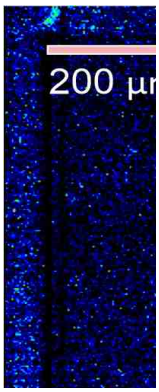

| | | | |
|---|---|---|---|
| -3261 | -6 | -16 | 0.000791031 |
| -3315 | -7 | -16 | 0.000765052 |
| -3369 | -8 | -17 | 0.000774299 |
| -3423 | -9 | -18 | 0.000728584 |
| -3478 | -10 | -19 | 0.000739651 |
| -3532 | -11 | -21 | 0.00061307 |
| -3586 | -11 | -22 | 0.000648854 |
| -3640 | -11 | -22 | 0.000554894 |
| -3695 | -11 | -22 | 0.00060175 |
| -3749 | -7 | -22 | 0.000417288 |
| | | | |
| -1331 | -19 | -17 | 0.000417081 |
| -1331 | -20 | -17 | 0.000423004 |
| -1331 | -20 | -17 | 0.000413843 |
| -1331 | -20 | -17 | 0.000399451 |
| | | | |
| | | | **0.0004227** |

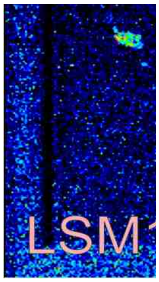


| | | | |
|---|---|---|---|
| 2989 | -15 | -6 | 0.0004155 |
| 2629 | -12 | -16 | 0.000387917 |
| 2587 | -19 | -5 | 0.00041913 |
| 2565 | -17 | -7 | 0.000526663 |
| 2543 | -17 | -8 | 0.000759426 |
| 2520 | -16 | -8 | 0.000674942 |
| 2485 | -14 | -9 | 0.000572205 |
| 1048 | -22 | -11 | 0.000408314 |
| 1428 | -18 | -7 | 0.000411743 |
| -1215 | -21 | -14 | 0.000378405 |
| -1266 | -20 | -15 | 0.000500078 |
| -4384 | -12 | -22 | 0.000596559 |
| -4420 | -14 | -21 | 0.000802076 |
| -4456 | -14 | -22 | 0.000655582 |
| -4492 | -14 | -23 | 0.004181011 |
| -4528 | -13 | -25 | 0.000570781 |
| -4565 | -13 | -26 | 0.000552443 |
| -4601 | -12 | -27 | 0.000557125 |
| -4637 | -11 | -27 | 0.000766271 |
| -4673 | -10 | -28 | 0.0007599 |
| | | | |
| -1351 | -20 | -18 | 0.000389316 |
| -1351 | -20 | -18 | 0.00041456 |
| -1351 | -20 | -18 | 0.000400483 |
| -1351 | -20 | -18 | 0.000385166 |
| | | | |
| | | | **0.000405363** |

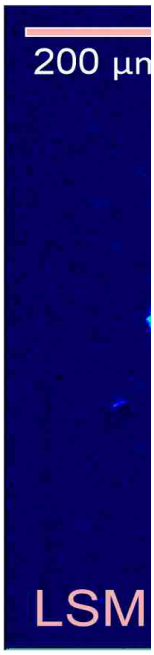


| | | | |
|---|---|---|---|
| -4710 | -8 | -28 | 0.000578133 |
| -3941 | -15 | -24 | 0.000863076 |

| | | | |
|---|---|---|---|
| -3976 | -12 | -24 | 0.000860303 |
| -3670 | -12 | -21 | 0.000703863 |
| -2192 | -9 | -15 | 0.000739032 |
| -2184 | -9 | -16 | 0.000705499 |
| -2175 | -11 | -15 | 0.000503533 |
| -2167 | -12 | -15 | 0.000455464 |
| -2158 | -12 | -15 | 0.000429677 |
| -2150 | -12 | -15 | 0.000470253 |
| -2142 | -12 | -15 | 0.000464728 |
| -2133 | -12 | -16 | 0.000467091 |
| -2125 | -12 | -16 | 0.000439952 |
| -2116 | -12 | -16 | 0.000391831 |
| -2108 | -11 | -16 | 0.000378045 |
| -2099 | -11 | -15 | 0.000375505 |
| -2091 | -11 | -15 | 0.000372192 |
| -2082 | -10 | -15 | 0.000374508 |
| -2074 | -10 | -15 | 0.000396482 |
| -2066 | -9 | -16 | 0.000382499 |
| | | | |
| -1371 | -20 | -19 | 0.000366287 |
| -1371 | -20 | -19 | 0.000385285 |
| -1371 | -20 | -19 | 0.000385521 |
| -1371 | -20 | -19 | 0.000364706 |
| | | | |
| | | | **0.000386415** |
| | | | |
| -2057 | -9 | -14 | 0.000501125 |
| -2049 | -9 | -15 | 0.00039952 |
| -2041 | -8 | -16 | 0.000522515 |
| -2032 | -7 | -15 | 0.000555443 |
| -2430 | -18 | -19 | 0.00037271 |
| -2429 | -17 | -19 | 0.000474038 |
| -2428 | -17 | -19 | 0.000392212 |
| -2427 | -17 | -18 | 0.00038333 |
| -2425 | -16 | -18 | 0.00052996 |
| -2424 | -16 | -18 | 0.000565558 |
| -2422 | -16 | -18 | 0.000641005 |
| -2421 | -16 | -18 | 0.000405183 |
| -2419 | -15 | -18 | 0.000499663 |
| -2418 | -15 | -18 | 0.000531048 |
| -2416 | -15 | -17 | 0.000507714 |
| -2414 | -14 | -18 | 0.000478194 |
| -2413 | -14 | -18 | 0.000527978 |
| -2411 | -13 | -18 | 0.00048105 |
| -2409 | -13 | -18 | 0.000439964 |
| -2408 | -12 | -18 | 0.00048224 |
| | | | |
| -1391 | -20 | -19 | 0.000357101 |

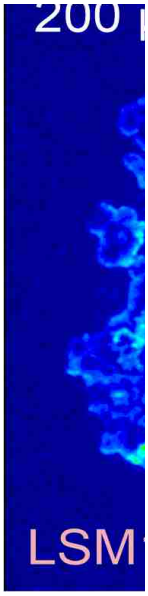


| | | | | |
|---|---|---|---|---|
| -1391 | -20 | -19 | 0.000372741 | |
| -1391 | -20 | -19 | 0.000374501 | |
| -1391 | -20 | -19 | 0.000351889 | |
| | | | **0.000369754** | |
| -2406 | -12 | -18 | 0.000455957 | |
| -2404 | -12 | -18 | 0.000515341 | |
| -2402 | -13 | -18 | 0.000445007 | |
| -2401 | -12 | -18 | 0.000380405 | |
| -1411 | -20 | -19 | 0.000353871 | |
| -1411 | -20 | -19 | 0.000392931 | |
| ~~-1411~~ | ~~-20~~ | ~~-19~~ | ~~0.000397239~~ | Low yield and higher 2SE |
| -1411 | -20 | -19 | 0.000354315 | |
| | | | **0.000365335** | |

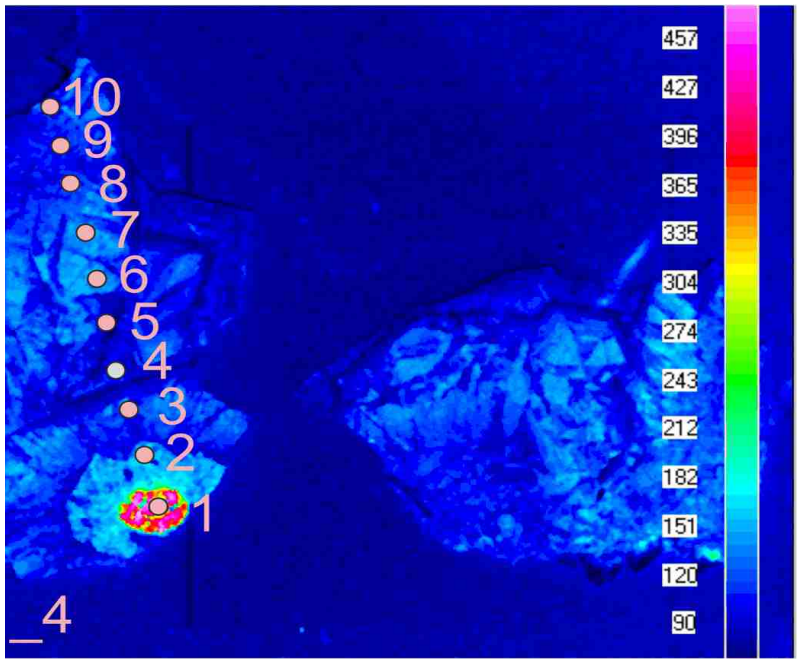
457
427
396
365
335
304
274
243
212
182
151
120
90
10
9
8
7
6
5
4
3
2
1
_4

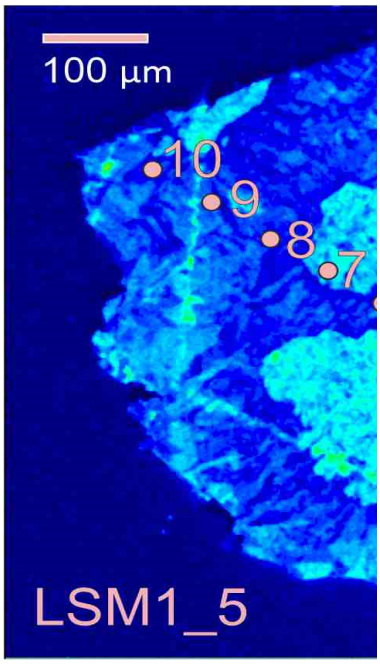
100 µm
10
9
8
7
LSM1_5

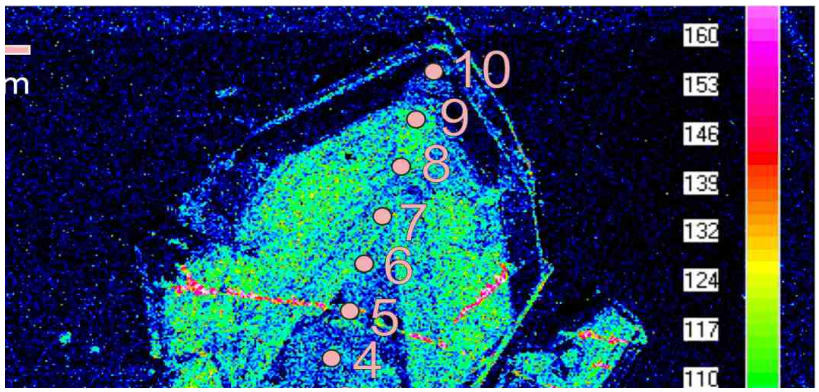
160
153
146
139
132
124
117
110
10
9
8
7
6
5
4

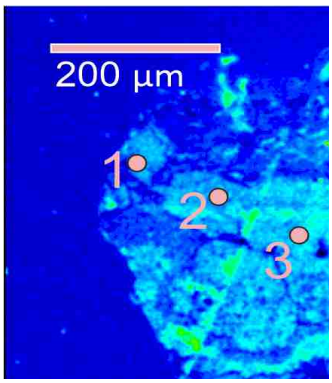
200 µm
1
2
3

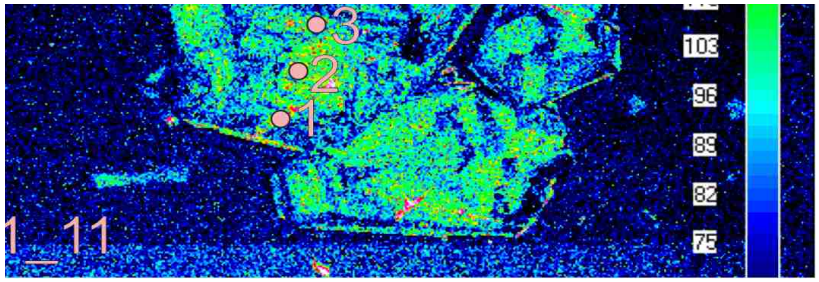
3
2
1
103
96
89
82
75
1_11

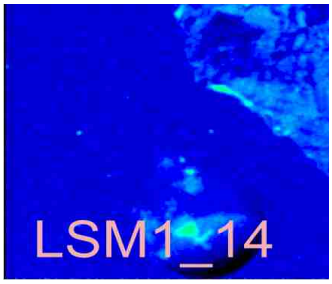
LSM1_14

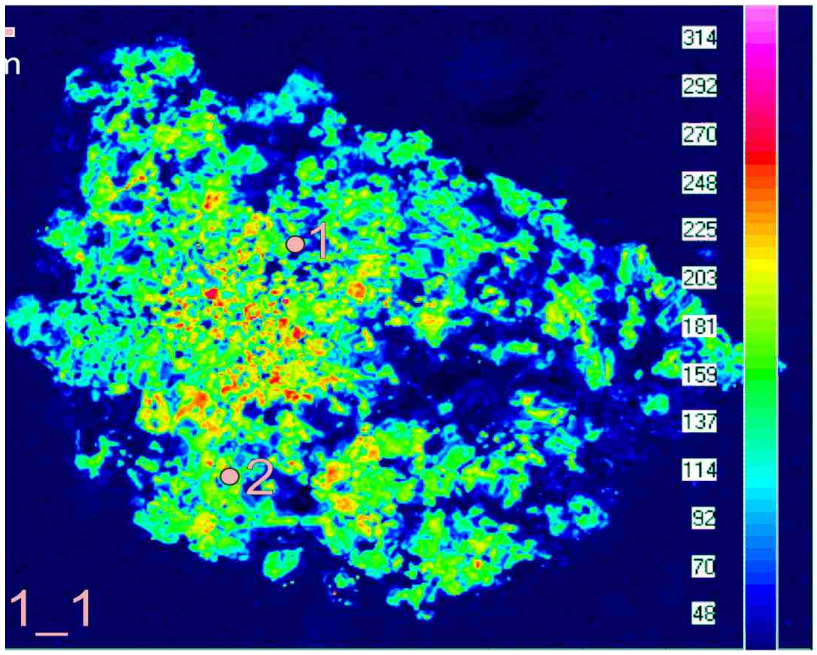
314
292
270
248
225
203
181
159
137
114
92
70
48
1
2
1_1

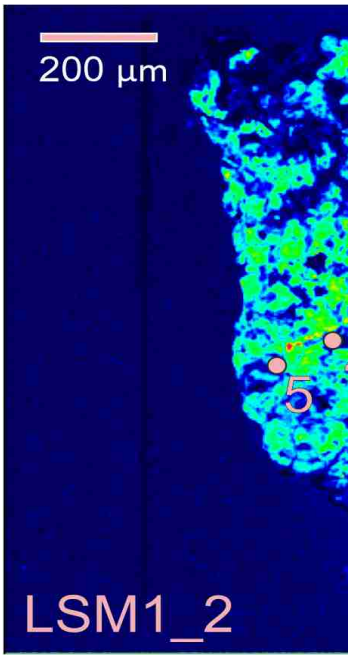
200 µm
5
LSM1_2


311

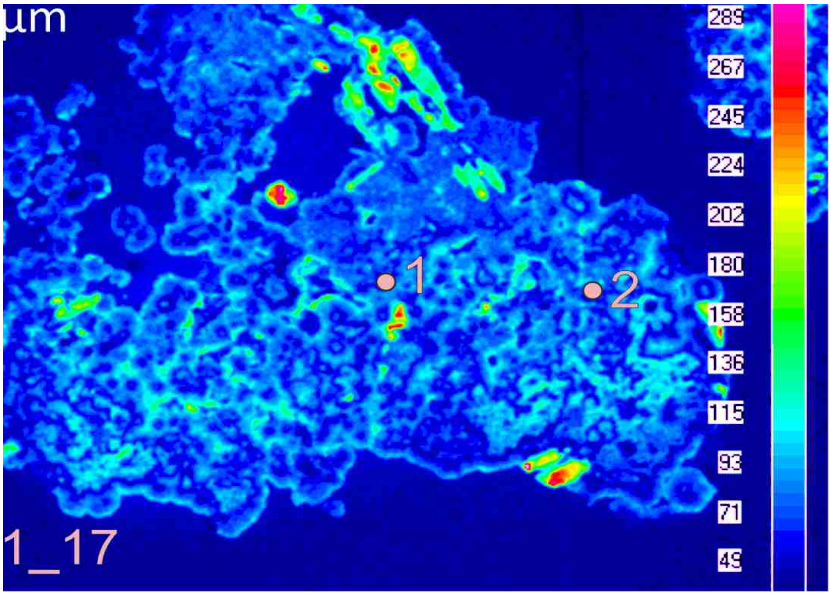
µm
289
267
245
224
202
180
158
136
115
93
71
49
1
2
1_17

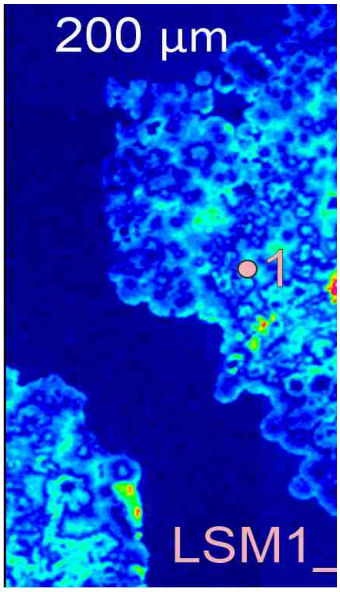
200 µm
1
LSM1_

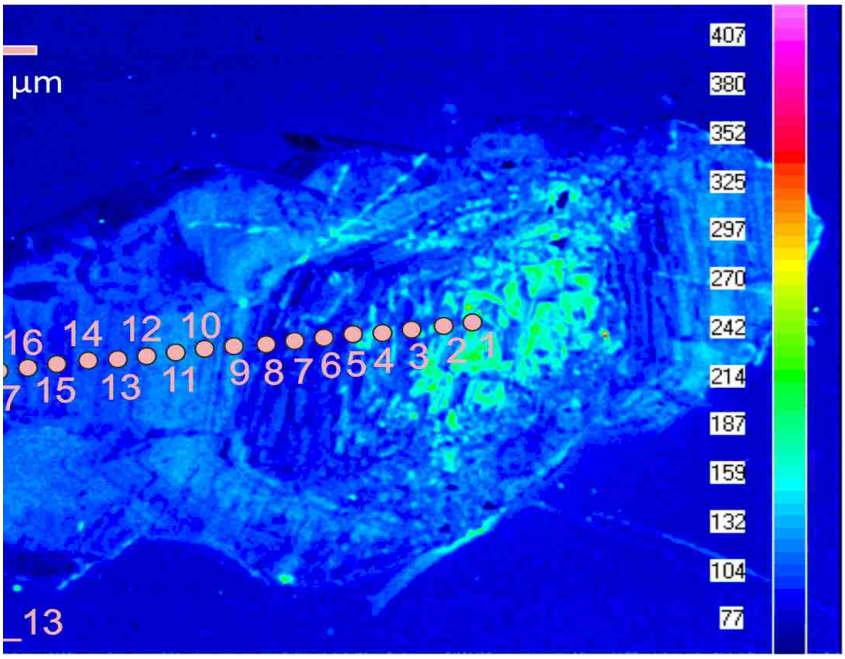
µm
407
380
352
325
297
270
242
214
187
159
132
104
77
16 14 12 10
7 15 13 11 9 8 7 6 5 4 3 2 1
_13

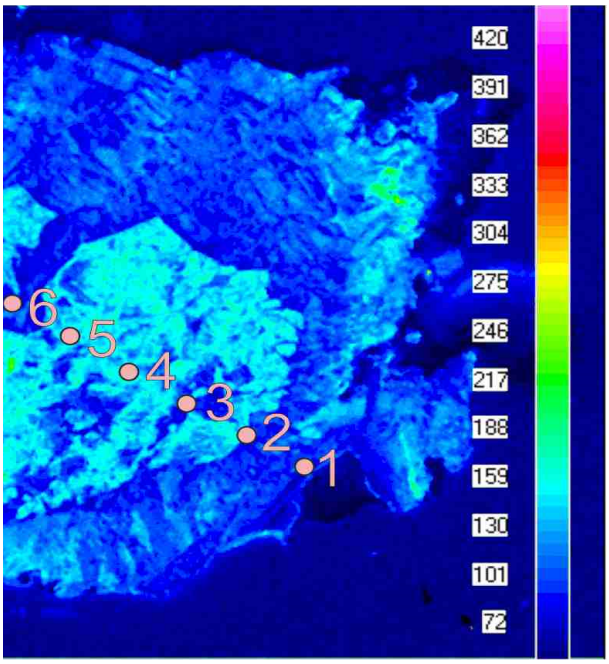
420
391
362
333
304
275
246
217
188
159
130
101
72
6
5
4
3
2
1

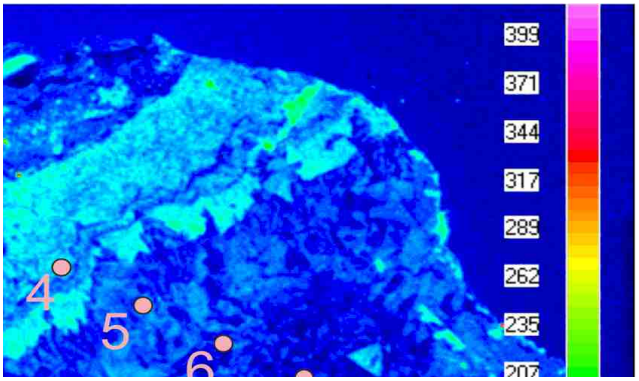
399
371
344
317
289
262
235
4
5
6

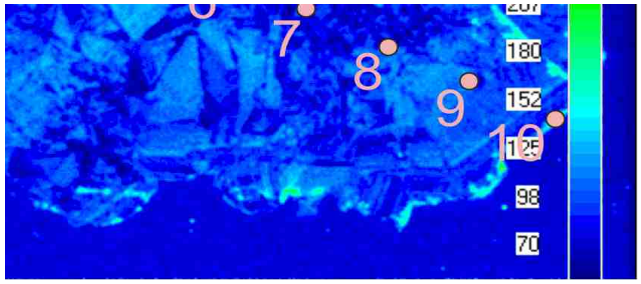
7
8
9
10
180
152
125
98
70

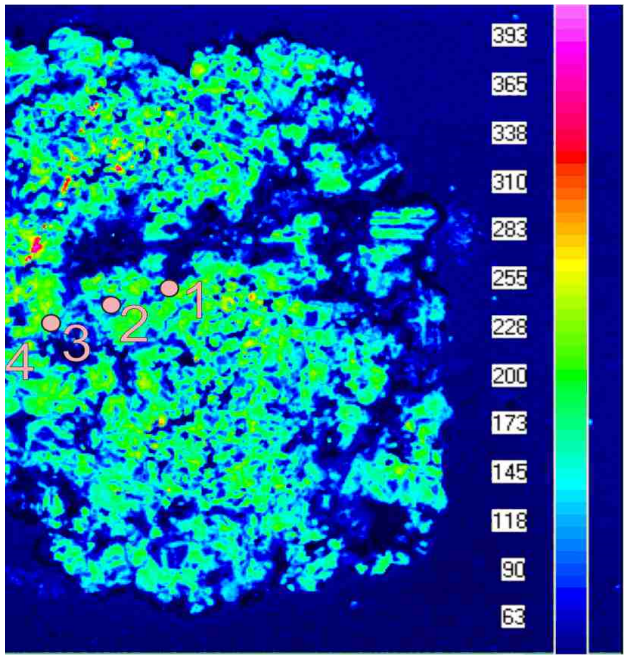
393
365
338
310
283
255
228
200
173
145
118
90
63
1
2
3
4

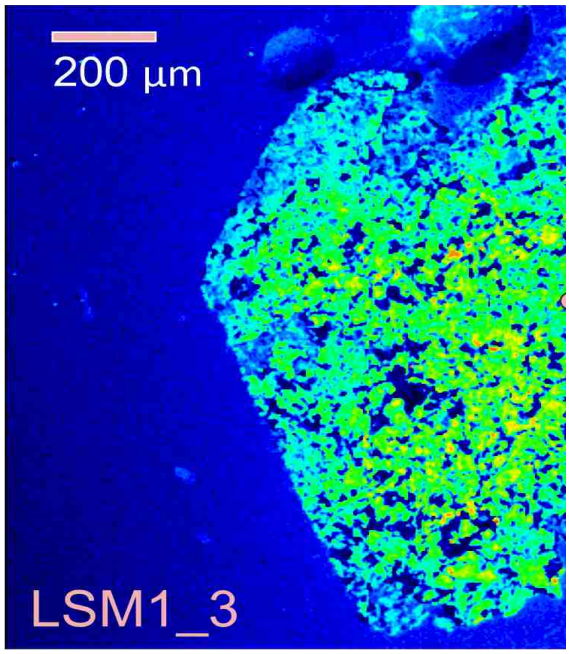
200 µm
LSM1_3


308

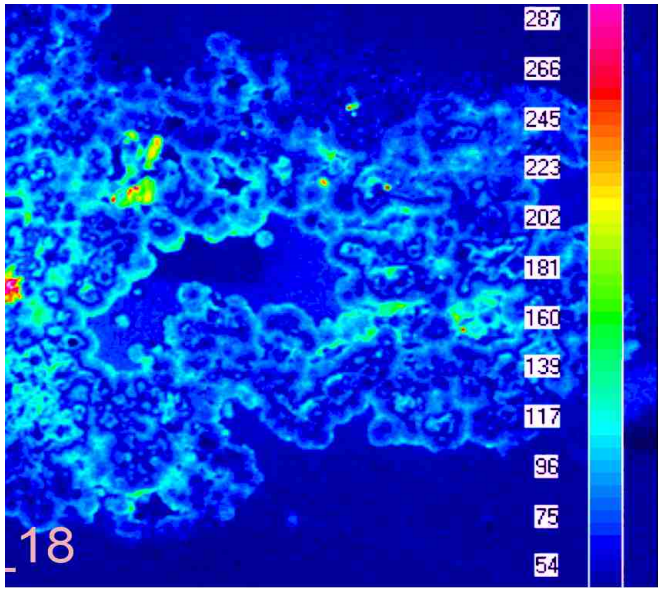
287
266
245
223
202
181
160
139
117
96
75
54
_18

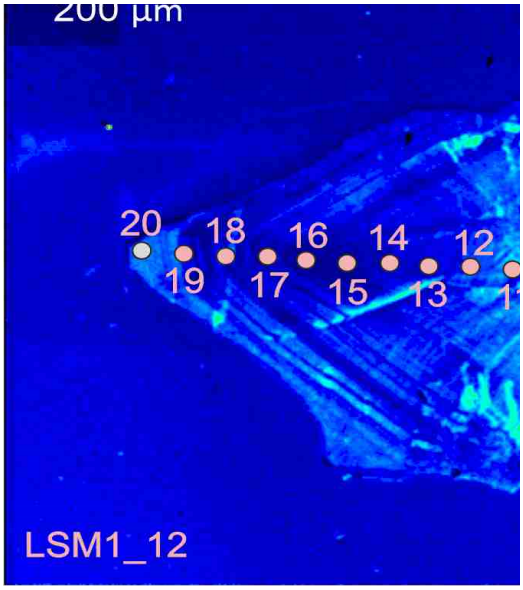
200 µm
20
18
16
14
12
19
17
15
13
LSM1_12

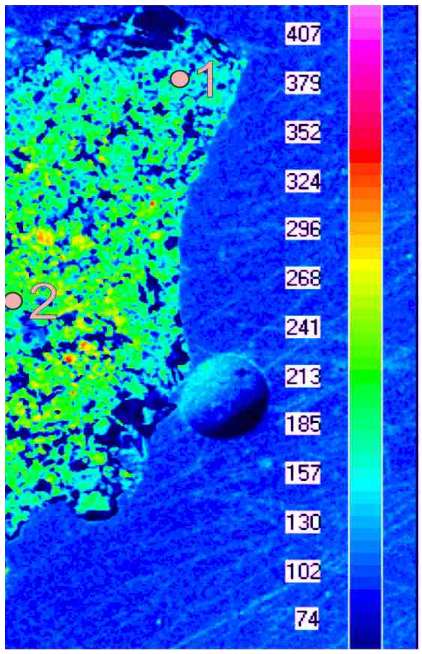
407
379
352
324
296
268
241
213
185
157
130
102
74
1
2

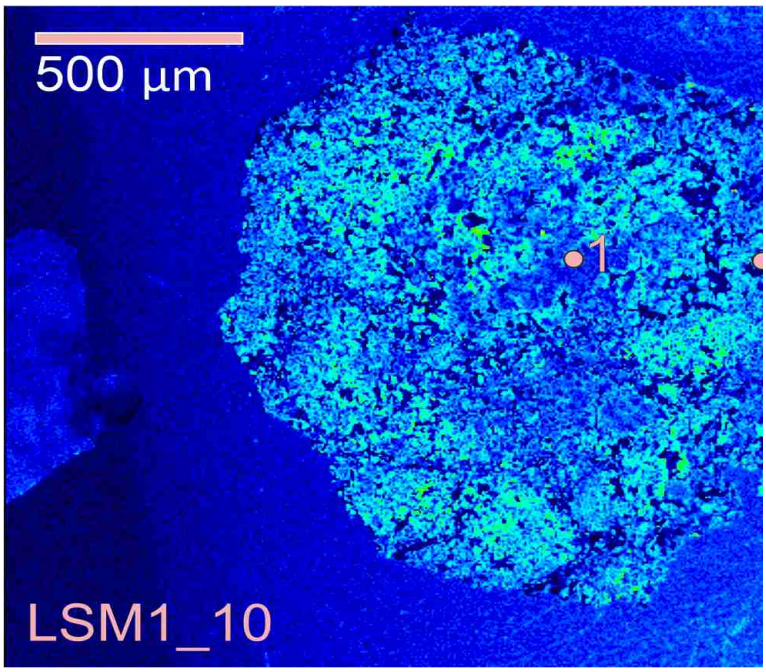
500 µm
1
LSM1_10


408

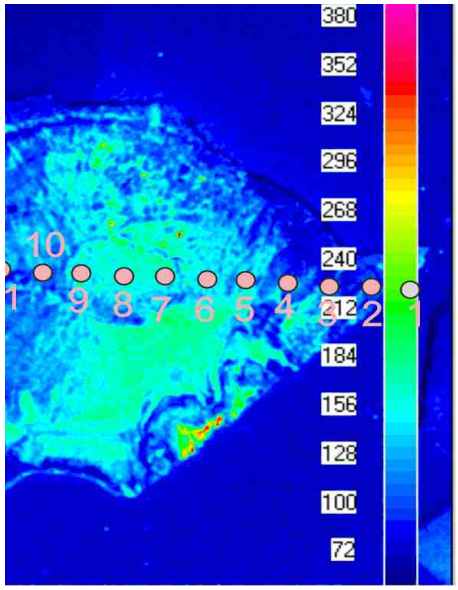
380
352
324
296
268
240
212
184
156
128
100
72
10
9
8
7
6
5
4
3
2
1

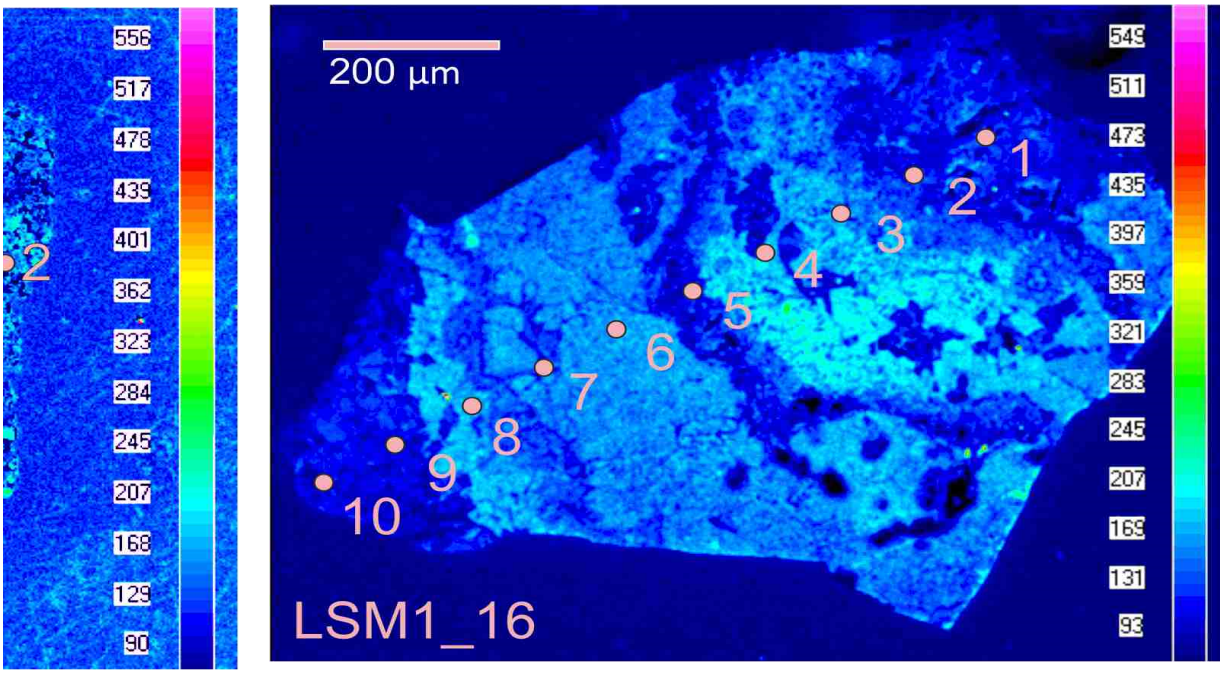
556
517
478
439
401
362
323
284
245
207
168
129
90
2
200 µm
549
511
473
435
397
359
321
283
245
207
169
131
93
1
2
3
4
5
6
7
8
9
10
LSM1_16